PHOTOCATALYTIC DEGRADATION OF PHTHALIC ANHYDRIDE AND DICARBOXYLIC ACIDS

by

Ayşe Neren Ökte

B.S. in Chem., Boğaziçi University, 1992

Submitted to the Institute for Graduate Studies in Science and Engineering in partial fulfillment of requirements for the degree of

Master of Science

in

Chemistry

Boğaziçi University

1994

"Gözlerimizi kapayıp tek başına yaşadığımızı düşünemeyiz. Memleketimizi bir çember içine alıp dünya ile ilgisiz yaşayamayız. Aksine yükselmiş, ilerlemiş, medeni bir millet olarak medeniyet düzeninin uzerinde yaşayacağiz. Bu hayat, ancak ilim ve fen ile olur. İlim ve fen nerede ise oradan alacağız ve her millet kafasına koyacağız."

Kasım 1922

Mustafa Kemal ATATÜRK

To my family

ACKNOWLEDGEMENTS

I would like to mention my gratitude to my thesis supervisor Prof. Dr. Yüksel İnel for his invaluable guidance, patience, suggestions and long-term encouragement throughout this study. I want to thank him for all the energy and time he put into this work.

I thank to my jury members, Assoc. Prof. Dr. Miray Bekbölet and Assoc. Prof. Dr. Dilek Çalgan for their critics and discussions to the manuscript.

I am also indebted to all my friends for their endless support and valuable discussions to overcome the difficulties on the preparation of this work.

I am especially grateful to Parisa Deljouie for her guiding comments and encouragement throughout this study.

I also thank to my classmates, Nuray Temel and Sibel Yazıcı Serhatkulu for their support and help on writing and printing the manuscript.

I would also like to thank Dr. Arlette İtken, Safiye Erdem, and Gökşin Apaydın for their valuable information on writing the manuscript.and drawing the figures.

I also thank to Emine Yıkılmaz and Hülya Metiner for their support and help during long periods of this work.

And, hearty thanks to my friend Vanya Bugarcıc, her presence made everything easier and tastier.

It is a great pleasure for me to express my deepest gratitude to my mother, my father and my brothers for their endless love, patience, and encouragement throughout this study.

ABSTRACT

Exposure of TiO_2 particles to light with an energy equal or greater than its bandgap leads to the creation of electrons and holes which are able to degrade toxic chemicals.

In this study, in the presence of Degussa P25 TiO_2, photocatalytic oxidation of phthalic anhydride, malonic acid, succinic acid, and adipic acid has been investigated by means of gas chromatography techniques following the CO_2 formation.

The alteration of pH of the aqueous suspension, TiO_2 loading, anhydride or acids concentrations, irradiation time, flow rate, and light intensity changed the rate of formation of CO_2 which has been investigated by the same method. It was also observed that the rate of CO_2 formation increases linearly by increasing the temperature of the suspension.

The order of the reactions as well as the rate constants could be determined for the photocatalytic oxidation processes. As a consequence, by altering the concentration of malonic, succinic, and adipic acids we observed that their disappearance fits a Langmuir-Hinshelwood kinetic model. In other words, the photoocatalytic xidation reactions take place in the adsorbed phase, i.e., on the surface of TiO_2.

Rate constants was also calculated by including the correction term $\alpha(T)$ which stands in order to take into account the decrease in the solubility of CO_2 with increasing temperature. These results led to the calculation of activation energy as: 3.19 kj/mole, 9.99 kj/mole, 15.59 kj/mole, and 14.38 kj/mole for phthalic anhydride, malonic acid, succinic acid, and adipic acid respectively.

Finally, 0.43×10^{-6} quantum yield for the CO_2 formation has been estimated from the proposed mechanisms.

ÖZET

TiO_2 parçacıklarının kendi bandgap enerjilerini eşit veya daha yüksek bir enerji ile ışıklandırılmaları sonucu oluşan elektronlar ve holler toksik kimyasalları degrede edebilme özelliğine sahiptirler.

Bu çalışmada, Degussa P-25 TiO_2 kullanılarak fitalik anhidrit, malonik, suksinik ve adipik asitlerin fotokatalitic yükseltgenmeleri gaz kromotografi tekniği ile CO_2 oluşumu üzerinden incelenmiştir. CO_2 oluşum hızı reaksiyon ortamının pH'sına, TiO_2 miktarına, anhidrit veya asit konsantrasyonuna, ışıklandırılma zamanına, akış hızına ve ışık şiddetine bağlı olarak değişmektedir. Sıcaklığa bağlı olarak ise CO_2 oluşum hızında doğrusal bir artış görülmüştür. Fotokatalitik yükseltgenme reaksiyonlarında reaksiyon derecelerini ve hız sabitlerini tesbit etmek mümkündür. Asit konsantrasyonlarının değişmesi Langmuir-Hinshelwood kinetik modeline uygun olduklarını, diğer bir değişle fotokatalitic yükseltgenme reaksiyonlarının emilme ortamında,.TiO_2 yüzeyinde gerçekleştiğini göstermiştir. Artan sıcaklıkla değişen CO_2 çözünürlüğü "$\alpha(T)$" ile tanımlanarak hız sabitleri hesaplanmıştır. Bu sabitlere göre fitalik anhidrit

için 3.19 kj/mol, malonik asit için 9.99 kj/mol, suksinik asit için 15.59 kj/mol ve adipik asit için 14.38 kj/mol aktivasyon enerjileri bulunmuştur.

CO_2 oluşumunda $0.43x10^{-6}$ kuantum verimi ileri sürülen mekanizmalara göre hesaplanmıştır.

TABLE OF CONTENTS

	Page
ACKNOWLEDGEMENTS	iv
ABSTRACT	v
ÖZET	vii
LIST OF FIGURES	ix
LIST OF TABLES	xiv
LIST OF SYMBOLS	xvi
I. INTRODUCTION	1
II. SEMICONDUCTORS	3
2.1. Basic Principles of Semiconductors	3
2.2. Conduction and Charge Carrier Generation	5
2.3. Fermi Level	7
2.4. Absorption of Light by Semiconductors	9
2.5. Semiconductor/Electrolyte Interface	9
2.6. Carrier Trapping	12
2.7. Photocatalytically Active Semiconductors	13
III. TITANIUM DIOXIDE: A PHOTOSENSITIVE SEMICONDUCTOR	14
3.1. Composition and Occurrence	14
3.2. Properties and Uses	15
3.3. Photocatalytic Activity of TiO_2	16
3.4. Surface Analysis of TiO_2	20
3.4.1. Adsorption Effect	22
3.4.2. Infrared Spectroscopy of Hydroxylated TiO_2	23
IV. EXPERIMENTAL	24
4.1. Properties of the Photocatalyst	24

	Page
4.2. Reagents and Sources of Light	24
4.2.1. Reagents	24
4.2.2. Sources of Light	24
4.3. Sample Preparation	27
4.4. Phthalic Anhydride	27
4.4.1. Reactors	28
4.4.2. Analysis	29
4.5. Dicarboxylic Acids	33
4.5.1. Reactor	34
4.5.2. Analysis	34
4.6. Actinometric Study	41
4.6.1. Preparation of the Actinometer Solution	41
4.6.2. Procedure for the Actinometric Measurements	42
V. RESULTS AND DISCUSSION	43
5.1. Results of Calibration Curves	43
5.1.1. Solubility of CO_2 in Water	43
5.2. Results of Phthalic Anhydride	46
5.2.1. Results for the Actinometric Measurement	46
5.2.2. Effect of Catalyst Concentration	46
5.2.3. Effect of pH	47
5.2.4. Effect of Phthalic Anhydride Concentration	50
5.2.5. Effect of Irradiation Time	50
5.2.6. Effect of Temperature	51
5.2.7. Effect of Flow Rate	55
5.2.8. Effect of Light Intensity	59
5.3. Results of Dicarboxylic Acids	61
5.3.1. Resuts for the Actinometric Measurements	61
5.3.2. Effect of pH	61
5.3.3. Effect of Irradiation Time	63
5.3.4. Effect of Acid Concentration	80
5.3.5. Effect of Temperature	93
5.3.6. Effect of Light Intensity	103
5.4. A Postulated Mechanism	117

Page

VI. CONCLUSION 120

BIBLIOGRAPHY 122

LIST OF FIGURES

		Page
FIGURE 2.1	Energy band diagram for a semiconductor.	4
FIGURE 2.2	Mechanisms of charge carrier.generation in semiconductor.	7
FIGURE 2.3	The Fermi level and the effects of doping.	8
FIGURE 2.4	Formation of space charge region in solution for an n-type semiconductor..	11
FIGURE 2.5	Formation of space charge region in solution for an p-type semiconductor.	11
FIGURE 2.6	The semiconductor particle as a redox catalyst.	12
FIGURE 3.1.	Relevant reduction potentials for couples in water/ oxygen system.	17
FIGURE 3.2	Generation of primary radicals at the surface of irradiated TiO_2 particles in water.	17
FIGURE 3.3	ESR signal of hydroxyl radical observed during UV irradiation of anatase TiO_2/water.	18
FIGURE 3 4	Formation of surface hydroxyls on the anatase (001)face.	21
FIGURE 3.5	Relevant groups present on TiO_2 surface in aqueous solution as a function of pH.	22
FIGURE 3.6	IR spectrum of TiO_2 (Degussa P-25).	23
FIGURE 4.1	Absorption spectrum of TiO_2 (anatase).	26

	Page
FIGURE 4.2 Emission spectrum of black light fluorescent lamps.	26
FIGURE 4.3 Reactor I.	30
FIGURE 4.4 Reactor II.	30
FIGURE 4.5 CO_2 calibration curve for phthalic anhydride.	31
FIGURE 4.6 Box design.	36
FIGURE 4.7 Experimental set-up.	37
FIGURE 4.8 CO_2 calibration curve for malonic acid.	38
FIGURE 4.9 CO_2 calibration curve for succinic acid.	39
FIGURE 4.10 CO_2 calibration curve for adipic acid.	40
FIGURE 5.1 Distribution of species diagram for CO_2,HCO_3^-,CO_3^{2-} system in water.	44
FIGURE 5 2 Effect of TiO_2 amount on CO_2 formation from phthalic anhydride.	48
FIGURE 5.3 Dependence of CO_2 formation on the pH of. phthalic anhydride.	49
FIGURE 5.4 Concentration effect on the CO_2 yield from phthalic anhydride.	52
FIGURE 5.5 CO_2 formation as a function of irradiation time for phthalic anhydride.	53
FIGURE 5.6 Temperature effect on the CO_2 formation from phthalic anhydride.	56
FIGURE 5.7 Arrhenius plot of phthalic anhydride.	57
FIGURE 5.8 CO_2 formation as a function of flow rate for phthalic.anhydride.	58

		Page
FIGURE 5.9	CO_2 evolution as a function of light intensity for.phthalic anhydride.	60
FIGURE 5.10	Effect of pH.on the CO_2 formation from malonic acid.	64
FIGURE 5.11	pH effect on the rate of CO_2 formation from. malonic.acid.	65
FIGURE 5.12	Effect of pH on the CO_2 formation from succinic acid.	66
FIGURE 5.13	pH effect on the rate of CO_2 formation from succinic acid.	67
FIGURE 5.14	Effect of pH on the CO_2 formation from adipic acid.	68
FIGURE 5.15	pH effect on the rate of CO_2 formation from succinic acid.	69
FIGURE 5.16	Irradiation time effect on the CO_2 formation from malonic,succinic.and adipic acids.	71
FIGURE 5.17	Malonic acid - CO_2 ml to mole conversion.	74
FIGURE 5.18	Succinic acid - CO_2 ml to mole conversion.	76
FIGURE 5.19	Adipic acid - CO_2 ml to mole conversion.	78
FIGURE 5.20	Rate of CO_2 formation after 60 min. irradiation time from malonic,succinic and adipic acids.	79
FIGURE 5.21	Effect of concentration on the CO_2 formation from malonic acid.	84
FIGURE 5.22	Effect of concentration on the rate of CO_2 formation from malonic acid.	85
FIGURE 5.23	1/R versus 1/conc for malonic acid.	86

			Page
FIGURE	5.24	Effect of concentration on the CO_2 formation from succinic acid.	87
FIGURE	5.25	Effect of concentration on the rate of CO_2 formation from succinic acid.	88
FIGURE	5.26	1/R versus 1/conc for succinic acid.	89
FIGURE	5.27	Effect of concentration on the CO_2 formation from adipic acid.	90
FIGURE	5.28	Effect of concentration on the rate of CO_2 formation from adipic acid.	91
FIGURE	5.29	1/R versus 1/conc for adipic acid.	92
FIGURE	5.30	Effect of temperature on CO_2 formation from malonic acid.	97
FIGURE	5.31	Arrhenious plot for malonic acid.	98
FIGURE	5.32	Effect of temperature on CO_2 formation from succinic acid.	99
FIGURE	5.33	Arrhenius plot for succinic acid.	100
FIGURE	5.34	Effect of temperature on CO_2 formation from adipic acid.	101
FIGURE	5.35	Arrhenius plot for adipic acid.	102
FIGURE	5.36	CO_2 formation from malonic acid as a function of number of lamps.	109
FIGURE	5.37	Light intensity effect on the rate of CO_2 formation from malonic acid.	110
FIGURE	5.38	Effect of square root of light intensity on the CO_2 formation from malonic acid.	111

Page

FIGURE 5.39 CO_2 formation from succinic acid as a function of number of lamps. 112

FIGURE 5.40 Light intensity effect on the rate of CO_2 formation succinic acid. 113

FIGURE 5.41 Effect of square root of light intensity on the CO_2 formation from succinic acid. 114

FIGURE 5.42 CO_2 formation from adipic acid as a function of number of lamps. 115

FIGURE 5.43 Light intensity effect on the rate of CO_2 formation from adipic acid. 116

FIGURE 5.44 Effect of square root of light intensity on the CO_2 formation from adipic acid. 117

LIST OF TABLES

	Page
TABLE 2.1. Bandgap energy and wavelength for some photochemically active semiconductors.	5
TABLE 3.1. Radicals formed on irradiated TiO_2 and their reactions	19
TABLE 4.1. Physicochemical data of TiO_2 (Degussa P-25).	25
TABLE 4.2. Reagents.	25
TABLE 4.3. Properties of phthalic anhydride.	28
TABLE 4.4. Analytical conditions for the gas chromatograph.	31
TABLE 5.1. The actinometric result for phthalic anhydride.	46
TABLE 5.2. Effect of TiO_2 loading on the CO_2 formation from phthalic anhydride.	47
TABLE 5.3. Effect of pH on the CO_2 formation from phthalic anhydride.	47
TABLE 5.4. Effect of phthalic anhydride concentration on theCO_2 formation.	50
TABLE 5.5. Effect of irradiation time on the CO_2 formation from phthalic anhydride.	51
TABLE 5.6. Effect of temperature on the CO_2 formation from phthalic anhydride.	51
TABLE 5.7. Arrhenius data for phthalic anhydride.	55

Page

TABLE 5.8. Effect of flow rate on the CO_2 formation from phthalic anhydride. 55

TABLE 5.9. Effect of light intensity on the CO_2 formation from phthalic anhydride. 59

TABLE 5.10. The actinometric results for dicarboxylic acids. 61

TABLE 5.11. Effect of pH on the CO_2 formation from malonic acid. 62

TABLE 5.12. Effect of pH on the CO_2 formation from succinic acid. 62

TABLE 5.13. Effect of pH on the CO_2 formation from adipic acid. 63

TABLE 5.14. Effect of irradiation time on the CO_2 formation from malonic,succinic and adipic acids. 70

TABLE 5.15. CO_2 volume to mole conversion for malonic acid. 73

TABLE 5.16. CO_2 volume to mole conversion for succinic acid. 75

TABLE 5.17. CO_2 volume to mole conversion for adipic acid. 77

TABLE 5.18. Effect of malonic acid concentration on the CO_2 formation. 80

TABLE 5.19. Effect of succinic acid concentration on the CO_2 formation. 81

TABLE 5.20. Effect of adipic acid concentration on the CO_2 formation. 81

TABLE 5.21. Effect of malonic acid concentration on the rate of CO_2 formation. 82

TABLE 5.22. Effect of succinic acid concentration on the rate of CO_2 formation. 82

TABLE 5.23. Effect of adipic acid concentration on the rate of CO_2 formation. 83

Page

TABLE 5.24. Rate constants and absorption equilibrium constants for acids. 83

TABLE 5.25. Effect of temperature on the CO_2 formation from malonic acid. 93

TABLE 5.26. Effect of temperature on the CO_2 formation from succinic acid. 93

TABLE 5.27. Effect of temperature on the CO_2 formation from adipic acid. 94

TABLE 5.28. Arrhenius data for malonic acid. 95

TABLE 5.29. Arrhenius data for succinic acid. 95

TABLE 5.30. Arrhenius data for adipic acid. 96

TABLE 5.31. Effect of light intensity on CO_2 formation from malonic acid. 103

TABLE 5.32. Effect of light intensity on CO_2 formation from succinic acid. 103

TABLE 5.33. Effect of light intensity on the CO_2 formation from adipic acid. 104

TABLE 5.34. Effect of light intensity on the rate of CO_2 formation for malonic acid. 105

TABLE 5.35. Effect of light intensity on the rate of CO_2 formation for succinic acid. 106

TABLE 5.36. Effect of light intensity on the rate of CO_2 formation for adipic acid. 107

TABLE 5.37. Postulated mechanism for dicarboxylic acids. 117

TABLE 6.1. Degradation percentages of dicarboxylic acids and phthalic anhydride. 121

LIST OF SYMBOLS

A	Acceptor
CB	Conduction band
D	Donor
e^-	Electron
E_{bg}	Bandgap energy
E_c	Conduction band energy
E_f	Fermi energy of the semiconductor
E_{rdx}	Fermi level of the solution
GC	Gas chromatography
h	Plank constant
h^+	Hole
IR	Infrared
k	Reaction rate constant
l	Path lenght
LD	Lethal dose
LH	Langmuir-Hinshlwood
n_{abs}	Number of absorbed photon
$N(CO_2)$	Total number of moles of CO2
OD	Optical density
SHE	Standard hydrogen electrode
t	Time
T	Temperature
TLV	Treshold limit value
VB	Valence band
VHS	Head space volume
VLP	Liquid phase volume
ε	Molar extinction coefficient
$\alpha(CO_2)$	Fraction of CO_2 in water
$\alpha(CO_3^-)$	Fraction of CO_3^- in water
$\alpha(HCO_3^-)$	Fraction of HCO_3^- in water
$\alpha(T)$	Correction term for CO_2 solubility
λ_{bg}	Bandgap wavelenght
ν	Frequency
Φ_λ	Quantum yield

I. INTRODUCTION

Biologically persistent and toxic organic compounds are present in waste waters as pollutants. They usually come from industrial manufacturers or even normal households. For the protection of the environment, these compounds have to be limited or decomposed into safe forms. Hence, during the last decade, studies have been focused on the semiconductor mediated photooxidative degradation of individual contaminants or families of compounds. This new approach, known also as photocatalytic mineralization, is an inexpensive but effective method of water treatment.

So far, TiO_2 suspended in aerated water has been proven as the most active photocatalyst with a bandgap of 3.2 eV. Absorption of light having energy greater than that of the band gap generates electron/hole pairs which, under the influence of the electric field, move into the conduction and valence bands respectively. It is the distribution of conduction band electrons, and valence band holes, which leads to various oxidation reduction processes.

Until recent years, extensive work has shown that many organic waste products could be completely mineralized on irradiated TiO_2 suspended in water. For example,highly toxic phenols and chlorophenols degraded to CO_2 and HCl in the presence of TiO_2 [1]. The complete degradation of 2-ethoxyethanol, a commonly used industrial solvent, and methyl vinyl ketone, an industrial pollutant found in waste water, can be efficiently carried out on irradiated TiO_2 [2]. Halogenated substrates have been decomposed successfully on irradiated semiconductor suspensions [3]. Extensive studies on the photocatalytic degradation of organo chlorine compounds known as carcinogenic, such as chloroethanes and chlorobenzenes have been carried out on irradiated TiO_2 suspensions [4]. Also,it has been reported that organophosphorus insecticides are efficiently degraded on suspended aqueous TiO_2, giving Cl^{-1}, PO_4^{-3}, H^+ and CO_2 as final products [5].

In this study, we have investigated photocatalytic degradation of phthalic anhydride and malonic, succinic and adipic acids as members of dicarboxylic acid family in the presence of TiO_2. These compounds were chosen as representatives of toxic pollutants. The aim of this work was to follow the possible decomposition of these compounds into CO_2. The disappearance of chemicals and the formation of intermediate products were not analyzed. In order to find the conditions for the highest yield of CO_2 formation, effects of various factors such as, catalyst concentration, pH, concentration of chemical, temperature, irradiation time, light intensity were investigated.

II. SEMICONDUCTORS

Heterogeneously dispersed semiconductor surfaces provide an environment to influence the chemical reactivity of a wide range of adsorbates and initiate light induced redox reactivity in these weakly associated molecules. Upon photoexcitation of several semiconductors, simultaneous oxidation and reduction reactions occur. The incident light that initiates this sequence is in a wavelength region (the visible or low energy range of the ultraviolet regions) absorbed by the semiconductor rather than by the substrate of interest. Furthermore, semiconductor particle that acts as the photocatalyst is stable to photolysis conditions and a large number of oxidative conversions can be attained without significant degradation of the semiconductor's redox capacity.

Initial interest in these photoinduced redox reactions was prompted by Fujishima and Honda's (1971) discovery that water could be simultaneously oxidized and reduced upon illuminating a TiO_2 electrode [7].

This observation produced extensive work focusing on the production of hydrogen (as a combustible fuel) from water as a means of solar energy conversion. It soon became apparent that redox reactions of organic and inorganic substrates could also be induced by bandgap irradiation of semiconductor particles.

The following section aims to give a summary about semiconductors.

2.1. Basic Principles of Semiconductors

By definition, a semiconductor has a band structure, roughly characterized as a series of energetically closed spaced energy levels associated with covalent bonding between atoms composing the crystallite (the

valence band) and a second series of spatially diffuse, energetically similar levels lying at higher energy and associated with conduction in the macromolecular crystallite (the conduction band) (Figure 2.1) [7].

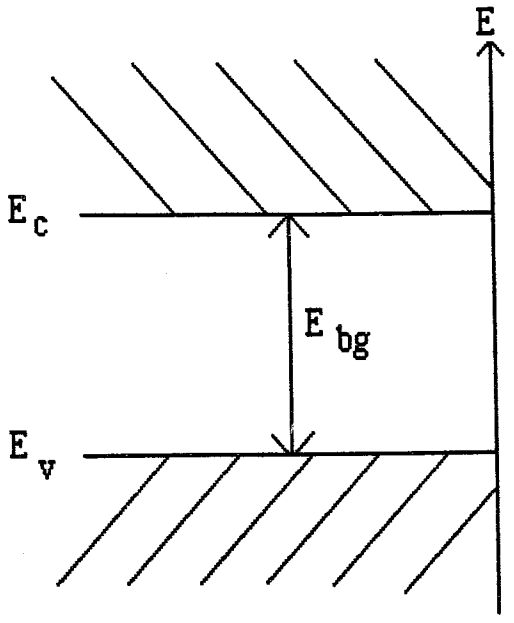

Figure 2.1. Energy band diagram for a semiconductor
E_c= lower edge of the conduction band; E_v= upper edge of the valence band; E_{bg}= bandgap energy.

If for a given solid, the valence band and the conduction band are separated by a gap devoid of energy levels, called the bandgap, the solid is either a semiconductor or an insulator.On the other hand, if these two bands overlap, then solid is a metal [8].

The magnitude of the fixed energy gap between the electronically populated valence band and the largely vacant conduction band governs the extent of thermal population of the conduction band (and hence the magnitude of the electrical conductivity of the particle) in its intrinsic (undoped) state.The bandgap also defines the wavelength sensitivity of the semiconductor to irradiation [7].

The bandgap energy (E_{bg}) is one of the primary determinants of the properties and behavior of the semiconductor electrode.It is defined as the

difference between the conduction and the valence band edges (Figure 2.1). The energy units for E_{bg} are electron-volts (eV) [8].

The bandgap energy distinguishes semiconductors from insulators. In general, solids with bandgap energies less than 3.5 eV are considered to be semiconductors, while insulators have bandgap energies larger than 3.5 eV.

Table 2.1 lists values of the bandgap energies and wavelengths for some important semiconductors.

Table 2.1. Bandgap energy and wavelength for some photochemically important semiconductors

Semiconductors	E_{bg} (eV)	λ_{bg} (nm)
SnO_2	3.5	350
TiO_2	3.2	390
CdS	2.4	520
GaP	2.3	540
GaAs	1.4	890
InP	1.3	950
Si	1.1	1130

2.2. Conduction and Charge Carrier Generation

In order for electrons to be mobile in a solid, they must be able to occupy a partially empty energy level within an energy band. In metals, empty levels are available immediately above the filled ones, and at room temperature it is easy for electrons to promote to the empty levels. However, in semiconductors and insulators, the filled energy levels are separated from the empty ones by the bandgap, i.e, a perfect semiconductor at absolute zero is a non-conductor [9].

Semiconductors can be made conductive either by putting extra electrons into the conduction band or by removing electrons from the valence band. Consequently, there are two modes of conduction in a semiconductor. The

first is the movement of electrons through the conduction band. The second mode is the electron flow in the valence band [9].

Mobile charge carriers can be generated by three different mechanisms.

Thermal Excitation Photo Excitation Doping

A) Thermal Excitation: If the bandgap energy is sufficiently small, thermal excitation can promote an electron from the valence band to the conduction band , (Figure 2.2 A), but this mechanism is important only for narrow bandgap semiconductors ($E_{bg} < 0.5$ eV).

B) Photo Excitation: An electron can be promoted from the valence band to the conduction band upon absorption of a photon of light. A necessary condition is that the photon energy exceeds the bandgap energy ($h\nu > E_{bg}$) (Figure 2.2 D).

C) Doping: Doping is the process of introducing new energy levels into the bandgap. It can be affected by either disturbing the stoichiometry of the semiconductor or by substituting a foreign element into the semiconductor lattice. Two types of doping can be distinguished.

When the doping entity is an electron donor and is located near the conduction band edge, then a large population of electrons is donated into the conduction band by thermal excitation.Electrical current is carried predominantly by negative charge carriers in the conduction band.The semiconductor is therefore called n-type (Figure 2.2 B).

p-type semiconductor is created when electron acceptors are near the valence band edge.Electrons are captured from the valence band, creating an excess population of positive charge carriers, holes (Figure 2.2 C).

Usually the electron donors and acceptors are neutral initially, and become charged due to loss or gain of an electron. These charged sites are fixed in the lattice [8].

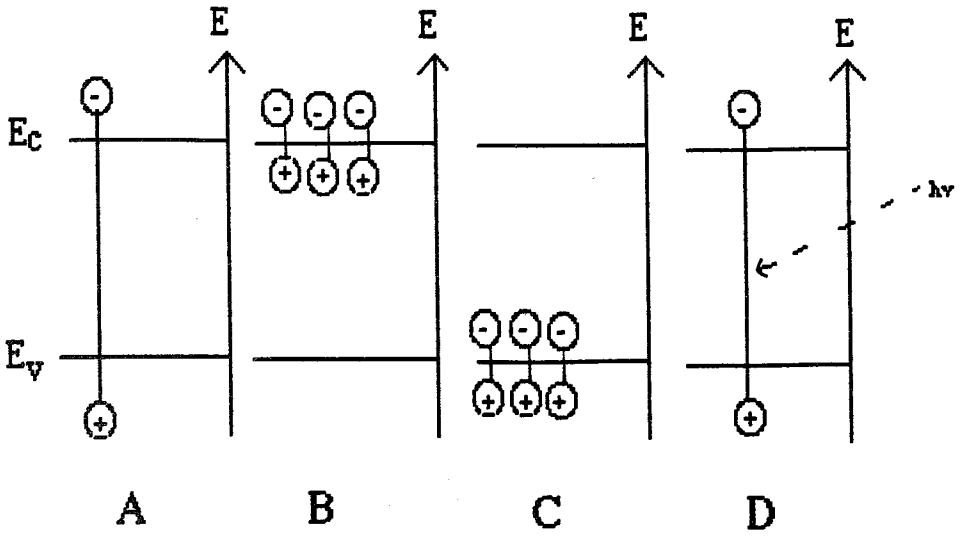

Figure 2.2. Mechanisms of charge carrier generation in a semiconductor. A: thermal generation; B: n-type doping; C: p-type doping; D: photoexcitation.

2.3. Fermi Level

The Fermi level is crucial in photoelectrochemistry since changes in the electrode potential correspond to changes in the position of the Fermi level with respect to a reference energy. By definition, the Fermi level is the energy E_f at which the probability of an energy level being occupied by an electron is exactly 1/2. In a semiconductor the Fermi level occurs in the bandgap. For an intrinsic (undoped) semiconductor E_f occurs approximately midway between the conduction and valence band edges (Figure 2.3).

Doping shifts the Fermi level with respect to band edges (Figure 2.3). The shift is consistent with the fact that the probability of occupancy of energy levels at E_c has increased; there are more electrons in the conduction band. Thus, the energy at which the probability equals 1/2 must be closer to E_c. Likewise, p-type doping shifts E_f nearer to E_v [9].

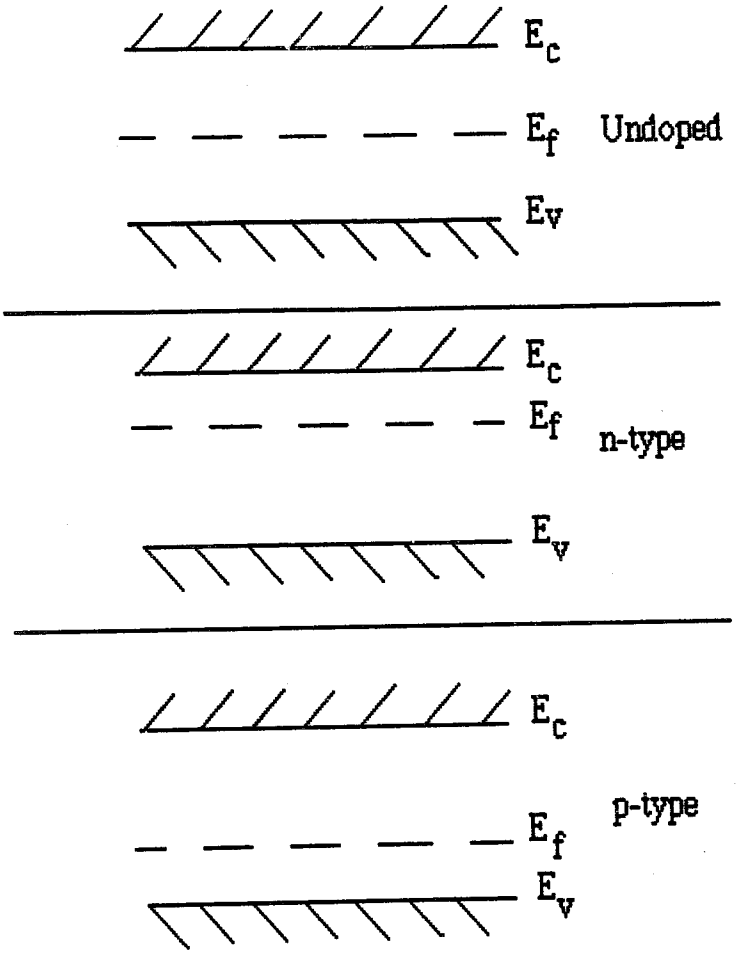

Figure 2.3- The Fermi level and the effects of doping.

2.4. Absorption of Light by Semiconductors

Photoexcitation with light of an energy greater than the bandgap promotes an electron from the valence band to the conduction band, creating an electronic vacancy or "hole" (h^+) at the valence band edge. The classical picture of a hole is that of a highly localized electron vacancy in the lattice of the irradiated semiconductor particle. This hole can be identified as a chemical entity. For example, a bound $O^{\bullet -}$ lattice radical or a surface associated $^{\bullet}OH$ radical in a metal oxide or an $S^{\bullet -}$ or $^{\bullet}SH$ radical in the substructure or a surface of metal chalcogenide. This hole can initiate further interfacial electron transfer or other chemical reactions to an adsorbate or, with the surface bound $^{\bullet}OH$ radical.

The photogenerated electron (e^-) relaxes thermally to the conduction band edge (and the hole to the valence band edge). The electrons which have a mobility at least $1x10^4$ m^2/V, are rapidly trapped through equilibrium localization at a trap, followed
by eventual recombination with a photogenerated hole at the semiconductor surface. Appreciable negative charge can be built up on a particle in the absence of an appropriate acceptor [10].

2.5. Semiconductor/Electrolyte Interface

Unlike metals, semiconductors lack a continuum of interband states to the recombination of the electron-hole pair. This assures an electron-hole pair lifetime sufficiently long to allow these species to participate in interfacial electron transfer Thus, the act of photoexcitation usually generates an electron-hole pair poised respectively at the conduction band and valence band edges (eq.2.1). The components of this activated pair, when transferred across the interface, are capable, respectively, of reducing and oxidizing a surface-adsorbed substrate, forming on a common surface a singly oxidized electron donor and singly reduced electron acceptor (eq.2.2 and 2.3).

$$\text{Semiconductor} \longrightarrow e^- + h^+ \quad (2.1)$$

$$h^+ + D \longrightarrow D^{\cdot+} \quad (2.2)$$

$$e^- + A \longrightarrow A^{\cdot-} \quad (2.3)$$

When the semiconductor is in contact with an electrolyte containing a redox couple, the Fermi level of the semiconductor moves to equilibrate with the potential of the redox couple. Contact between the semiconductor and the electrolyte establishes a Schottky barrier. The electric field of this Schottky barrier induces spatial separation between e- and h+ by driving the photogenerated e- and h+ in opposite directions, causing the bands to bend at the solid-liquid interface. The Fermi level of the semiconductor then moves to equilibrate with the potential of the redox couple. Charge carriers are driven to surface trapping sites either by diffusion or by migration induced by the space-charge gradient (Figure 2.4, Figure 2.5)

If a photogenerated hole reaches the surface of the semiconductor, it can react with an adsorbed substrate by interfacial electron transfer, assuming that the adsorbate possesses a redox potential appropriate for a thermodynamically allowed reaction. Thus, an adsorbed electron donor can be oxidized by transferring an electron to a photogenerated hole on the surface, and an adsorbed acceptor can be reduced by accepting an electron from the surface. Hole trapping generates a cation radical, $D^{\cdot+}$ (eq 2.2), and an electron trapping generates an anion radical, $A^{\cdot-}$ (eq.2.3) (Figure 2.6).

These radical ions can participate in several pathways: 1) They may react chemically with themselves or other adsorbates 2) They may recombine by back electron transfer to form the excited state of one of the reactants or to waste the excitation energy by a nonradiative pathway. 3) They may diffuse from the semiconductor surface and participate in chemical reaction in the bulk solution. If the rate of formation of $D^{\cdot+}$ is kinetically competitive with he rate of back electron transfer, photoinduced oxidation will occur for any molecule with an oxidation potential less positive than the semiconductor valence band edge. By similar considerations, the photoinduced reduction can occur to any molecule possessing a reduction potential less negative than the conduction band edge [7].

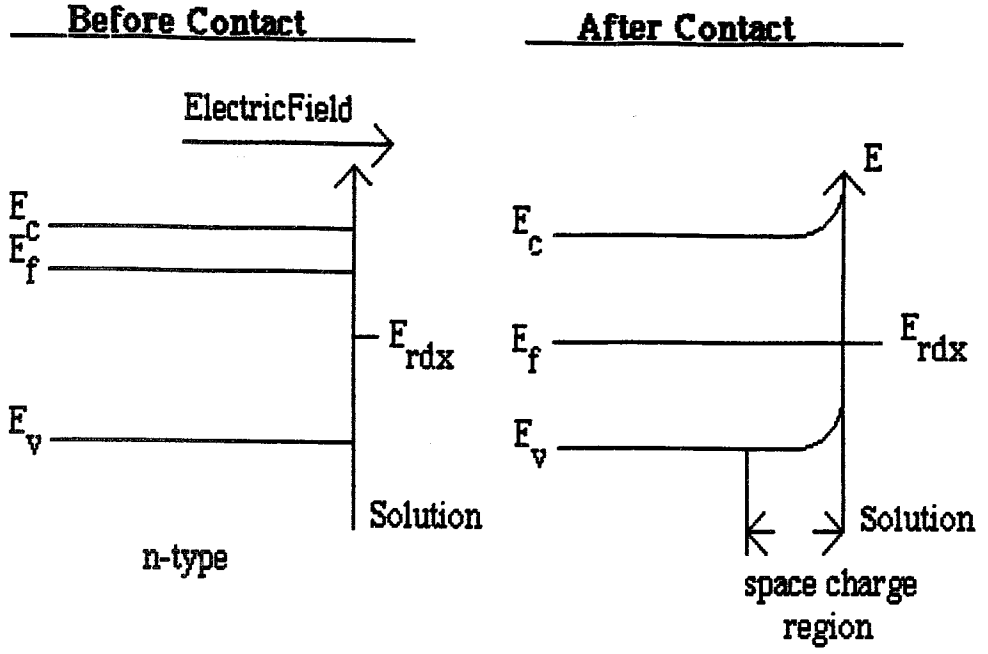

Figure 2.4. Formation of space charge region in solution for an n-type semiconductor.

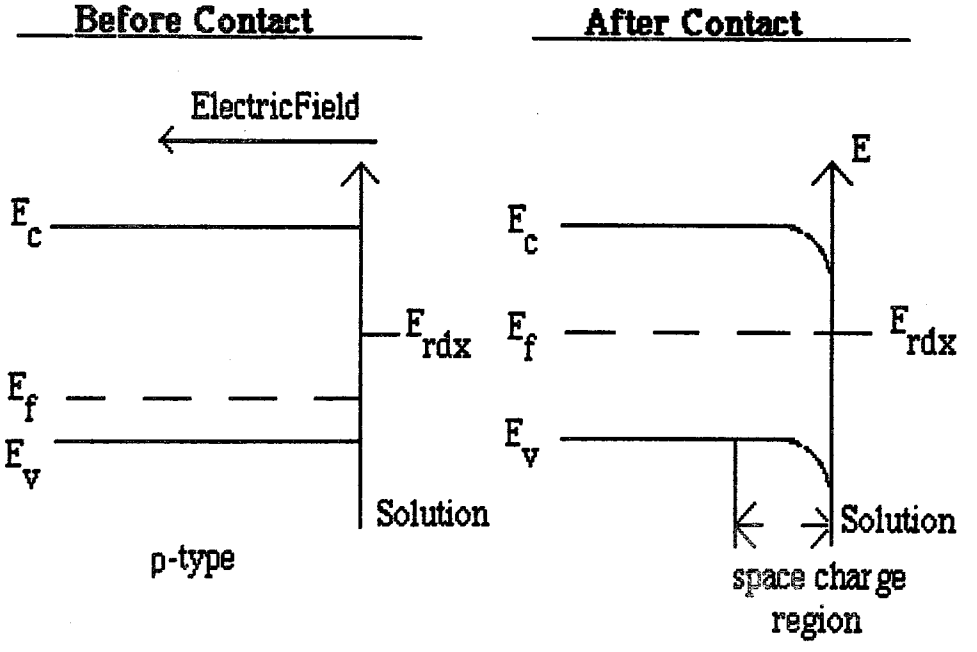

Figure 2.5. Formation of space charge region in solution for a p-type semiconductor.

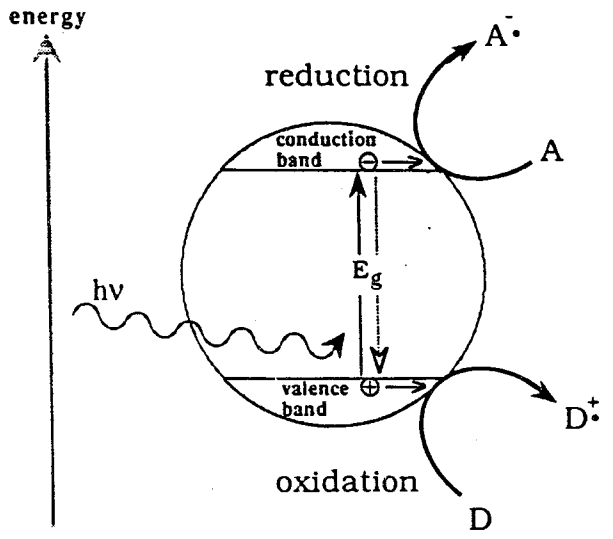

Figure 2.6. The semiconductor particle as a redox catalyst.

2.6 Carrier Trapping

In order for photocatalysis to be productive chemically, electron-hole pair recombination must be suppressed. This can be accomplished by trapping either the photogenerated electron or the photogenerated hole.

Hole trapping is usually achieved by the use of degradable adsorbates or a sacrificial reagent. For example, triethylamine and hydroquinone have been used successfully as sacrificial electron donors in CdS mediated photoreductions, functioning as hole traps so that the conduction band electron can be transferred more slowly without significant electron-hole recombination.

Electron trapping similarly suppresses electron-hole recombination. Adsorbed oxygen serves as a trap for the photogenerated conduction band electron in many heterogeneous photocatalytic reactions [11]. It is often found that photocatalytic activity is nearly completely suppressed in the absence of

oxygen, possibly because of back interfacial electron transfer from active species present on the photocatalyst surface. The resulting species, superoxide O_2^-, is highly active and can attack either organic molecules or adsorbed intermediates or, after protonation, can provide another source for surface-bound hydroxyl radicals.

2.7. Photocatalytically Active Semiconductors

Because of their resistance to photocorrosion, wide bandgap metal oxides have found greatest utility in heterogeneous photocatalysis. Metal chalcogenides such as CdS and CdSe have narrower bandgaps, making them sensitive to incident light in the visible spectrum. With these semiconductors, however, photocorrosion is significant. Hematite (α-Fe_2O_3), for example, is absorptive in the visible region, but shows much lower photocatalytic activity than does TiO_2 or ZnO, probably because of corrosion or the formation of short-lived metal-to-legand or legand-to-metal charge transfer states [12].

The most commonly studied photocatalysts are TiO_2, ZnO, and CdS. Because of its high photocatalytic activity, titanium dioxide has become the benchmark photocatalyst against which photocatalytic activity is measured. SnO_2 and WO_3 demonstrate much lower levels of photoactivity. Although cadmium sulfide is not as photoactive as TiO_2, it has been extensively studied because of its good spectral response to wavelengths of the solar spectrum. Like ZnO, CdS suffers from photocorrosion.

$$CdS + 2\,h^+ \longrightarrow Cd^{+2} + S \qquad (2.4)$$

$$ZnO + 2\,h^+ \longrightarrow Zn^{+2} + 1/2\,O_2 \qquad (2.5)$$

These competing reactions lead to depressed photoactivity and the release of sometimes dangerous metal ions (e.g.,Cd^{+2}) into solution [7].

III. TITANIUM DIOXIDE: A PHOTOSENSITIVE SEMICONDUCTOR

Titanium is very widely distributed in the earth's crust, comprising 0-58 per cent of all terrestrial matter and standing ninth in order of abundance of the elements. It is a constituent, generally in minor proportions, of almost all igneous rocks, is widely distributed in soils and clays, and has been detected in peats, ashes of certain coals and woods, and in the bones of man and animals.

The element titanium does not occur free in nature, but it forms a number of oxides, the most important being the dioxide, TiO_2. Titanium bearing minerals include ilmenite $FeTiO_3$, perovskite $CaTiO_3$, titanite (sphene) $CaTiSiO_5$, and titaniferous magnetite.

A brief review of the composition, occurrence and different properties of TiO_2 is given below.

3.1. Composition And Occurrence

Titanium dioxide contains not less than 99 percent and not more than 100.5 percent O_2 calculated on the dry basis [13]. The theoretical composition of the oxide is titanium 60 percent, oxygen 40 percent. It contains Iron, Columbium and Tantalum in important amounts; Tin, Chromium and Vanadium have also been reported [14].

Titanium dioxide is polymorphic and occurs naturally in three crystalline modifications as the minerals rutile, anatase, and brookite. By far the most abundant in nature, rutile crystallizes in the tetragonal system, is usually prismatic. Anatase is also tetragonal and usually appears as octahedra. Brookite, the rarest and least important modification, is orthorhombic. Rutile is the thermostable modification, and on heating anatase at high temperatures

transformation to rutile occurs. Anatase and rutile differ in their surface area, the state of surface hydration and hydroxylation, surface crystallinity, surface charge caused by an excess of cations or anions on the surface, and the presence of dopants and impurities.

3.2 Properties And Uses

TiO_2 is stable thermally and resistant to chemical attack. On drying at 105°C for three hours it loses not more than 0.5 percent of its weight [13]. It loses a small amount of oxygen when heated strongly in vacuum. It is inert to most acids and alkalis. Chlorination is possible only if a reducing agent is present. The oxide is soluble in boiling $(NH_4)_2SO_4$ plus concentrated H_2SO_4, in the proportions 5 5 g + 8 g + 20 ml H_2O [15]. It is also reported to be more soluble in a solution of NaF than in H_2O.

TiO_2 owes its importance as a pigment chiefly to its uniquely high hiding power and whiteness, and these in turn depend on three main properties:
1) refractive index; 2) particle size; 3) absence of undesirable impurities [16].

TiO_2 pigments find their greatest use in paint and allied products, although they are used in almost every pigment consuming industry, notably rubber, vitreous enamelling, paper, linoleum, plastics, textiles and leather. In paints the desirable properties of titanium dioxide pigments are extreme opacity and consequent economy in use, good whiteness, chemical inertness, and non-toxicity.

Another property of TiO_2 arouse interest when in the 1950's Renz showed that TiO_2 becomes markedly photosensitive, in the presence of certain organic liquids and reducing solutions. Since then, the ability of TiO_2 to mediate photoelectrochemical reactions in solution has been explored. It has been shown that particulate suspensions and colloidal dispersions of TiO_2 act as photocatalysts for a number of reactions. Many aspects of the photoelectrochemistry of the oxide have been investigated with the main interest focused on the establishment of charge transfer mechanisms, the development of radiant energy converts to the electrical and/or chemical energy, and the development of functional devices.

3.3. Photocatalytic Activity Of TiO_2

TiO_2 is an n-type semiconductor, and it is the presence of physical defects that causes semiconductivity of the oxide to appear. These imperfections introduce quantum levels in the energy gap between the valence and conduction band edges [17]. Two types of paramagnetic defects involving Ti^{+3} were identified by E.S.R. spectra on the surface of titania. In the first type of defects, these ions are either in normal or in interstitial positions. In the second type, Ti^{+3} ions are associated with one or two oxygen vacancies [18]. More recently, evidence for the presence of Ti^{+2} species was obtained by photoelectron spectroscopy investigations of a titanium surface.

An additional photolysis effect is the ejection of oxygen from the crystal lattice, leaving Ti^{+3} defect; reoxidation to Ti^{+4} in the absence of a redox couple by molecular oxygen, occurs readily [19]. Light absorption takes place predominantly in a layer of a few hundred A° inside the solid and the transport of the excitation to the surface occurs in a second step creating positive holes and electrons [20]. The above leads to the conclusion that sites do not preexist on a surface, but are produced on contact between the solid and the light [21].

When the semiconductor absorbs light, an electron from the valence band (the ground electronic state) moves to the conduction band (the excited state). For the anatase form of TiO_2 this requires photons having energies greater than 3.2 eV (about 380 nm). The resulting hole (electron vacancy in the valence band) and electron in the conduction band serve as oxidizing and reducing sites, respectively. Each is characterized by a reduction potential in volts relative to the NHE, which is defined as 0.0 V (Figure 3.1). Relevant reduction potentials for couples in the water oxygen system are also shown in Figure 3.1 [22].

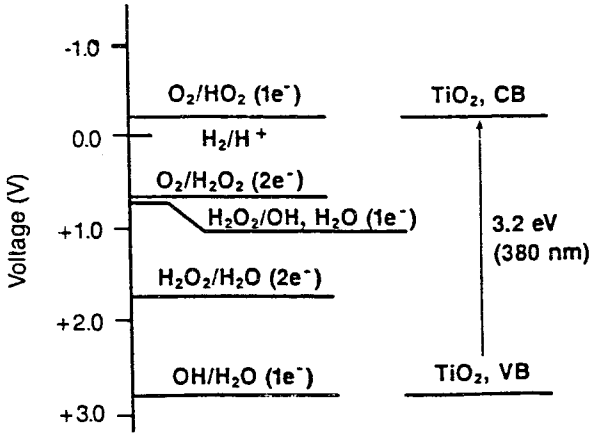

Figure 3.1. Relevant reduction potentials for couples in water/oxygen system

It is thermodynamically favorable for the hole site in the valence band of TiO_2 to oxidize water to hydroxyl radical and for the conduction band electron to reduce either oxygen or hydrogen peroxide at -0.13 and +0.71 V, respectively [20]. Oxidation and reduction reactions both must occur in order to maintain charge neutrality in the semiconductor particle. Figure 3.2 shows a simplified picture of generation of primary radicals at the surface of irradiated TiO_2.

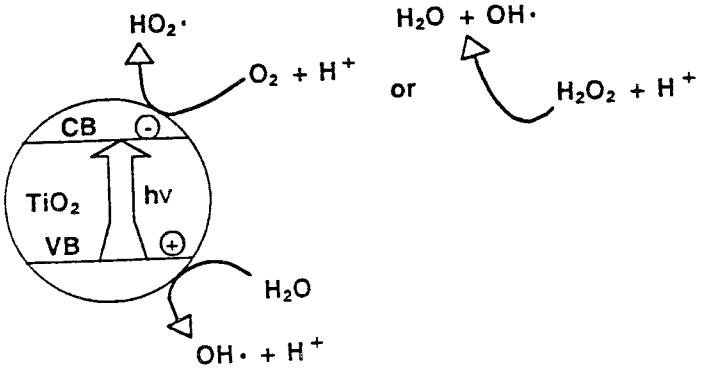

Figure 3.2. Generation of primary radicals at the surface of irradiated TiO_2 particles in water

The reactions that occur in the TiO_2/ H_2O/ O_2 organic compound system, summarized in Table 3.1, can be placed in three categories. The first includes productive reactions which convert the electrons and holes produced on the semiconductor particle to active chemical species.The second group includes the steps that destroy the organic contaminant. The third group are reactions that consume the hydroxyl radicals in non-productive ways. It is desirable to maximize the efficiency of the reactions in the first two categories and to minimize the third category of reactions [22].

The first event in the photocatalytic process is the absorption of a photon to produce the electron-hole pair on a particle. The electron in the conduction band can be removed by reaction with hydrogen ion (H^+), O_2 or H_2O_2. The hole in the valence band can react with surface-bound water or hydroxide groups (OH^-) to give the $OH^{\cdot}$ radical (Figure 3.3) [23].

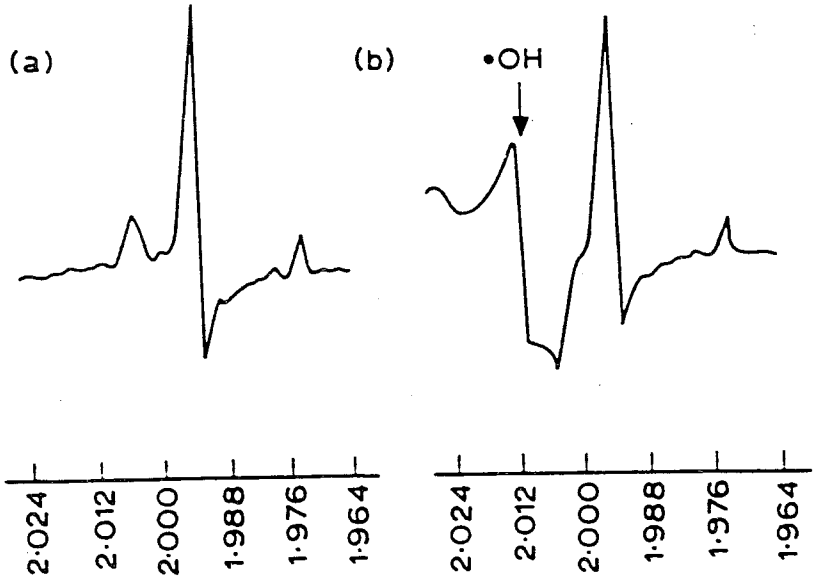

Figure 3.3. ESR signal of hydroxyl radical observed during UV irradiation of anatase TiO_2/water: a) before irradiation and b) after irradiation

Once formed, the hydroxyl radical can react with the organic contaminant to initiate a sequence of reactions. After formation of the initial organic radical, breakdown may occur via reaction with oxygen or water.

The third set of reactions that consume hydroxyl radical in non-productive ways. These include the recombination of the hydroxyl radical with the conduction band electron and the reaction of two hydroxyl radicals to give hydrogen peroxide. The perhydroxy radical $HO_2^{\cdot}$ formed in the reaction of O_2 with electron can consume hydroxyl radical.

Additional pathways for loss of hydroxyl radical are possible when the water to be treated contains significant levels of dissolved carbondioxide in the form of carbonate or hydrogen carbonate ions. These species can react with hydroxyl radical as shown in Table 3.1. Oxidizable metal ions can also provide loss pathways which may be amplified if they can participate in cyclic oxidation-reduction reactions.

Table 3.1. Radicals formed on irradiated TiO_2 and their reactions.

Electron/hole pair formation	Electron removal
$TiO_2 \xrightarrow{hv} e^- + h^+$	$e^- + O_2 + H^+ \longrightarrow HO_2^{\cdot}$ $e^- + H_2O_2 + H^+ \longrightarrow OH^{\cdot} + H_2O$

Destruction of organic compounds	Nonproductive radical reactions
e.g:([22]) $Cl_2C{=}CHCl + OH^{\cdot} \longrightarrow Cl_2C(OH){-}\dot{C}HCl$ $Cl_2\dot{C}CHCl(OH) + (O_2, H_2O_2, ..) \longrightarrow CO_2 + HCl + H_2O$	$e^- + OH^{\cdot} + H^+ \longrightarrow H_2O$ $2OH^{\cdot} \longrightarrow H_2O_2$ $2HO_2^{\cdot} \longrightarrow H_2O_2 + O_2$ $HO_2^{\cdot} + OH^{\cdot} \longrightarrow H_2O + O_2$ $HCO_3^- + OH^{\cdot} \longrightarrow CO_3^{-2} + H_2O$ $M^{+3} \xrightarrow{e^-} M^{+2}$

3.4. Surface Analysis Of TiO_2

Most metal oxides are hydroxylated under normal conditions, i.e, at room temperature and when water or its vapor has had access to the surface [24]. The reason for this hydroxylation is that a surface of an ionic crystal is more stable when it preserves its electroneutrality.

Titanium dioxide surfaces are covered with surface hydroxyls of an amphoteric character. How the adsorption of water leads to the formation of hydroxyls on the anatase single crystal surface is shown in Figure 3.4.

Chemisorption of water molecules on the surface Ti^{+4} ions is expected since vacant coordination sites would be filled. However, proton transfer to neighboring oxide ions should result in better charge neutralization. For anatase, approximately 40 percent of the surface is hydroxylated [25].

In the model of Figure 3.4 B, two types of hydroxyl groups can be identified: terminal, in which the OH is bonded to a single Ti atom, and a bridging, in which the OH is shared by two Ti atoms [24]. The doubly-coordinated OH groups should be strongly polarized by the cations, thus loosening the bond to hydrogen and resulting in acidic character. The acidic character should be much weaker with the singly-coordinated OH groups, and one would expect a tendency for dissociation as hydroxide ions. These groups should be predominantly basic in character and might be exchangeable for other anions.

Depending upon the pH, these surface groups may add or abstract protons. Therefore, it can be said that surface nature of TiO_2 is pH dependent [26]. The corresponding acid-base equilibria can be written as follows:

$$Ti^{IV}\text{-}OH + H^+ \longrightarrow TiOH^{2+} \qquad (3.1)$$

$$TiO^- + H^+ \longrightarrow TiOH \qquad (3.2)$$

At pH<6 TiO_2 surface accumulates a net positive charge due to the increasing fraction of total surface sites present as $TiOH^{2+}$. At high pH, the surface has a net negative charge due to a significant fraction of total surface sites present as TiO^- [27].

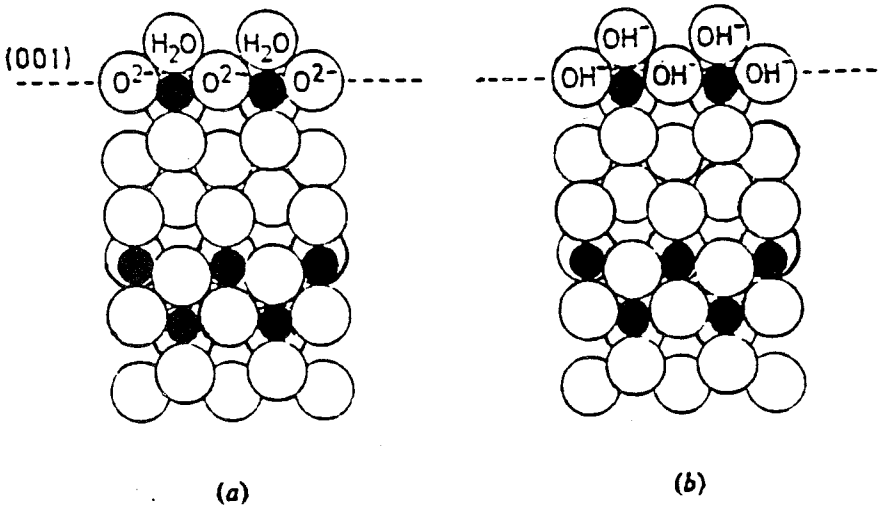

Figure 3.4. Formation of surface hydroxyls on the anatase TiO_2 surface: a) coordination of Ti^{+4} ions by water molecules ; and b) the formation of surface hydroxyl ions by proton transfer from water. (● : Ti^{+4})

The influence of electrostatic interactions between the charged surface of the photocatalyst and charged reactants has been investigated for the photocatalytic degradation of trichloroacetate and chloroethylammonium chloride on TiO_2 at various pH values.

In the examined pH range trichloroacetate was dissociated and therefore negatively charged, while the chloroethylammonium ion is positively charged. The rate of degradation of trichloroacetate was found to be high at low pH when the TiO_2 surface is positively charged while it approached zero at pH>6. On the other hand, the rate of degradation of the chloroethylammonium cation was zero at pH 3 and reached a maximum around pH 8 when catalyst surface is negatively charged [26].

Figure 3.5 shows the surface composition of a TiO_2 particle in aqueous medium at various pH values [26].

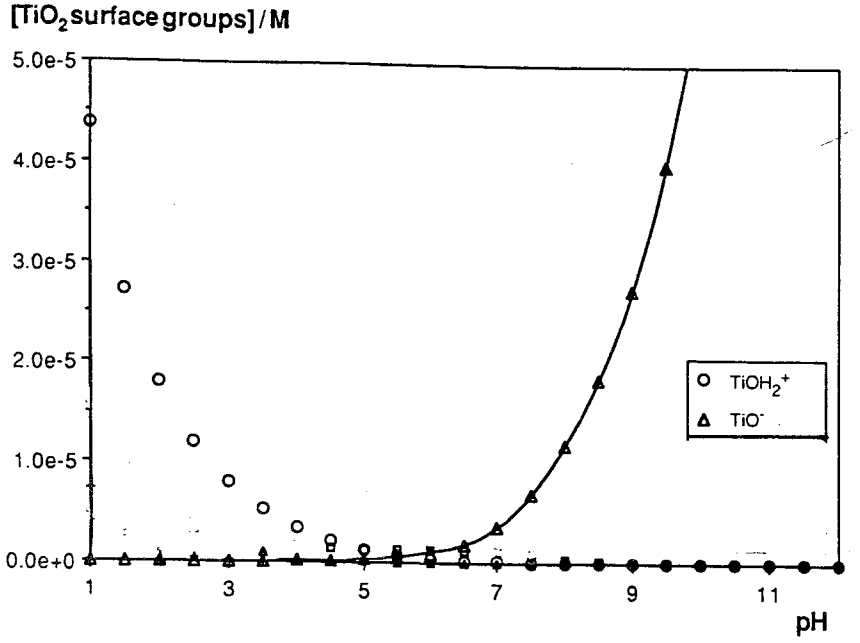

Figure 3.5. Relevant groups present on the TiO_2 surface in aqueous solution as a function of pH.

3.4.1. Adsorption Effect

The importance of substrate adsorption on the TiO_2 surface can be explained by the use of the Langmuir-Hinshelwood (LH) kinetic model [7]. This model assumes that:

1) at equilibrium, the number of surface adsorption sites is fixed;
2) only one substrate may bind at each surface site;
3) the heat of adsorption by the substrate is identical for each site and is independent of surface coverage;
4) there is no interaction between adjacent adsorbed molecules;
5) the rate of surface adsorption of the substrate is greater than the rate of any subsequent chemical reactions;
6) no irreversible blocking of active sites by binding to product occurs [7].

Assuming that the adsorption equilibrium follows a Langmuir isotherm, then surface coverage, θ is related to the initial concentration of the substrate and the adsorption equilibrium constant κ as follows:

$$\theta = \kappa C/(1+\kappa C)$$

Then, LH kinetic rate expression becomes:

$R = dC/dt = k(\kappa C)/1+\kappa C$

where C is the initial concentration of the substrate,and k is the reaction rate constant. The linearity of a plot of 1/R versus 1/C, where 1/k is the y intercept and $1/\kappa k$ is the slope, indicates that the LH model is valid [7].

3.4.2 Infrared Spectroscopy Of Hydroxylated TiO_2

The most important technique used to identify the nature of the surface hydroxyls on TiO_2 is FTIR spectroscopy [23].

The IR spectra show two distinct groups:

(A) The group at 3000-3700 cm^{-1} contains distinct peaks at 3420, 3632, 3647, 3659 and 3676 cm^{-1} (Figure 3.6) and shoulders at 3614, 3639, and 3728 cm^{-1}, which can be attributed to OH stretching vibrations of free and hydrogen-bonded surface OH groups (chemisorbed water).

(B) The group at 1200-1700 cm^{-1} containing peaks at 1361, 1454, 1624, 1585 and 1622 cm^{-1}, which can be assigned to physically adsorbed water (H-O-H bending).

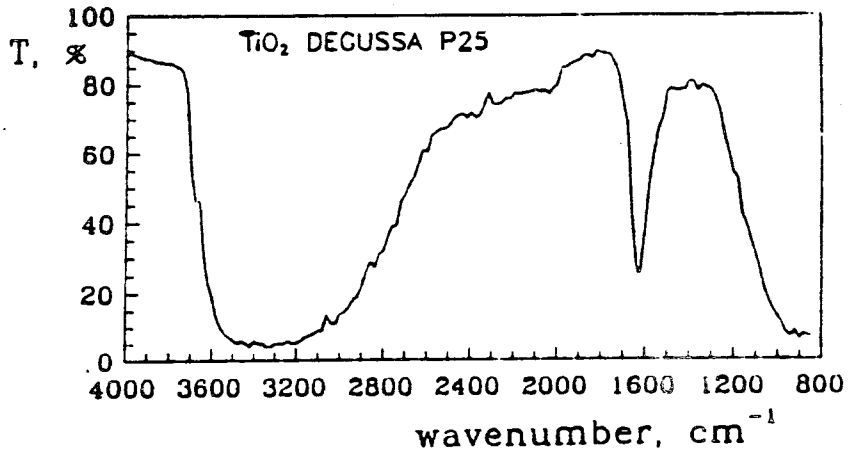

Figure 3.6- IR spectrum of original Degussa P-25 without any treatment (pressed between two KBr pellets) [29].

IV. EXPERIMENTAL

4.1. Properties of the Photocatalyst

Most commercial semiconductor samples exhibit photocatalytic activities that can vary from one batch to another [30,31] because surface characteristics are influenced by physicochemical features determined by the catalyst's origin and preparation. Among the variables which alter photocatalytic activity are surface area (roughness), surface crystallinity, surface charge, the state of surface hydration, annealing pretreatment, and the presence of dopants and impurities.

The titanium dioxide which has a BET surface area of 50 m^2/g and an average particle size of 30 nm was Degussa P25 grade. It was shown by X-ray diffraction analysis that the material used in the experiment is predominantly in the anatase form. Table 4.1 lists some specifications of TiO_2 used in this work [32].

4.2. Reagents and Sources of Light

4.2.1. Reagents

All chemicals (Table 4.2) that were used in the experiments were of laboratory reagent grade and they were used without further purification.

4.2.2. Sources of Light

TiO_2 has a bandgap energy of 3.2 eV which corresponds to a wavelength of 380 nm. Anatase absorption is given in Figure 4.1.

Table 4.1. Physicochemical data of TiO_2 (Degussa P-25).

Appearance	Fluffy white powder
Compacted apparent density	Appr 150 (g/L)
Moisture(2 hrs at 105°C)	< 1.5%
Ignition loss(2 hrs at 1000°C)	< 2.0%
SiO_2	<0.2%
Al_2O_3	<0.3%
Fe_2O_3	<0.01%
TiO_2	>99.5%
HCl	<0.3%

Table 4.2. Reagents.

Name	Formula	Molecular Weight (g/mole)	Supplier	% Purity
Adipic Acid	$C_6H_{10}O_4$	146.14	Eastman org.chem.	—
Malonic Acid	$C_3H_4O_4$	104.06	Merck	99
Succinic Acid	$C_4H_6O_4$	118.09	Merck	99.5
Phthalic Anhydride	$C_8H_4O_3$	148.12	Fisher	100
Perchloric Acid	$HClO_4$	100.46	Merck	70
Sodium Hydroxide	NaOH	40.00	Merck	98

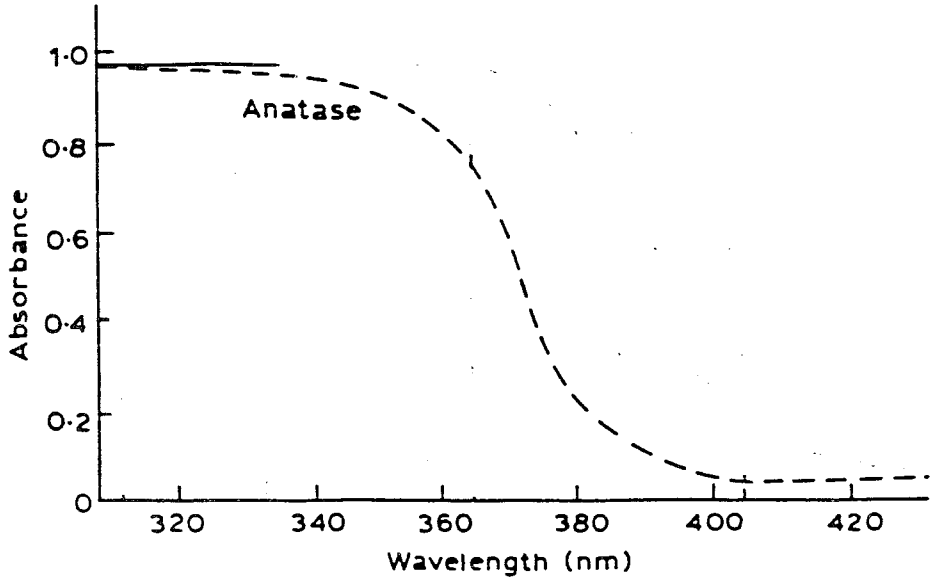

Figure 4.1. Anatase absorption.

Wavelength < 400 nm is necessary to produce the reactions considered.

The light source was 20W black light fluorescent lamp (General Electric F 20 T 12/BLB) that provides light of wavelength 320-440 nm. Its emission spectrum is given in Figure 4.2 [37]. The inside wall of the lamp is coated with a fluorescent substance which emits in a broad band around 365 nm.

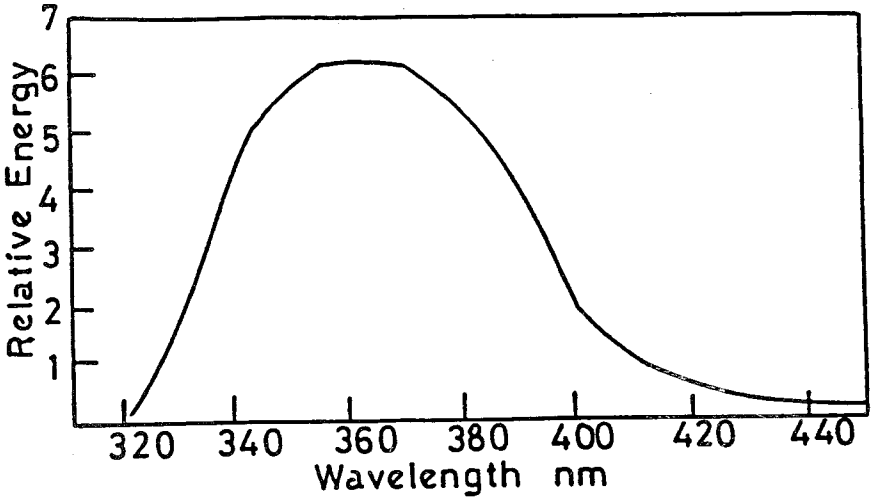

Figure 4.2. Emission spectrum of a black light fluorescent lamp.

By comparing Figure 4.1 and Figure 4.2, it can be seen that the lamp emits in the region of maximum absorption of the catalyst. Actinometric measurement of light intensity is given in a later section.

4.3. Sample Preparation

Deionized water was used in all solutions. Stock solutions of phthalic anhydride and dicarboxylic acids were prepared as $1x10^{-3}M$ in their natural pH's. Phthalic anhydride and dicarboxylic acid suspensions were prepared in the same way, a known volume of phthalic anhydride or dicarboxylic acid was mixed with the catalyst, TiO_2 as being 1 g/L. Sonicator was used to ensure the uniform mixing of the suspensions for about ten minutes before being added into the reactor. Solutions were kept in dark or wrapped with Al foil in order to prevent any interference from surrounding light before irradiation. The pH values of the reaction solutions were adjusted by adding $HClO_4$ or NaOH. H_2SO_4, HCl and H_3PO_4 were not used to adjust the pH of solutions because inorganic anions, sulfate in the case of sulfuric acid, chloride in the case of hydrochloric acid, and phosphate in the case of phosphoric acid are rapidly adsorbed by the catalyst and reduce the observed oxidation rate of organic compounds [7]. These observations suggest that inorganic anions may compete with the organic substrate for surface active sites or can form a highly polar environment near the particle surface, thus blocking the diffusion or organic to the active site. But perchlorate and nitrate had very little effect on the photooxidation rates.

A digital pH meter (Orion SA520) was used to measure the pH of the reaction solution.

4.4. Phthalic Anhydride

Phthalic anhydride is the principle commercial form of phthalic acid. The worldwide production capacity was $1.36x10^6$metric tons in 1976. It is

mainly used as intermediate for phthalic plasticizers, paints, polyester resins, dyes, pharmaceuticals, perfumes and analytical reagents.

Phthalic anhydride is a severe irritant to the eyes, respiratory tract, and skin and especially to moist tissue. If in contact with the skin for a significant amount of time, the solid may burn the tissue. Repeated exposure may result in asthma, irradiation of the mucous membranes, and diseases of the respiratory and digestive organs [36].

Table 4.3. Properties of phthalic anhydride [36].

mol.wt.	148.12
mp,°C	131
sp. gr.	1.53
Solubility	0.69 g /100 g (In water at 25°C)
TLV	2 mg/L
LD_{50}	4 g/kg (In rat)

It should be taken into account that the complete photooxidation of phthalic anhydride proceeds according to the following equation:

$$C_8H_4O_3 + 15/2O_2 \longrightarrow 8CO_2 + 2H_2O \qquad (4.1)$$

4.4.1. Reactor

Four black light fluorescent lamps combination were used for the experiments.

The experiments were conducted with two different photocatalytic reactors. The first reactor was containing two parts: a Pyrex glass tube (7.2 cm in outer diameter and 39 cm in length) positioned parallel to the lamps, and an erlenmeyer flask (250 mL) mixed with a magnetic stir bar (Figure 4.3). The two parts of the reactor were connected by Tygon tubing and the contents circulated continuously with a Cole Palmer Standard Servodyne Peristaltic Pump at a flow rate of 144 mL/min. All samples were obtained through the mouth of the erlenmeyer flask, which was tightly closed with a

glass stopper on which a Mini Valve was attached. Experiments , performed by using this reactor, were all at room temperature. Under equilibrium conditions, the ratio of the liquid volume in the erlenmeyer flask to that in the glass tube was approximately 2:1.

In order to investigate the temperature effect, a second reactor was used. It was made out of a borosilicate glass (Pyrex) tube of 36.2 cm length and 13 cm outer, 3.5 cm inner diameters. It contained an inner glass tube with a thickness of 2 cm (Figure 4.4). The temperature of the system was controlled by a Julabo F40 Ultratemp 2000 water circulator connected to the inner glass tube. The suspension was contained in the annulus between the two tubes. A sintered glass disk placed at the bottom of the reactor which provides circulation of air,to prevent the settlement of the suspension. There were two sampling ports: a gas and a liquid sampling port. The gas sampling port, a Mini Valve, attached to a glass stopper (12.4 cm length, 4 cm inner diameter (below), 1.2 cm inner diameter (above)) on top of the reactor. The glass stopper was connected to the pump in order to allow the gas to recycle continuously through the reactor. The liquid sampling port was a glass outlet pipe (26.2 cm below the mouth, 7.8 cm above the bottom part of the reactor) connected to the reactor

4.4.2. Analysis

Gas samples were taken from the gas sampling port and injected to the gas chromatograph (Gow Mac) fitted with a column packed with Porapak N and thermal conductivity detectors. The carrier gas was helium at a flow rate of 60 mL/min. Other analytical conditions are given in Table 4.4. Flow rates were measured using a soap bubble flow meter and a stopwatch. The GC was calibrated by the addition of known volumes of CO_2 to the photochemical reactor under the identical conditions with the experiments. The gas recycling rate in both reactors was held constant at 144 mL/min [37] in all experiments and calibrations. In Figure 4.5 calibration curve for CO_2 at different pH values are given. The values in the curves were corrected for the blank values of CO_2.

A Shimadzu C-R3A Chromatopac recorder-integrator was used to investigate the peak areas automatically. All parameters of the chromatopac recorder-integrator were kept constant in all analysis. The chart speed was

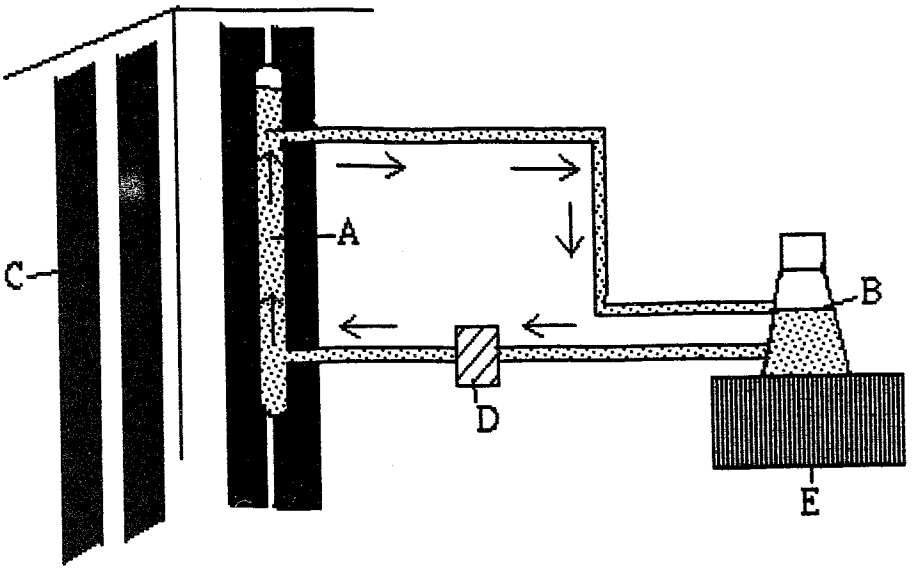

Figure 4.3. Reactor I.

A:Tube;
B:Erlenmeyer flask;
C:Lamps;
D:Pump;
E:Magnetic stirrer.

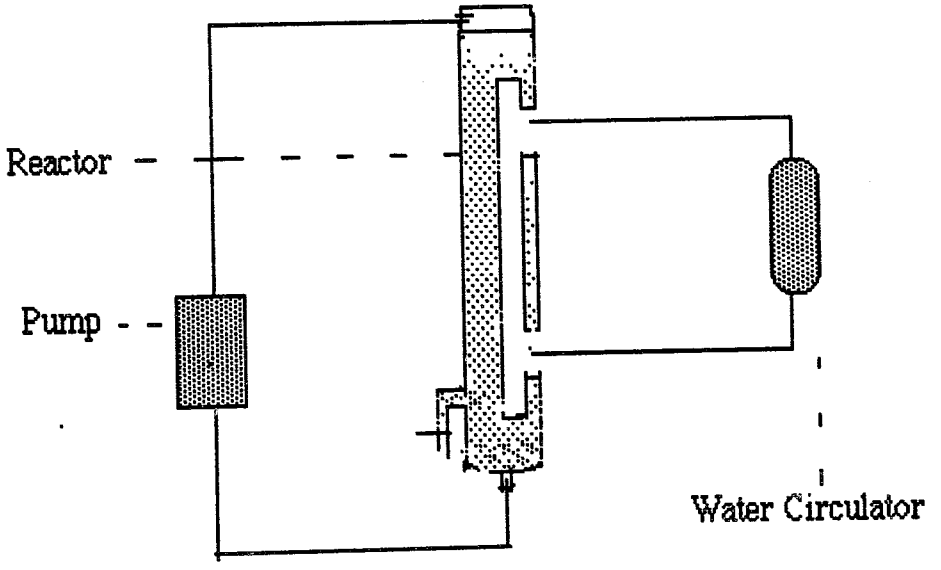

Figure 4.4. Reactor II.

10 mm/min. The minimum peak area to be detected was set at 100 counts, since a lower setting caused too many unwanted noise signals.The slope was set at 20 mV/min. The instrument automatically calculated a slope value according to the noise level. When noise level was high, the automatic slope setting was also high. Therefore, it was decided to set the slope at a constant value.

Table 4.4. GC Conditions.

Helium Pressure	10 kg/cm^2
Helium Flow Rate	60 ml/min
Injection Port Temperature	160°C
Column Temperature	110°C
Detector Temperature	220°C
Bridge Current	200 mA
Retention Time for:	
Composite Air Peak	~1 min
Carbon Dioxide Peak	~2 min
Water Vapor Peak	~10 min

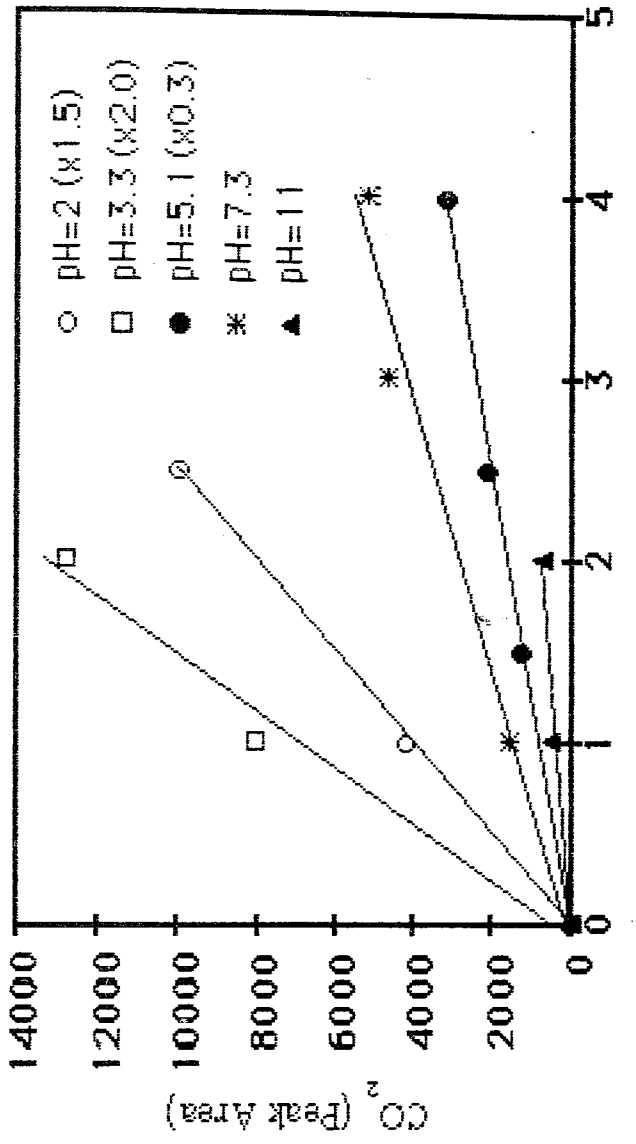

Figure 4.5. Calibration of CO_2 for phthalic anhydride.

4.5. Dicarboxylic Acids

Aliphatic dicarboxylic acid family has five members: oxalic, malonic, succinic, glutaric, and adipic acids. In this study malonic, succinic and adipic acids were investigated.

Malonic acid is a strong acid. It is harmful if swallowed, inhaled or absorbed through skin. It is also causes severe irritation. High concentrations are extremely destructive to tissues of the mucous membrane and upper respiratory tract, eyes and skin [36].

Succinic acid is a constituent of almost all plant and animal tissues. Uses of succinic acid range from scientific applications such as radiation dosimetry to applications in agriculture, food, medicine, plastics, cosmetics, textiles, and plating. Caution is advised when dealing with hot vapors given off from succinic acid, which is harmful to nasal passages [36].

Adipic acid, from a commercial viewpoint, is the most important of all the aliphatic dicarboxylic acids, with a world wide annual production of about 1.8 million metric tons. Its primary use is in the manufacture of nylon-6,6. Other applications are in plasticizers, resins, and plastics. The principal hazard in handling of adipic acid is the danger of dust explosions. Minimum explosive concentration (dust) is 0.010-0.015 g/L In high dust areas, exposure may cause irritation to neck, ankles and to the mucous membranes of nose and throat [36].

Table 4.5 gives some properties of malonic, succinic and adipic acids [38].

It should be taken into account that the complete photooxidation of malonic, succinic, and adipic acids proceed according to the following equations:

$$C_3H_4O_4 + 2O_2 \longrightarrow 3CO_2 + 2H_2O \quad (4.2)$$

$$C_4H_6O_4 + 7/2O_2 \longrightarrow 4CO_2 + 3H_2O \quad (4.3)$$

$$C_6H_{10}O_4 + 13/2O_2 \longrightarrow 6CO_2 + 5H_2O \quad (4.4)$$

Table 4.5. Some properties of acids.

	Malonic Acid	Succinic Acid	Adipic Acid
Molecular weight	104.06	118.09	146.14
Melting point°C	136	185	151
Solubility (g/100 g H_20 at 20°C)	74	6	2
LD_{50} mg/kg (in rat)	1310	2200	3600
pK_1	2.85	4.19	4.43
pK_2	5.69	5.64	5.41

4.5.1. Reactor

The experiments were conducted with reactor II which was also used to determine the temperature effect for phthalic anhydride. Reactor II was put in a box made of wood (70 cm in length, 22 cm in width) (Figure 4.6).

Six black light fluorescent lamps were settled in the box. They were two together attached to the right and left sides and also to the back side of the box. It was possible to light them on one by one. The front side of the box was designed to operate as a door and the reactor was attached to the the front side in order to maintain a uniform geometry all through the experiments. A ventilator was placed at the top of the box and air was also continually circulated through the box in order to eliminate the heating effect of the lamps.

4.5.2. Analysis

A heated gas sampler (Shimadzu Type HGS-2) was used to send the gas samples into the gas chromatograph (Gow Mac) automatically so that errors coming from hand made injections were canceled (Figure 4.7) GC was fitted with a Porapak N column and thermal conductivity detectors. Other analytical conditions were the same given in Table 4.4.

In the gas line, between the glass stopper of the reactor and the gas sampler, $CaCl_2$ was used to eliminate the water peaks.

Calibrations were carried out using measured volumes of carbon dioxide added to the circulating gas phase loop under identical conditions with the experiments. In Figure 4.8, Figure 4.9, Figure 4.10 calibration curves for CO_2 at different pH values are given. The values in the curves were corrected for the blank values of CO_2.

Peak areas were automatically investigated with the recorder-integrator. The chart speed was 5 mm/min. The minimum peak area was 100 counts. The slope was set at 20 mV/min.

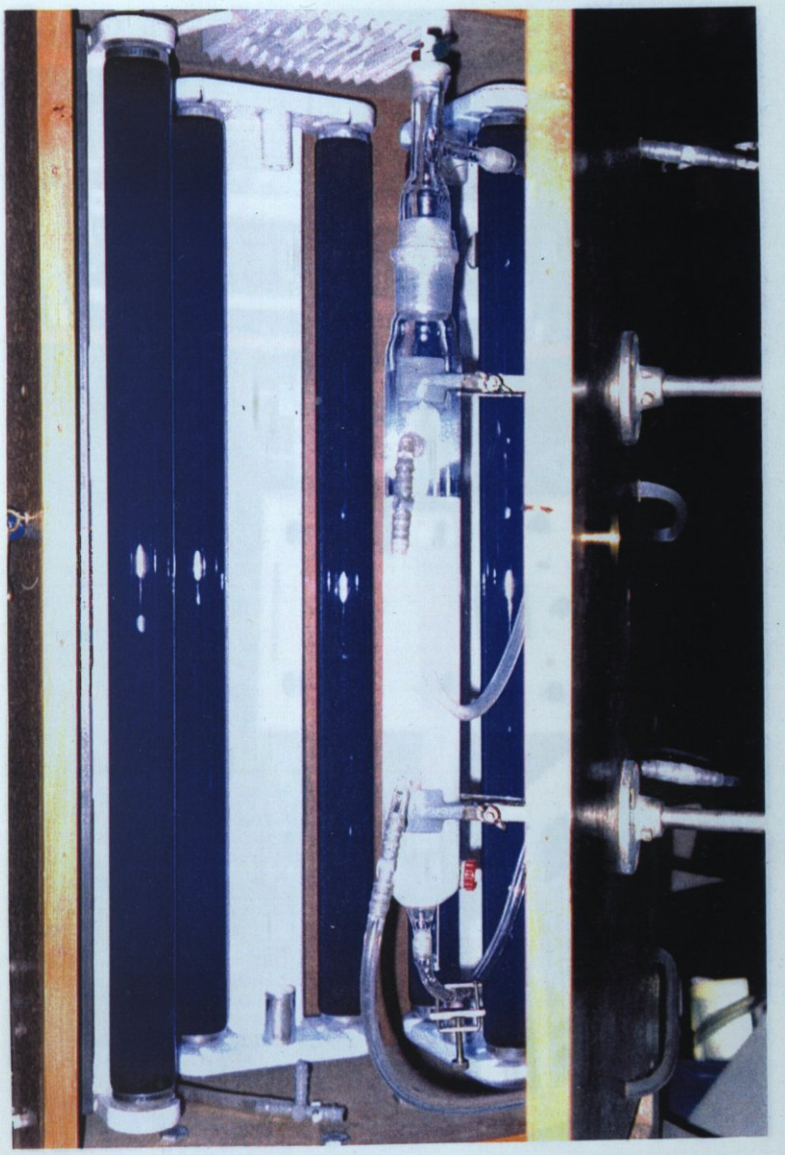

Figure 4.6. Box design.

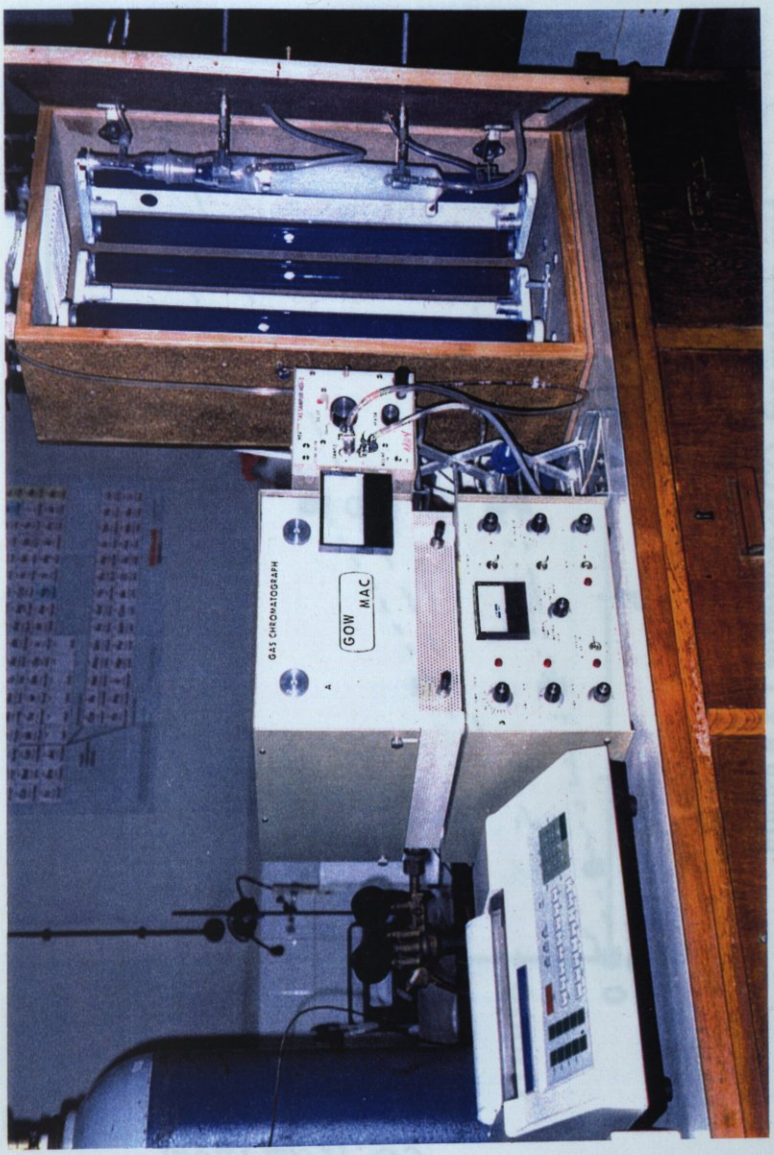

Figure 4.7. Experimental set-up.

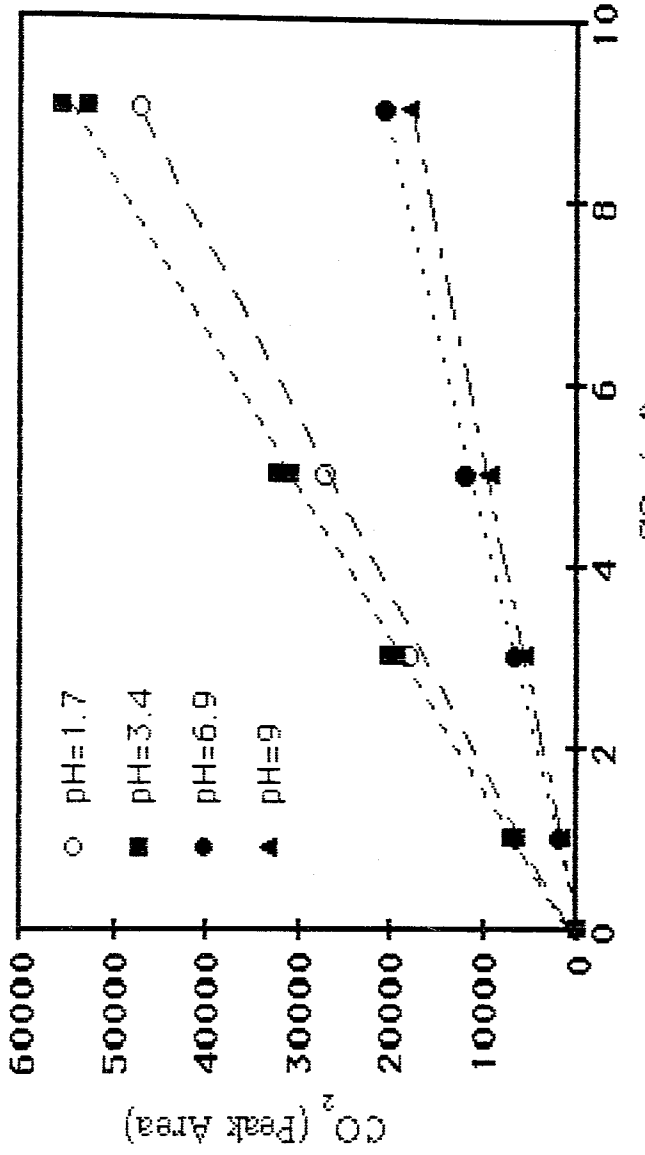

Figure 4.8. Calibration of CO_2 for malonic acid.

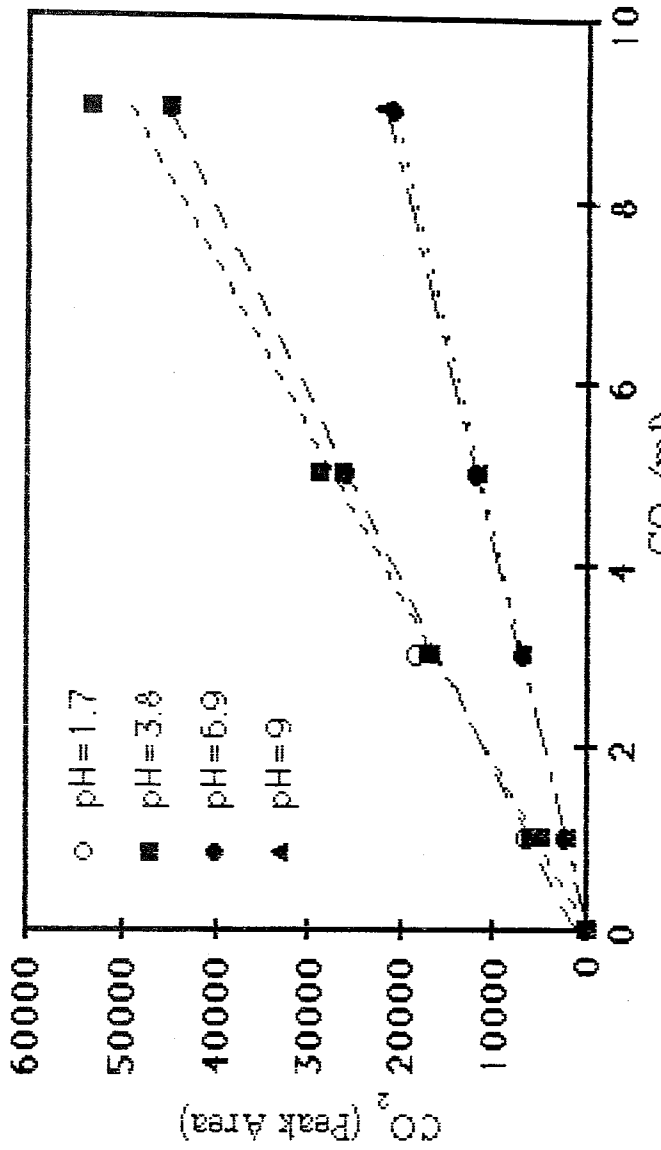

Figure 4.9. Calibration of CO_2 for succinic acid.

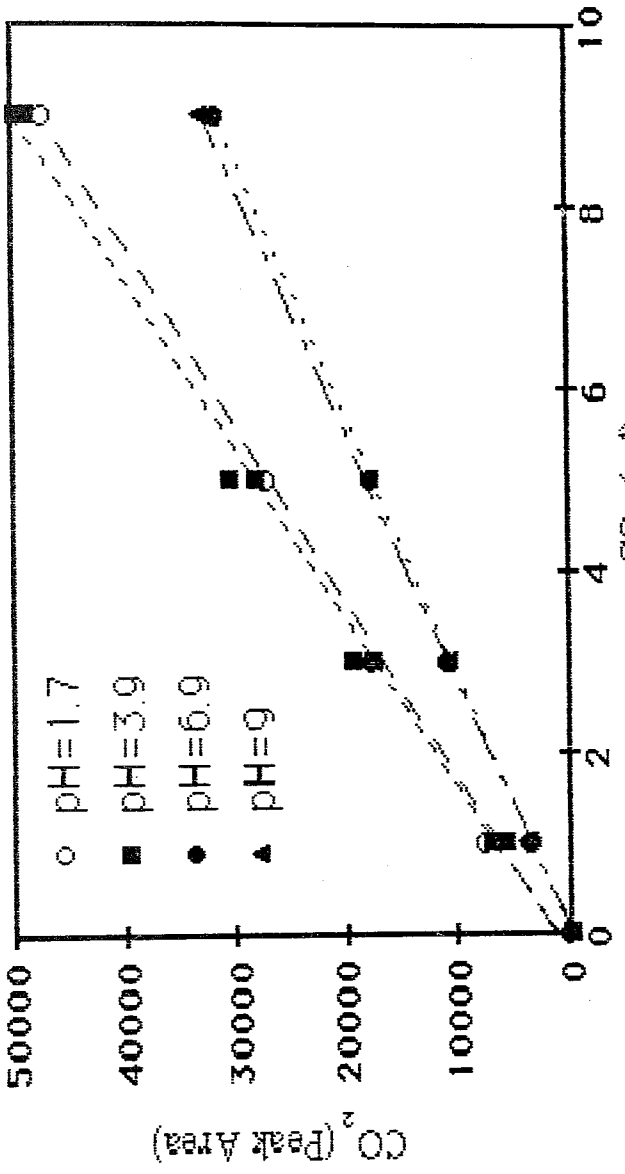

Figure 4.10. Calibration of CO_2 for adipic acid.

4.6. Actinometric Study

Several physical means for the calibration of light sources are known. With chemical systems, however, it is much easier to mimic the experimental situation of the sample. Many chemical actinometers that can be used to determine the number of photons in a beam per unit time are known in the liquid phase [39].

Potassium ferrioxalate actinometer developed by Hatchard and Parker [40] was chosen for this study It has many advantages: high sensitivity, high quantum efficiency over a wide wavelength range (254-510 nm), simplicity of operation, greater stability of photolyte and photolysis products, operation of a wide range of intensities and applicability to the measurement of a wide range of values of total radiation dose.The principle of potassium ferrioxalate actinometer is the reduction of ferric ions to ferrous state.When the solution of potassium ferrioxalate in sulfuric acid is irradiated within the 254-510 nm range, the Fe^{+3} ions are reduced to Fe^{+2} ions.The formed Fe^{+2} ions form a red-colored complex has an absorption maximum at 510 nm and can be measured spectrophotometrically.

4.6.1. Preparation of the Actinometer Solution

For all quantitative work the preparation and manipulation of the ferrioxalate solutions were carried out in a dark room using a red photographic safe light. Green crystals of $K_3Fe(C_2O_4)_3.3H_2O$ were prepared by mixing 3 volumes of 1.5 molar potassium oxalate solution with 1 volume of 1.5 molar ferric chloride solution with vigorous stirring [40]. Green crystals was then recrystallized three times from water and then dried at 45°C. The crystals was kept in the dark. Generally, 0.006, 0.012 or 0.15 M solutions can be used for actinometric studies. A one-actinometer depth of a 0.006 M solution absorbs 99 percent or more of light of wavelengths up to 390 nm. In both gas recycling reactor and optical bench reactors the 0.006 M $K_3Fe(C_2O_4)_3.3H_2O$ solution was used. In order to prepare the 0.006 M solution, 2.947 g of the crystals were dissolved in 800 mL of water, 100 mL of 1 N H_2SO_4 was added to the solution and this mixture was diluted to one liter.

The phenanthroline solution was 0.1 percent by weight 1,10-phenanthroline monohydrate in water. It was prepared by dissolving 0.1 g of the solid in water and completing the volume to one liter. Solutions of phenanthroline were freshly prepared and kept in the dark, to avoid the slow photodegradation of the phenanthroline solution.

A buffer solution was prepared from 600 mL of 1 N $NaC_2H_3O_2$ and 360 mL of 1 N H_2SO_4 diluted to one liter.

4.6.2. Procedure for Actinometric Measurements

The actinometric solution of volume V_1 was irradiated in the reaction vessel for an appropriate period of time t determined experimentally, so as to produce a Fe^{+2} concentration between $1x10^{-6}$ and $3x10^{-6}$ mole/mL. At time t, an aliquot volume V_2 pipetted in a volumetric flask V_3. A volume of buffer equal to about one half the volume of the photolyte taken is added, prior to the addition of 2 mL of phenanthroline solution, as recommended [41]. After dilution to V_3 with water and mixing, the solution is allowed to stand for 30 minutes. An identical but unirradiated solution is used as the blank. All these operations are performed in the absence of actinometrically active light.

When $K_3Fe(C_2O_4)_3$ solutions in H_2SO_4 were irradiated simultaneous reduction of ferric ion to the ferrous state and oxidation of oxalate ion occur. The complex mechanism can be simplified to the overall reaction represented by [42]:

$$2Fe(C_2O_4)_3^{3-} + hv \longrightarrow 2Fe^{2+} + 5C_2O_4^{2-} + 2CO_2 \qquad (4.5)$$

The number of moles of Fe^{2+} formed are determined spectrophotometrically by development with 1,10-phenanthroline resulting in the formation of a red $Fe(phen)_3]^{+2}$moiety (l max=510 nm). The absorbance of this solution is a measure of the quantity of light absorbed by the actinometer [42]. The measured optical density corresponds to the net ferrous ions value.

The formula stated below was used for calculating the number of photons incident on the cell per second [43].

$$n_{abs}=\Sigma n_{abs}/t = \frac{6.023x10^{20}\, V_1\, V_3\, (OD)}{V_2\, 1\, (\varepsilon)\, (\phi\lambda)\, t}$$

where:

t = irradiation time of the actinometer (sec)

V_1 = volume of the actinometer solution irradiated (mL)

V_2 = volume of aliquot taken for analysis (mL)

V_3 = final volume to which V_2 is diluted (mL)

1 = path length of the spectrophotometric cell (1.0 cm)

OD = measured " optical density difference " of the final solution at 510 nm

ε = the molar extinction coefficient of the Fe^{+2} complex ($1.11x10^4$ L/mol.cm)

$\phi\lambda$ = quantum yield for the Fe^{+2} formation selected from table [49].

It has been reported that at least 10^{14} photons are necessary to initiate a photochemical reaction [40].

V. RESULTS AND DISCUSSION

5.1. Results of Calibration Curves

5.1.1. Solubility of CO_2 in Water

Carbon dioxide, CO_2, is a weak acid in water. Because of the presence of CO_2 in air and its production from microbial decay of organic matter, dissolved CO_2 present in all natural waters and waste waters [44]. The most important acid-conjugate base system in air water interactions is the carbonate system. It controls the pH of water and consists of following species:

Carbon dioxide, CO_2, in gaseous form $CO_2(g)$ or dissolved in water $CO_2(aq)$
Carbonic acid, H_2CO_3
Bicarbonate ion, HCO_3^-
Carbonate ion, CO_3^{2-} [44].

The CO_2, HCO_3^-, CO_3^{-2} system in air and water may be described by the following equations:

Air⟶Water: $CO_2(g) \longrightarrow CO_2(aq)$ $K=3.2\times10^{-2}$ (5.1)

In Water: $CO_2(aq)+H_2O \longrightarrow H_2CO_3$ $K=1.6\times10^{-3}$ (5.2)

$H_2CO_3+H_2O \longrightarrow HCO_3^-+H_3O^+$ $K_1=4.45\times10^{-7}$ (5.3)

$HCO_3^-+H_2O \longrightarrow CO_3^{2-}+H_3O^+$ $K_2=4.8\times10^{-11}$ (5.4)

The predominant species formed by CO_2 dissolved in water depend upon pH (Figure 5.1).

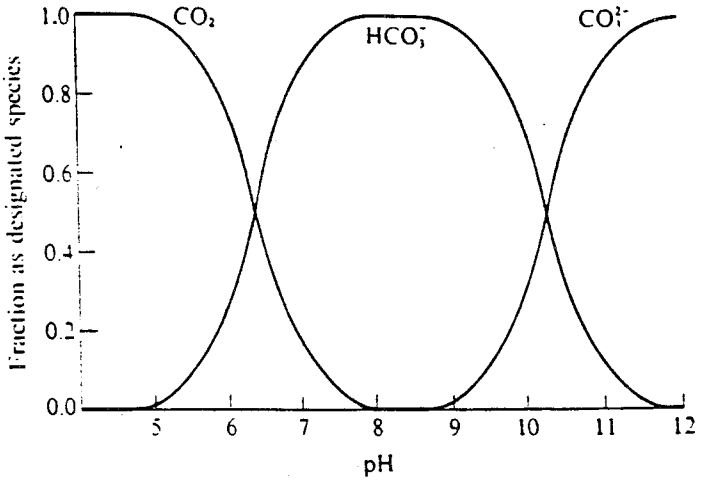

Figure 5.1. Distribution of species diagram for the CO_2, HCO_3^-, CO_3^{2-} system in water.

Such a diagram shows the major species present in solution as a function of pH. The fractions of CO_2, HCO_3^- and CO_3^{2-} present in water are given by the following expressions:

$$\alpha CO_2 = \frac{[CO_2]}{[CO_2]+[HCO_3^-]+[CO_3^{2-}]}$$

$$\alpha HCO_3^- = \frac{[HCO_3^-]}{[CO_2]+[HCO_3^-]+[CO_3^{2-}]}$$

$$\alpha CO_3^{2-} = \frac{[CO_3^{2-}]}{[CO_2]+[HCO_3^-]+[CO_3^{2-}]}$$

Substitution of the expressions for K_1 and K_2, into the above equations leads to the following:

$$\alpha CO_2 = \frac{[H^+]^2}{[H^+]^2+K_1[H^+]+K_1K_2}$$

$$\alpha HCO^{3-} = \frac{K_1[H^+]}{[H^+]^2+K_1[H^+]+K_1K_2}$$

$$\alpha CO_3^{2-} = \frac{K_1K_2}{[H^+]^2+K_1[H^+]+K_1K_2}$$

Calculations from these expressions show that for pH significantly below pK_1, αCO_2 is essentially 1, when $pH=pK_1$, $\alpha CO_2=\alpha HCO_3^-$; when $pH=1/2(pK_1+pK_2)$, αHCO_3^- is at its maximum value of 0.98; when $pH=pK_2$, $\alpha HCO_3^-=\alpha CO_3^{2-}$; and for pH significantly above pK_2, αCO_3^{2-} is essentially 1 [44].

According to the above expressions when various pH values for phthalic anhydride and dicarboxylic acids were taken into account the following results were obtained:

1)When pH(<5.1) is lower than the pK_1(6.35) value, αCO_2 is essentially 1 which indicates the highest evolution of CO_2.

2)When pH(7.3) is approximately equal to pK_1(6.35) value, αCO_2 is equal to αHCO_3^- which leads to a low evolution of CO_2 compared to the first case.

3)At pH(9.0) ,the formation of HCO_3^- and CO_3^{2-} would be the predominant species in the medium which leads to a lower evolution of CO_2.

4) When pH(11) is above the pK_2(10.33) value, αCO_3^{2-} is essentially 1 which leads to the lowest evolution of CO_2.

5.2. Results of Phthalic Anhydride

5.2.1. Results for the Actinometric Measurement

The results of the actinometric study is given in Table 5.1.

Table 5.1. The Actinometric results for phthalic anhydride.

V_1 = 300 mL
V_2 = 2 mL
V_3 = 10 mL
t = 3600 sec
OD = 3.89
$\varphi\lambda$ = 1.21
n_{abs}= 7.28×10^{16} photon/sec or 1.21×10^{-7} einstein/sec

5.2.2. Effect of Catalyst Concentration

Dependence of TiO_2 concentration on CO_2 formation was followed in the range of 0.1-3.1 g/L (Table 5.2, Figure 5.2). Each point in the figure shows the result for one hour irradiation.

CO_2 formation was found to increase with increasing TiO_2 concentration up to 0.8 g/L. With further increase of TiO_2 concentration, the CO_2 formation appeared to reach a limiting value, representing contribution of two main factors. One of these factors may be aggregation of TiO_2 particles at high concentrations, causing a decrease in the number of surface active sites. The other factor is that higher catalyst concentration, because of the opacity and light scattering properties of the particles, can also decrease the passage of irradiation through the sample. Thus, a TiO_2 amount of 1 g/L was chosen near the beginning of the plateau for the further experiments.

Table 5.2. Effect of TiO_2 loading on the CO_2 formation.

TiO_2 (g/L)	CO_2 (µmole)
0.1	0.66
0.2	1.6
0.3	1.6
0.7	2.3
1.4	2.4
2.1	2.3
3.1	2.2

5.2.3. Effect of pH

CO_2 photogeneration was determined as a function of reaction solution pH over the pH range 2.1-11. The results of this study are illustrated in Table 5.2 and Figure 5.3.

Different pH values affected the competitive adsorption of phthalate ion and hydroxyl ions on the TiO_2 surface, which consequently affected the generation of hydroxyl radicals on the catalyst surface.

Table 5.3. Effect of pH on the CO_2 formation.

pH	CO_2 (µmole)
2.1	98.2
3.3	95.3
5.1	143
7.3	150
11	0

At pH values lower than 7.3, an increase in phthalate ion adsorption was observed on the positively charged TiO_2 surface. A maximum CO_2 was

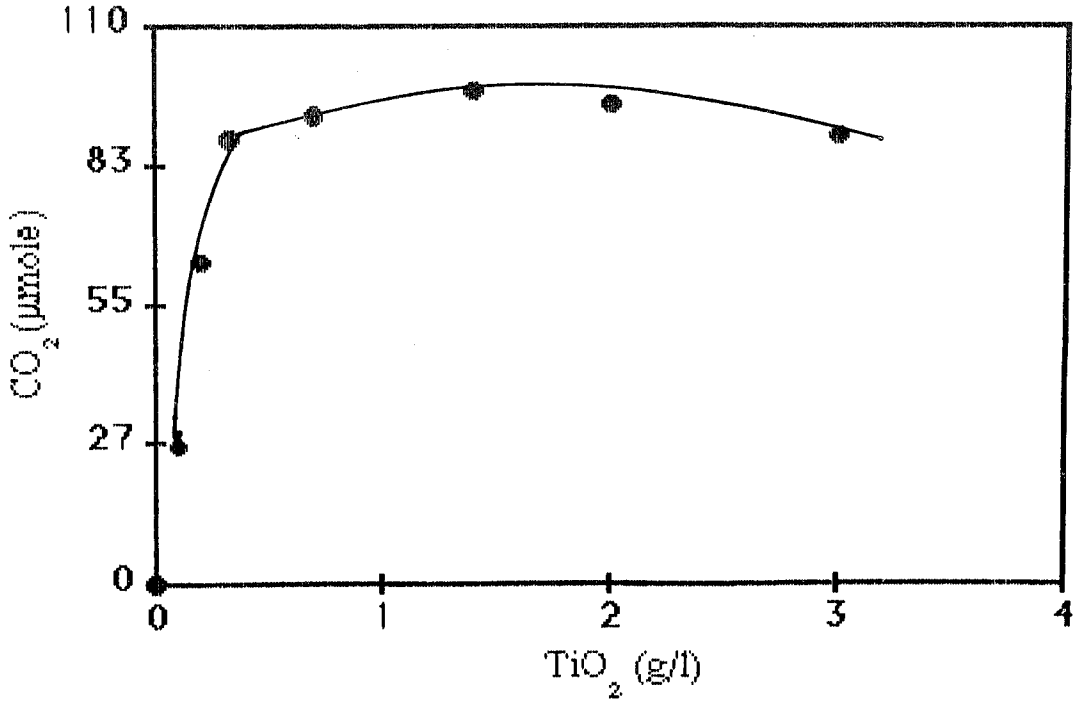

Figure 5.2. Effect of TiO_2 amount on the CO_2 formation.
Conditions: pH=3.3(natural), [anhydride]=$1x10^{-3}$ M, T=298 K, Intensity=$1.21x10^{-7}$ einstein/sec, Irradiation time=60 min,
Flow Rate= 144 ml/min.

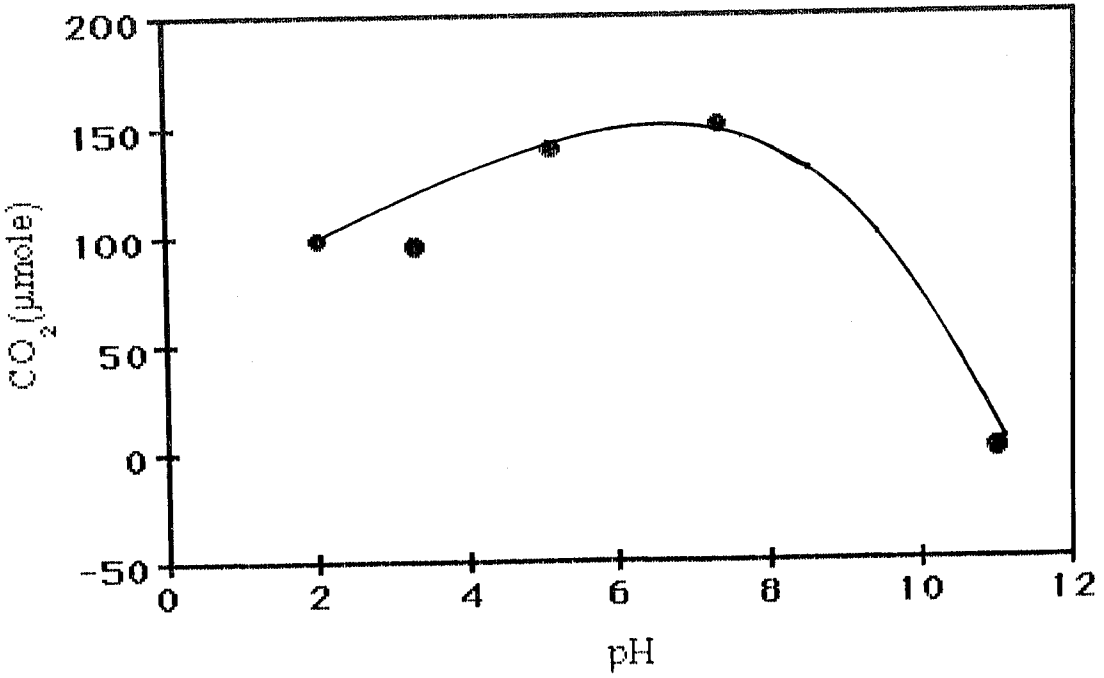

Figure 5.3. Dependence of CO_2 formation on the pH of the solution. Conditions: [phthalic anhydride]=$1x10^{-3}$ M, T=298 K, Intensity=$1.21x10^{-7}$ einstein/sec, [TiO_2]=1 g/L, Irradiation time=60 min, Flow Rate=144 ml/min.

obtained at pH=7.3. At pH=11, however, CO_2 generation drastically decreased due to the competitive adsorption of OH^-(number of OH^- at the active sites increased with an increase in pH values) and phthalate ion on the TiO_2 surface. In other words, when pH is greater than 7.3 the replacement of physisorbed OH^- by phthalate anions would be more favorable which can be represented as:

$$Ti^{+n}(OH)_n + Ph(COO^-)_2 \text{ ---------> } Ti^{+n}(OH)^{n-1}(Ph(COO^-)_2) + OH^-$$

5.2.4. Effect of Phthalic Anhydride Concentration

The phthalic anhydride concentration effect was investigated in the (0.01-1)x10^{-3} M range by using slurries at natural pH and in the presence of 1g/L TiO_2 (Table 5.4).

The formation of CO_2 versus phthalic anhydride concentration represented in Figure 5.4, and from the figure it is observed that the amount of the adsorbate reaches a finite limit which implies that the reaction takes place in the adsorbed phase.

Table 5.4. Effect of phthalic anhydride concentration on the CO_2 formation.

[Phthalic Anhydride] (x10^{-3}M)	CO_2 (µmole)
0.01	182
0.1	224
0.5	361
1	432

5.2.5. Effect of Irradiation Time

The effect of irradiation time on CO_2 formation from phthalic anhydride in the presence of suspended TiO_2 was investigated. Results are given in Table 5.5 and Figure 5.5 show a linear increase in CO_2 amount with irradiation time.

Table 5.5. Effect of irradiation time on the CO_2 formation.

Irradiation time (min)	CO_2 (µmole)
0	0
30	59.3
60	95.3
120	204
160	240

5.2.6. Effect of Temperature

The variation in CO_2 formation with temperature was followed over the range 21-54°C. An increase in CO_2 generation was observed at higher temperatures. Results are given in Table 5.6 and shown in Figure 5.6.

Table 5.6. Effect of temperature on the CO_2 formation.

Time (min)	CO_2 (µmole)		
	294 K	313 K	327 K
0	0	0	0
5	2.86	43.8	87.2
20	118	211	331
40	224	376	481
60	360	521	693

The formation of CO_2 from phthalic anhydride was determined at three different temperatures namely 21°C, 40°C and 54°C. A correction term $\alpha(T)$ is needed to take into account the decrease in the solubility of CO_2 with increasing temperature.

In all experiments, gas chromatography is used to measure the temporal variation in the percentage CO_2 in the gas phase. The corresponding temporal

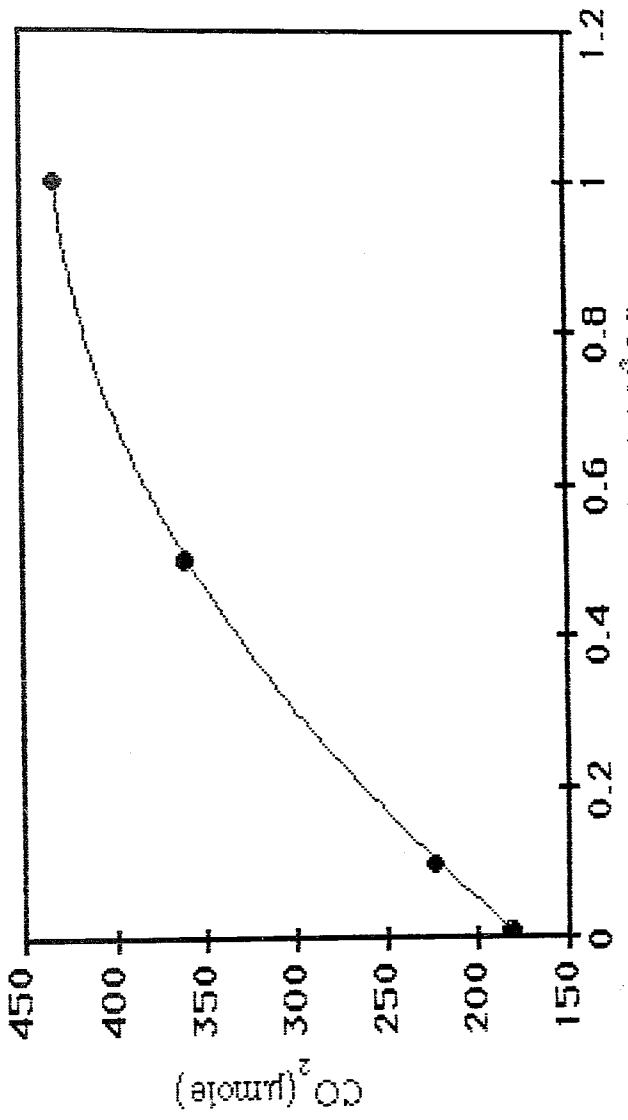

Figure 5.4. Concentration effect on the CO_2 yield.
Conditions: pH=3.3(natural), T=298 K, Intensity=$1.21x10^{-7}$ einstein/sec, [TiO2]=1 g/L, Irradiation time=60 min, Flow Rate=144 ml/min.

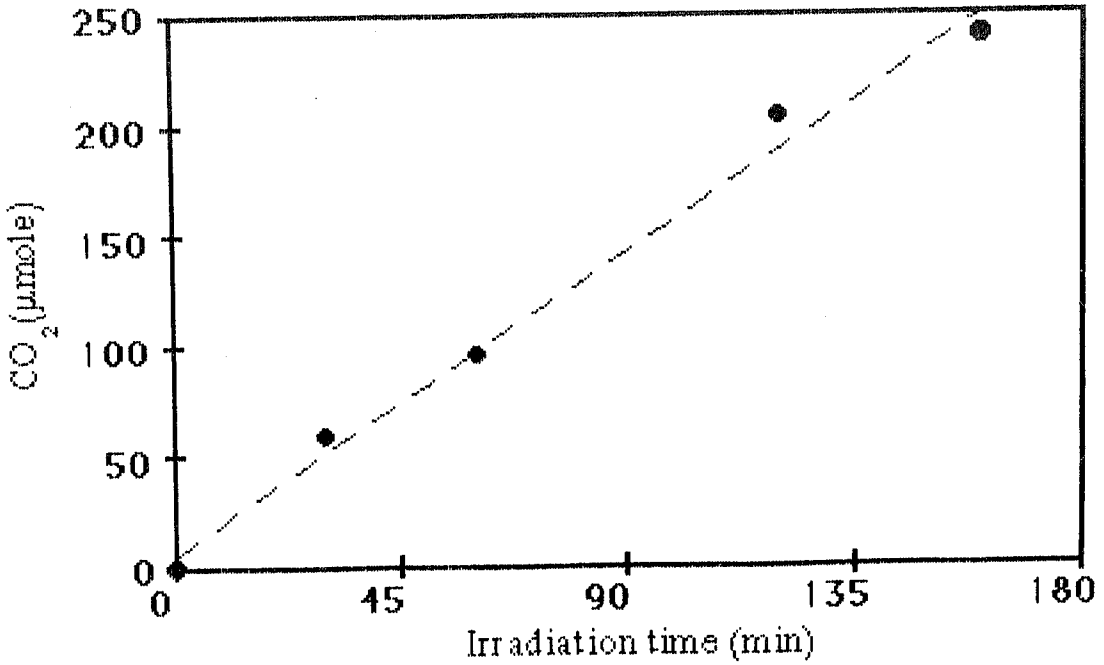

Figure 5.5. CO_2 formation as a function of irradiation time.
Conditions: pH=3.3(natural), [phthalic anhydride]=$1x10^{-3}$ M, T=298 K, Intensity=$1.21x10^{-7}$ einstein/sec, [TiO2]=1 g/L, Flow Rate=144 ml/min.

variation in the total number of moles of CO_2, i.e., $N(CO_2)$ can be determined using the formula [45]:

$$N(CO_2) = [CO_2] (V_{HS}/V + V_{LP}\ K_{CO_2}\ T/294) / 100$$
$$= \alpha(T)\ [CO_2]$$

where;

V_{HS} = Volume of the head space (0.100 L)

V = Volume of one mole of gas at T=21°C and P=1 atm (24.11 L)

V_{LP} = Volume of the liquid phase (0.300 L)

K_{CO_2} = Equilibrium constant for the process $CO_2(g) \xrightarrow{K_{CO_2}} CO_2(aq)$

where $K_{CO_2}=3.9\times10^{-2}$ mol/L atm at 21°C [46].

In this study most of the experiments were done at T=21°C, therefore, $\alpha(T) = (V_{HS}/V + V_{LP}\ k_{CO_2})/100$ is constant and calculated as 15.84×10^{-5} mol/$[CO_2]$.

In the experiments where CO_2 formation was followed as a function of temperature, the term $\alpha(T)$ was no longer constant and at each temperature, a measure of the true relative rate of CO_2 photogeneration was given by the term $\alpha(T) \times k_{CO_2}$, where values for $\alpha(T)$ at different temperatures are calculated using the above formula.

$$\alpha(T)=\alpha(40°C)=(V_{HS}/V + V_{LP}\ K_{CO_2}\ T/294) / 100$$

where;

V_{HS} =Volume of the head space (0.100 L)

V =Volume of one mole of gas at T=40°C and P=1 atm (25.67 L)

V_{LP} =Volume of the liquid phase (0.300 L)

K_{CO_2} = 2.3×10^{-2} mol/L atm at 40°C [46]

$\alpha(40°C)$ = 11.24×10^{-5} mol/$[CO_2]$.

$$\alpha(T)=\alpha(54°C)=(V_{HS}/V + V_{LP}\ K_{CO_2}\ T/294) / 100$$

where;

V_{HS} =Volume of the head space (0.100 L)

V =Volume of one mole of gas at T=54°C and P=1 atm (26.81 L)

V_{LP} =Volume of the liquid phase (0.300 L)

K_{CO_2} =1.85×10^{-2} mol/L atm at 54°C [46]

$\alpha(54^{\circ}C) = 9.90x10^{-5}$ mol/$[CO_2]$.

The Arrhenious data is given in Table 5.7 and is plotted as $\ln(\alpha(T) \times k_{CO_2})$ versus 1/T in Figure 5.7 whose whose slope leads to the calculation of activation energy (3.19 kj/mole).

Table 5.7. Arrhenious data for phthalic anhydride.

Equation $y=CO_2(\mu M)$ x=time(min)	$\ln(\alpha(T) \times k_{CO_2})$	$1/T\ K^1(x10^{-3})$
y=40.72+20.41x R=0.9971	-19.55	3.401
y=36.68+29.22x R=0.9971	-19.53	3.191
y=126.2+37.41x R=0.9901	-19.41	3.061

5.2.7. Effect of Flow Rate

In all experiments air was circulated through reactor to prevent the settlement of the catalyst particles. In Figure 5.8 and Table 5.8, results of CO_2 formation as a function of flow rate are shown. Experiments were carried out at three different flow rates. Although low CO_2 was formed at low flow rates, 144 mL/min was used in order to prevent the overflow of the solution out of the reactor and also not to harm the tygon tubing which passes through the peristaltic pump

Table 5.8. Effect of flow rate on the CO_2 formation.

Flow Rate (mL/min)	CO_2 (µmole)
144	95.3
432	132
720	143

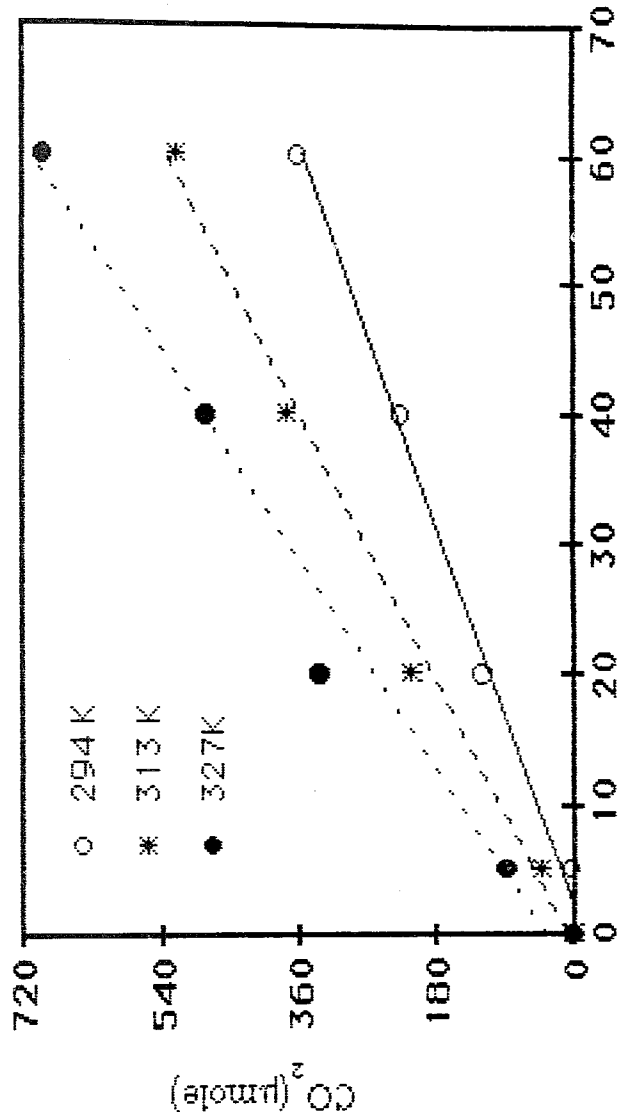

Figure 5.6. Temperature effect on the rate of CO_2 formation.
Conditions: pH=3.3(natural), [phthalic anhydride]=1x10-3 M, Intensity=1.21x10-7 einstein/sec, [TiO_2]=1 g/L, Irradiation time=60 min, Flow Rate=144 ml/sec.

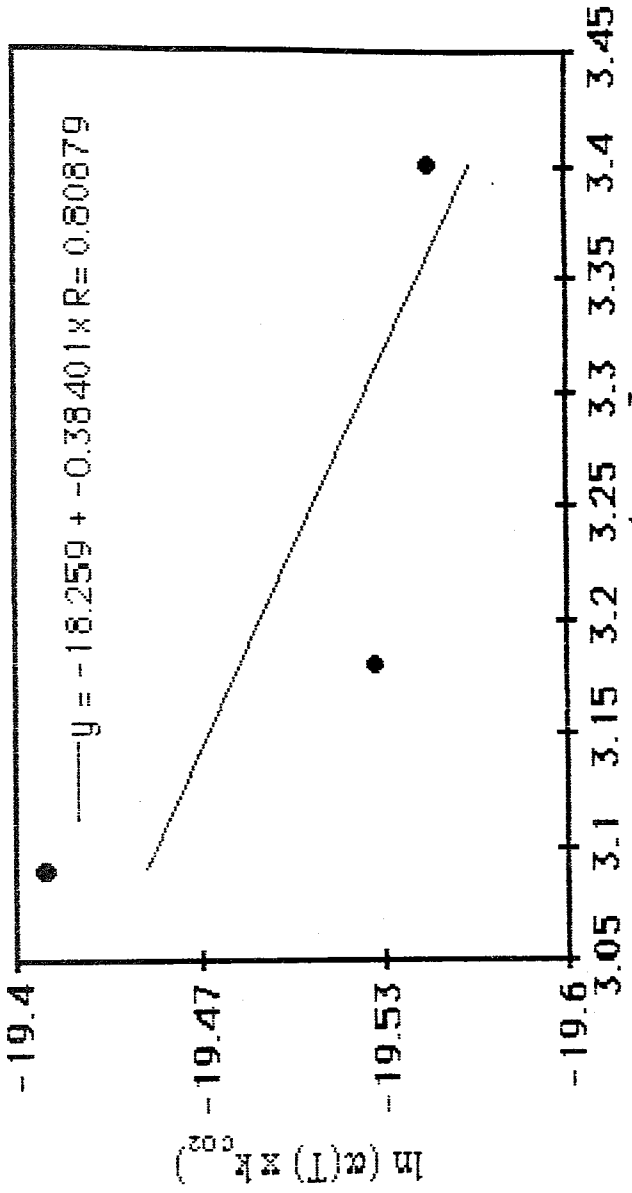

Figure 5.7. Arrhenious plot of phthalic anhydride.
Conditions: pH=3.3(natural), [phthalic anhydride]=1x10^{-3} M,
Intensity=1.21x10^{-7} einstein/sec, [TiO_2]=1 g/L, Irradiation time=60 min,
Flow Rate=144 ml/min.

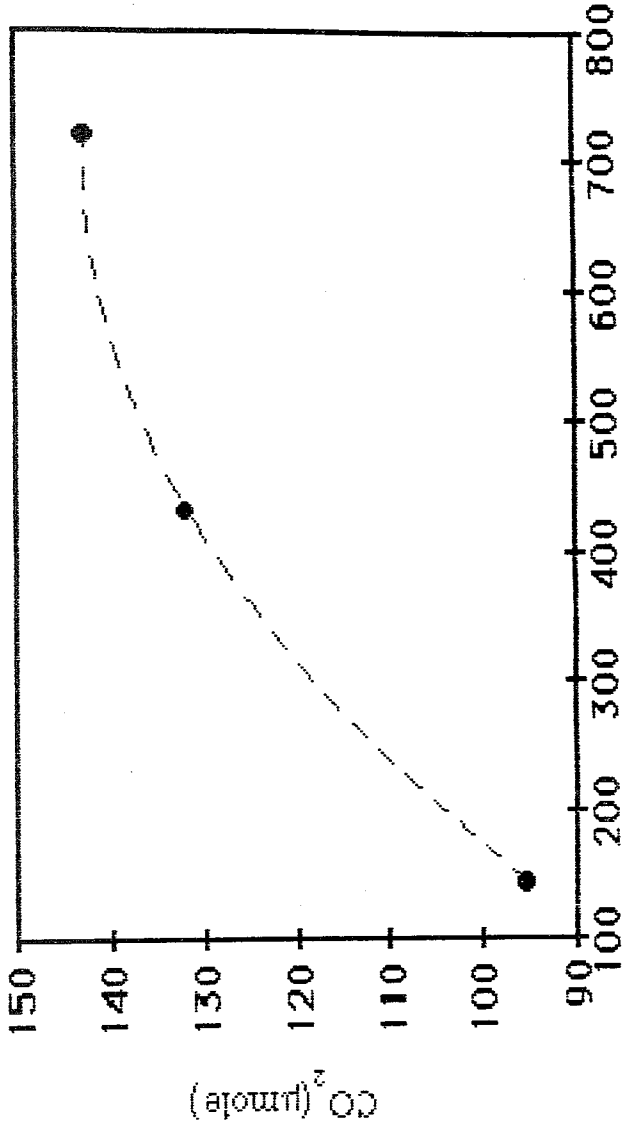

Figure 5.8. CO_2 formation as a function of flow rate
Conditions: pH=3.3(natural), [phthalic anhydride]=1x10^{-3} M, Intensity=1.21x10^{-7} einstein/sec, [TiO_2]=1 g/L, Irradiation time=6.0 min.

5.2.8. Effect of Light Intensity

CO_2 generation was followed with two ($0.61x10^{-7}$ einstein/sec) and four ($1.21x10^{-7}$ einstein/sec) lamps (Table 5.9, Figure 5.9). In the case of four lamps CO_2 formation was higher but not proportionally increased compared to the amount obtained with two lamps. That can be explained by the fact that electron/hole recombination is faster at higher light intensities.

Table 5.9. Effect of light intensity on the CO_2 formation.

Intensity ($x10^{-7}$) einstein/sec	CO_2 (µmole)
0	0
0.611	74.5
1.21	95.3

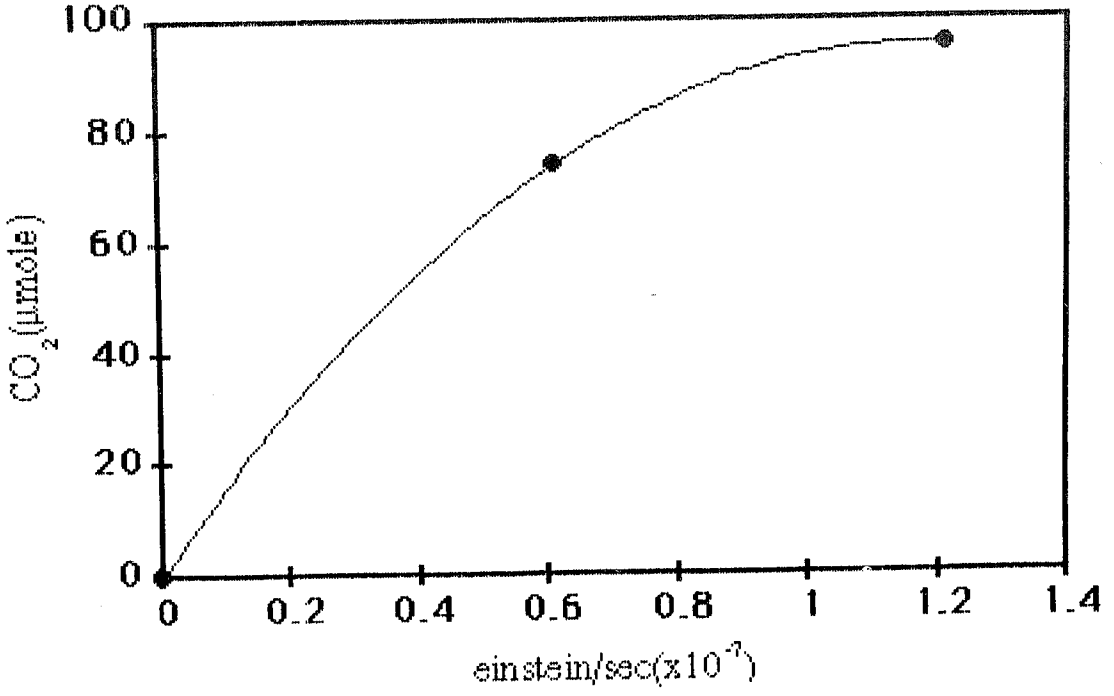

Figure 5.9. CO_2 evolution as a function of light intensity.
Conditions: pH=3.3(natural), [phthalic anhydride]=$1x10^{-3}$ M, [TiO_2]=1 g/L,
Irradiation time=60 min, Flow Rate=144 mL/min.

5.3. Results of Dicarboxylic Acids

The amount of TiO_2 loading and the flow rate which were optimized in the phthalic anhydride experiments were used in the subsequent studies for dicarboxylic acids.

5.3.1 Results for the Actinometric Measurements

The result of the actinometric study is given in Table 5.10. From right to left side of the box, lamps are numbered as one to six.

Table 5.10. The Actinometric Results.

Conditions
V_1 = 200 mL
V_2 = 2 mL
V_3 = 10 mL
t = 3600 sec
$\varphi\lambda$ = 1.21

No of lamps	OD	n_{abs} (photon/sec)($x10^{16}$)	n_{abs} (einstein/sec)($x10^{-7}$)
No=1	1.26	1.54	0.251
No=2	1.52	1.85	0.312
No=3	1.61	1.95	0.321
No=4	1.62	1.98	0.323
No=5	1.49	1.82	0.301
No=6	1.44	1.76	0.291

5.3.2. Effect of pH

Formation of CO_2 determined as a function of solution pH over the pH range 1.7-9. The results are represented in Tables 5.11, 5.12, 5.13.and are

plotted in Figures 5.10, 5.12, and 5.14.

Table 5.11. Effect of pH on the CO_2 formation from malonic acid.

time (min)	CO_2 (µmole) pH=1.7	pH=3.4	pH=6.9	pH=9
0	0	0	0	0
10	0.121	33.2	52.3	43.1
20	8.11	73.1	92.5	79.2
30	13.3	96.2	123	118
40	21.2	124	160	153
50	27.8	152	192	176
60	30.7	185	207	211

Table 5.12. Effect of pH on the CO_2 formation from succinic acid.

time (min)	CO_2 (µmole) pH=1.7	pH=3.4	pH=6.9	pH=9
0	0	0	0	0
10	0	43.9	42.3	25.7
20	8.29	78.8	80.5	61.4
30	15.4	107	122	95.4
40	23.6	145	174	138
50	32.8	169	215	172
60	36.9	187	257	215

Ionizable hydrogens of acids can be abstracted according to their pK_1 and pK_2 values. The following results were obtained when rates of CO_2 formation are plotted against pH (Figure 5.11, 5.13, 5.15):

1) When pH of the medium was below pK_1, the rate of formation of CO_2 was the least. This can be explained by the presence of acid in its acidic form (i.e, no hydrogen is lost) which obstructs the formation of CO_2.

2) There is a small difference between natural pH of acids and the pK_1 values, therefore, one of the hydrogens can be lost which facilitates the rate of CO_2 formation.

Table 5.13. Effect of pH on the CO_2 formation from adipic acid

time (min)	CO_2 (µmole) pH=1.7	pH=3.4	pH=6.9	pH=9
0	0	0	0	0
10	0	19.9	11.6	9.96
20	0	47.7	29.9	24.5
30	0	80.5	47.3	46.1
40	3.32	117	73.8	66.4
50	8.71	146	107	95.4
60	12.4	174	141	117

3) At pH around 7 both ionizable hydrogens were abstracted which leads to an effective formation of CO_2. However, adipic acid was contradictory to this result may be due to the formation of some intermediates which can block the surface active sites of TiO_2, leading to a decrease in the rate of CO_2 formation.

4) At pH=9, hydroxyl anions are introduced into the system which can block the surface active sites of semiconductor, however, these anions are capable of producing hydroxyl radicals which cause oxidation of dicarboxylic acids to CO_2.

5.3.3. Effect of Irradiation Time

The yield of CO_2 from 200 mL solutions of $1x10^{-3}M$ malonic, succinic and adipic acids at their natural pH's containing 0.2 g of TiO_2 was followed to extended irradiation times. For malonic acid after irradiation for 150 minutes, for succinic acid after irradiation for 160 minutes, and for adipic acid after irradiation for 240 minutes, CO_2 formation reached a plateau (Figure 5.16). Table 5.14 represents the effect of irradiation time results for each dicarboxylic acid.

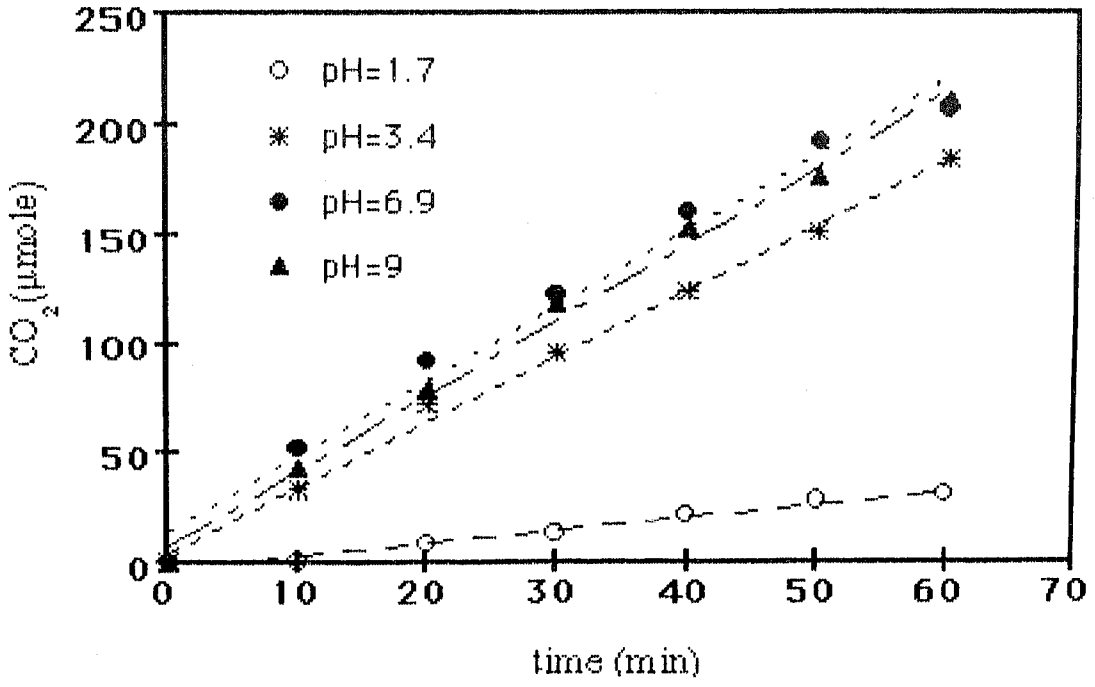

Figure 5.10. Effect of pH on the CO_2 formation from malonic acid
Conditions: [malonic acid]=$1x10^{-3}$ M, T=294 K, Intensity=$1.81x10^{-7}$ einstein/sec, [TiO_2]=1 g/L, Flow Rate=288 mL/min.

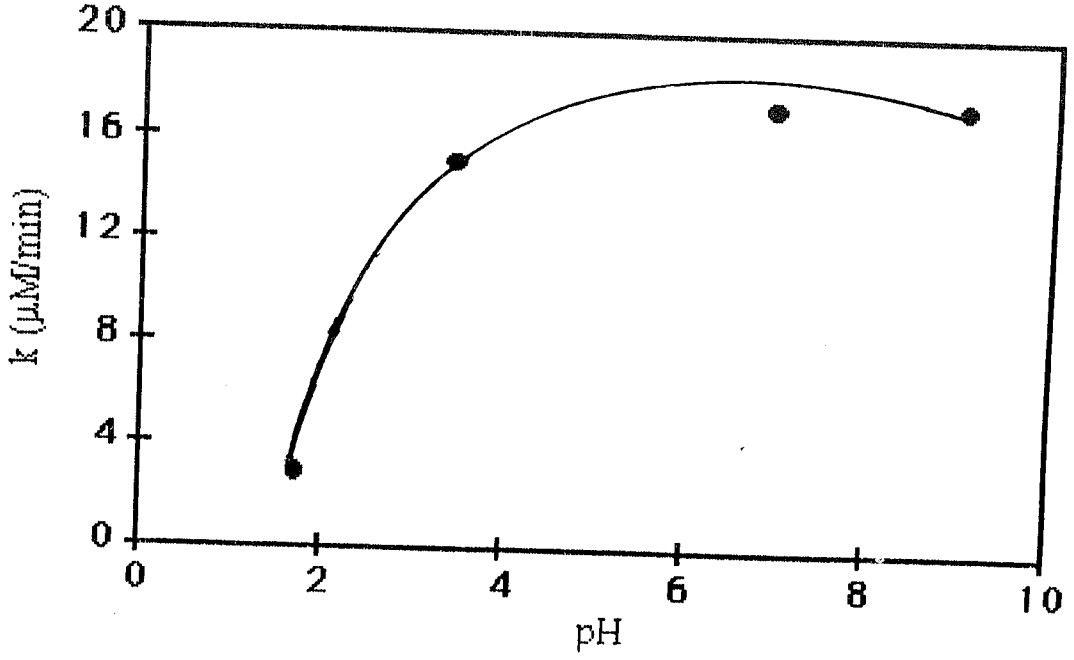

Figure 5.11. pH effect on the rate of CO_2 formation from malonic acid
Conditions: [malonic acid]=$1x10^{-3}$ M, T=294 K, Intensity=$1.81x10^{-7}$ einstein/sec, [TiO_2]=1 g/L, Flow Rate=288 mL/min.

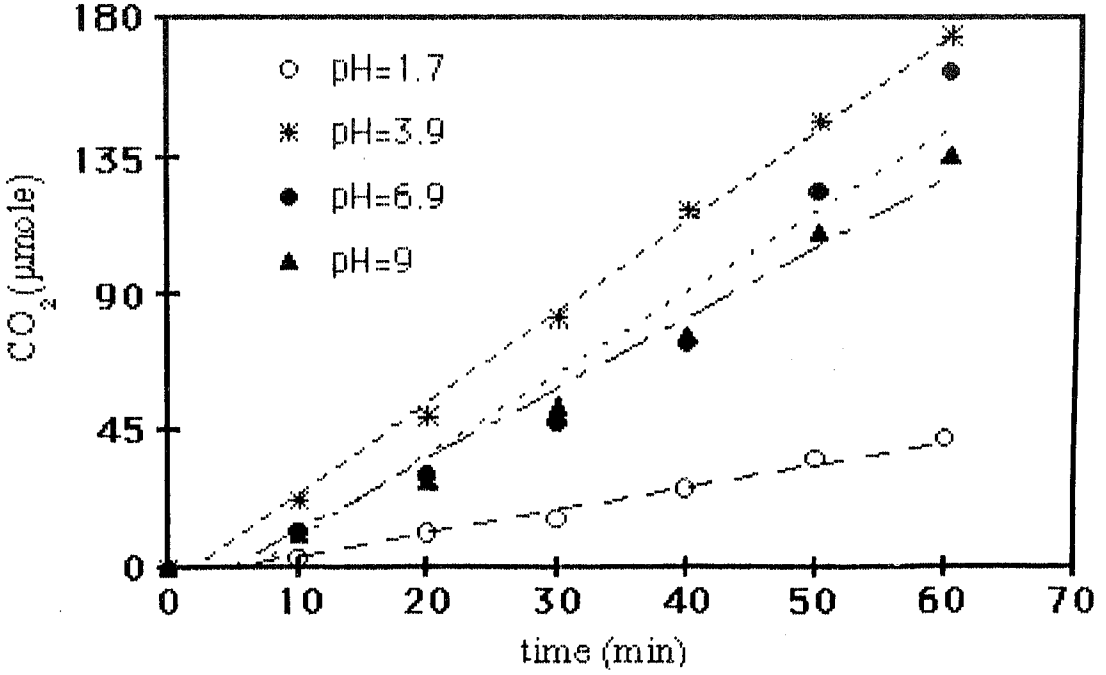

Figure 5.12. Effect of pH on the CO_2 formation from succinic acid
Conditions: [succinic acid]=$1x10^{-3}$ M, T=294 K, Intensity=$1.81x10^{-7}$ einstein/sec, [TiO_2]=1 g/L, Flow Rate=288 mL/min

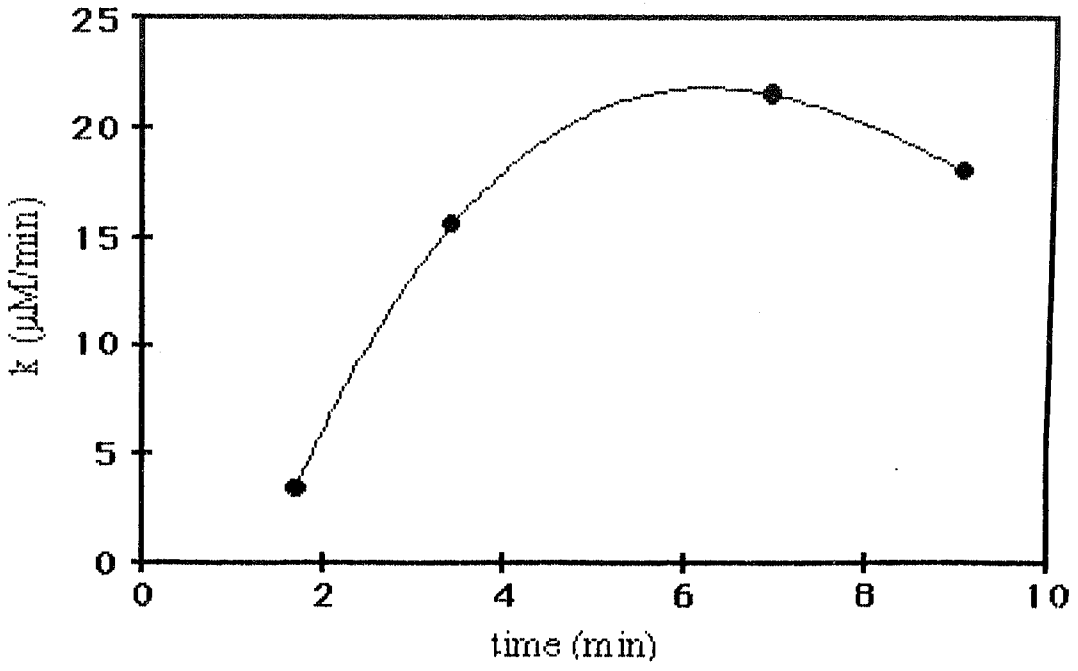

Figure 5.13. pH effect on the rate of CO_2 formation from succinic acid
Conditions: [succinic acid]=$1x10^{-3}$ M, T=294 K, Intensity=$1.81x10^{-7}$ einstein/sec, [TiO_2]=1 g/L, Flow Rate=288 mL/min

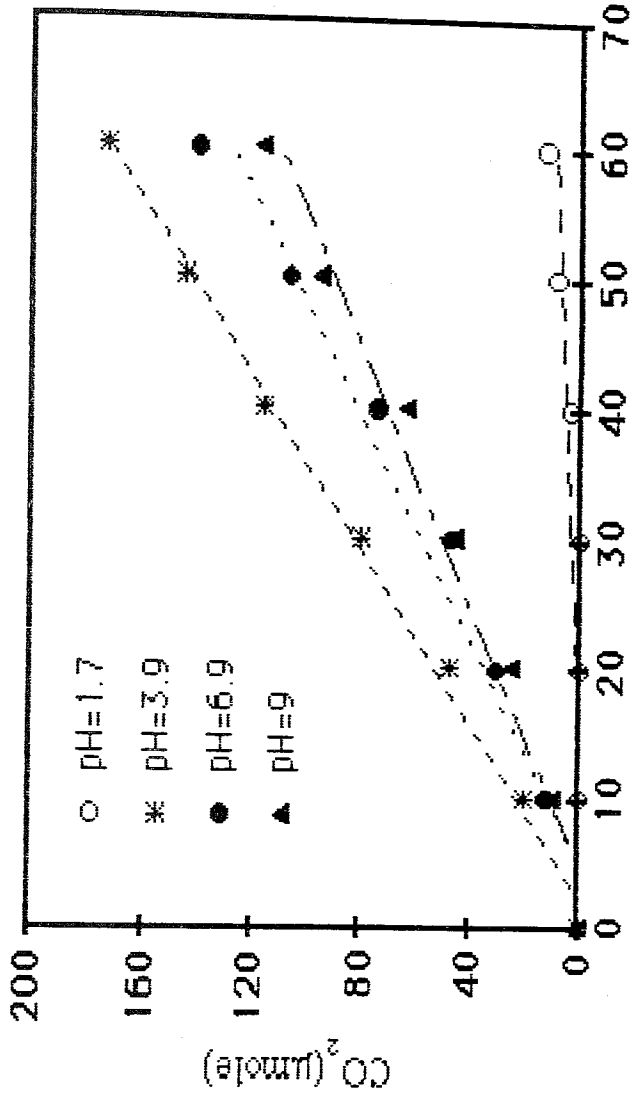

Figure 5.14. Effect of pH on the CO_2 formation from adipic acid
Conditions: [adipic acid]=1x10^{-3} M, T=294 K, Intensity=1.81x10^{-7} einstein/sec, [TiO_2]=1 g/L, Flow Rate=288 mL/min.

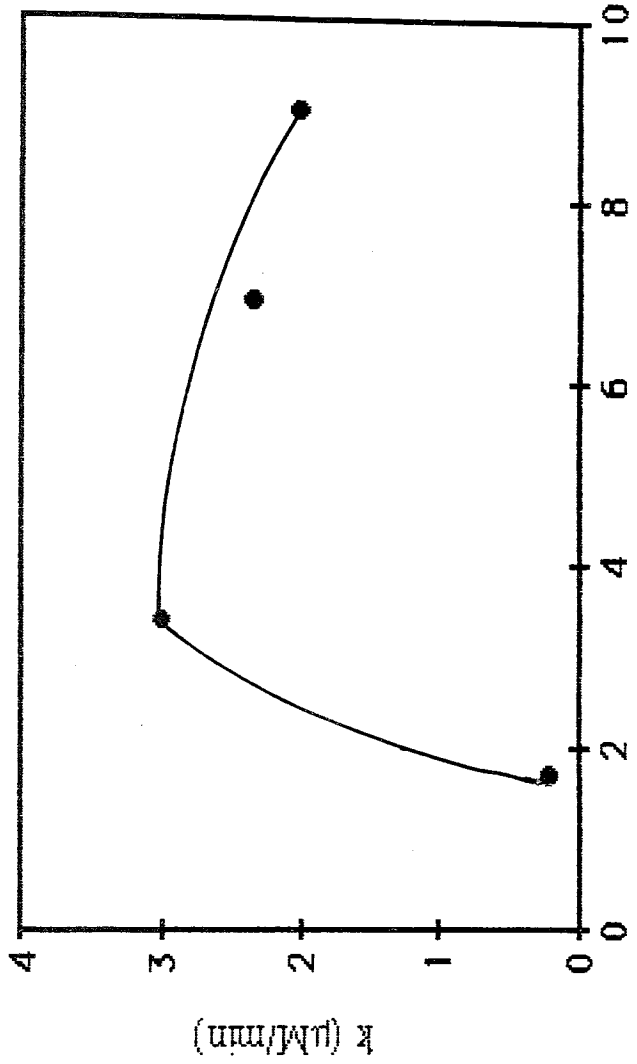

Figure 5.15. pH effect on the rate of CO_2 formation from adipic acid
Conditions: [adipic acid]=1x10^{-3} M, T=294 K, Intensity= 1.81x10^{-7} einstein/sec,
[TiO_2]=1 g/L, Flow Rate=288 mL/min

Table 5.14. Effect of irradiation time on the CO_2 formation.

Time (min)	CO_2 (µmole)		
	Malonic Acid	Succinic Acid	Adipic Acid
0	0	0	0
10	33.2	43.9	19.9
20	73.1	78.8	47.7
30	96.2	107	80.4
40	124	145	116
50	152	169	146
60	185	187	174
80	217	238	211
100	260	270	273
120	289	281	326
140	320	316	370
160	320	325	388
180	-	335	442
200	-	-	416
220	-	-	467
240	-	-	480

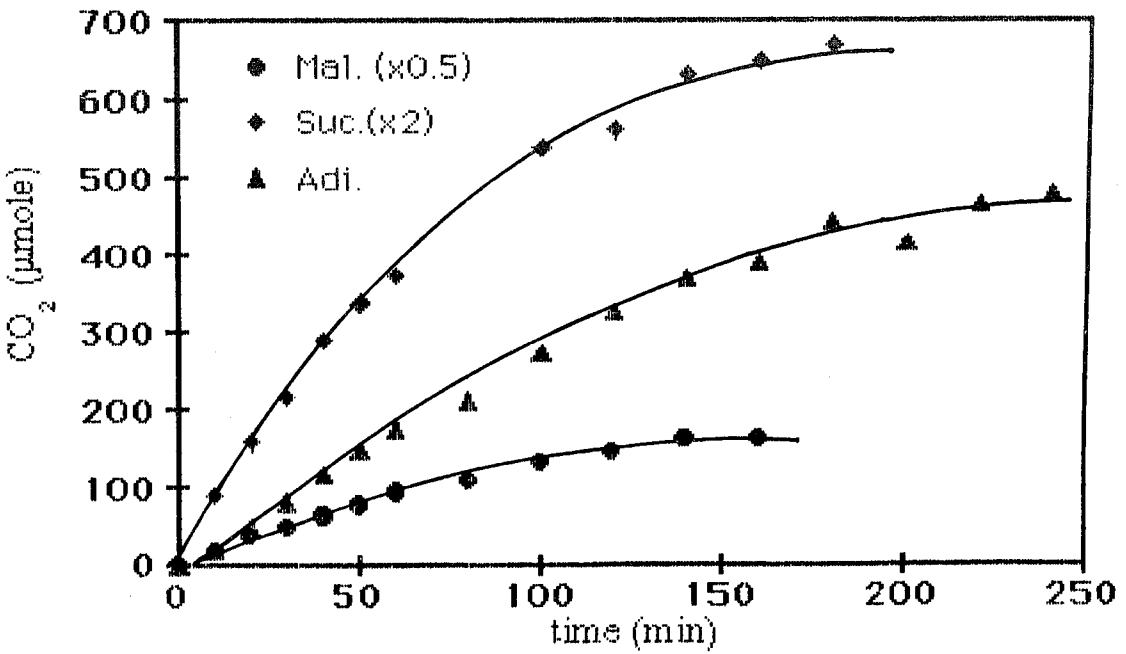

Figure 5.16. Irradiation time effect on the CO_2 formation from malonic,succinic and adipic acids.
Conditions: pH=natural, [dicarboxylic acid]=$1x10^{-3}$M, T=294 K, Intensity=$1.81x10^{-7}$ einstein/sec, [TiO_2]=1 g/L, Flow Rate=288 mL/min.

Figure 5.16 suggests that the formation of CO_2 increases by increasing the irradiation time. This can be explained by the fact that the amount of CO_2 evolved may be directly related to the number of carbons that are present in the acid, in other words, the more carbon containing the acid the more formation of CO_2 would be expected.

It is assumed that dicarboxylic acids may produce CO_2 according to their number of carbons, i.e., malonic acid ($HOOC-CH_2-COOH$) possessing three carbons is capable of producing 1, or 2, or 3 carbon dioxides depending on the number of carbons which undergo photooxidation. Likewise, succinic acid ($HOOC-CH_2-CH_2-COOH$) may produce 1,or 2, or 3, or 4 carbon dioxides and adipic acid ($HOOC-CH_2-CH_2-CH_2-CH_2-COOH$) can generate 1, or 2, or 3, or 4, or 5, or 6 carbon dioxides. These theoretical CO_2 mole numbers are plotted versus CO_2 volumes in Figures 5.17, 5.18, 5.19 whose straight line equations lead to the conversion of CO_2 volumes to the experimental CO_2 mole numbers which are represented in Tables 5.15, 5.16, 5.17. Comparing the dicarboxylic acids CO_2 evolution after similar irradiation period (160 min) one can conclude that adipic acid generates the highest amount of CO_2, succinic acid gives a lower amount than adipic acid and malonic acid produces the lowest.

Table 5.15. CO_2 volume to mole conversion for malonic acid.

Equation $y=-1.98x10^{-8}+0.21x$	y=mole numbers of CO_2 ; x=volume of CO_2 (mL)	
Time(min)	CO_2 (ml)	CO_2(mol)
0	0	0
10	0.81	0.17
20	1.8	0.37
30	2.3	0.48
40	3.1	0.62
50	3.7	0.76
60	4.5	0.93
80	5.2	1.08
100	6.3	1.32
120	6.9	1.44
140	7.7	1.61
160	7.7	1.61

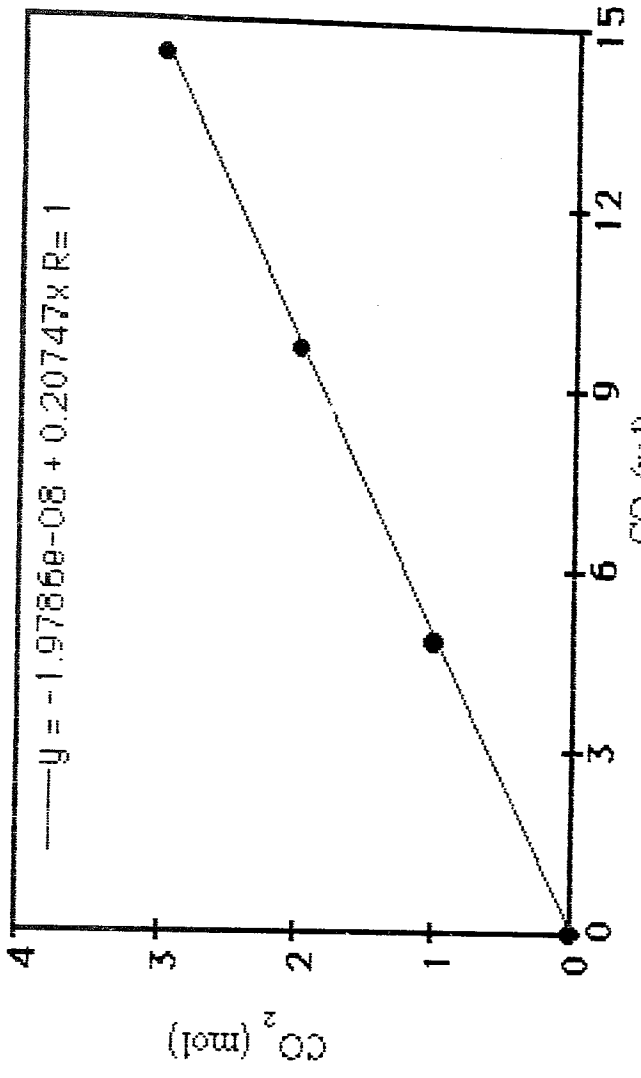

Figure 5.17. Malonic acid - CO_2 mL to mole conversion.

Table 5.16. CO_2 volume to mole conversion for succinic acid.

Equation $y=-4.15x10^{-4}+0.21x$	y=mole numbers of CO_2 ; x=volume of CO_2 (mL)	
Time (min)	CO_2 (mL)	CO_2 (mol)
0	0	0
10	1.1	0.22
20	1.9	0.39
30	2.6	0.54
40	3.5	0.72
50	4.1	0.84
60	4.5	0.93
80	5.7	1.2
100	6.5	1.4
120	6.8	1.4
140	7.6	1.6
160	7.8	1.6
180	8.1	1.7

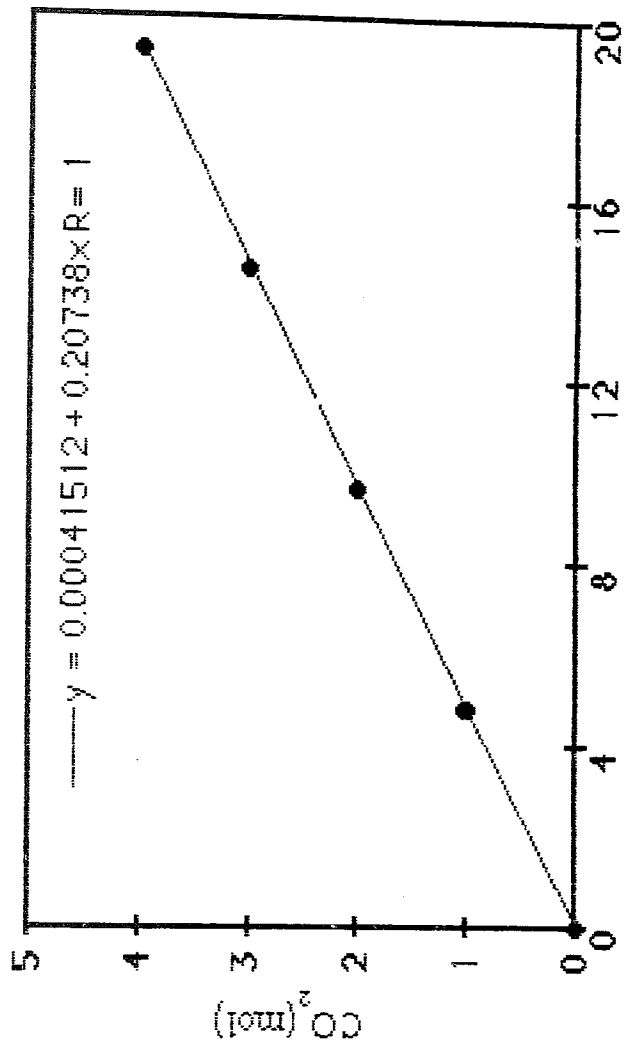

Figure 5.18. Succinic acid - CO_2 mL to mole conversion.

Table 5.17. CO_2 volume to mole conversion for adipic acid.

Equation $y=-4.00x10^{-4}+0.21x$	y=mole numbers of CO_2 ; x=volume of CO_2 (mL)	
Time (min)	CO_2 (mL)	CO_2 (mol)
0	0	0
10	0.48	0.09
20	1.2	0.24
30	1.9	0.41
40	2.8	0.58
50	3.5	0.73
60	4.2	0.87
80	5.1	1.1
100	6.6	1.4
120	7.9	1.6
140	8.9	1.8
160	9.4	1.9
180	11	2.2
200	10	2.1
220	11	2.3
240	12	2.4

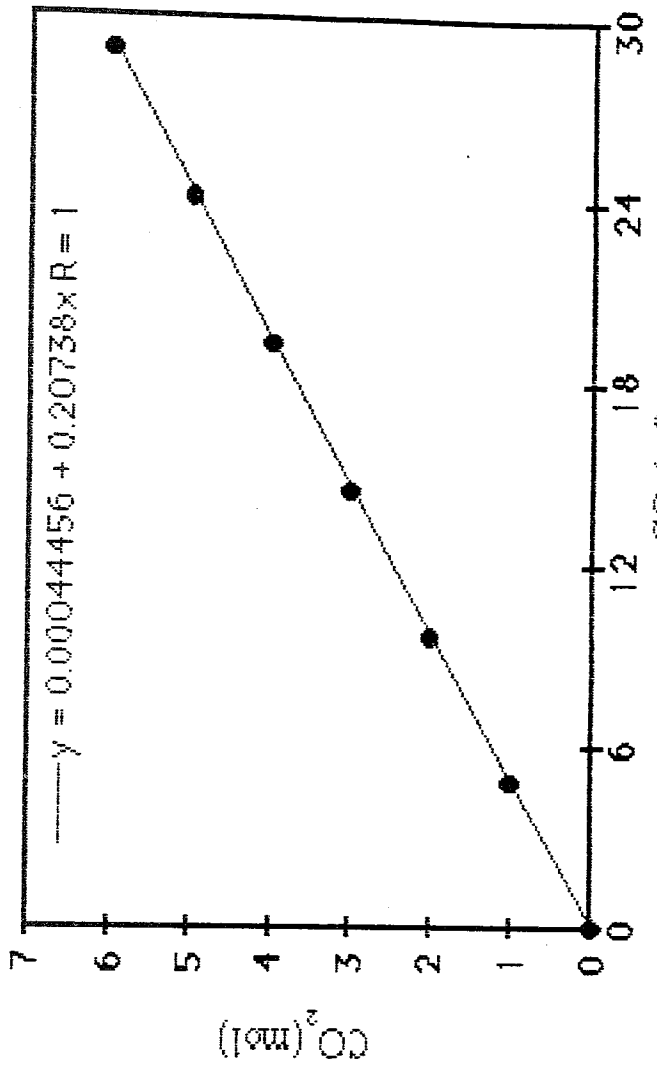

Figure 5.19. Adipic acid - CO_2 mL to mole conversion.

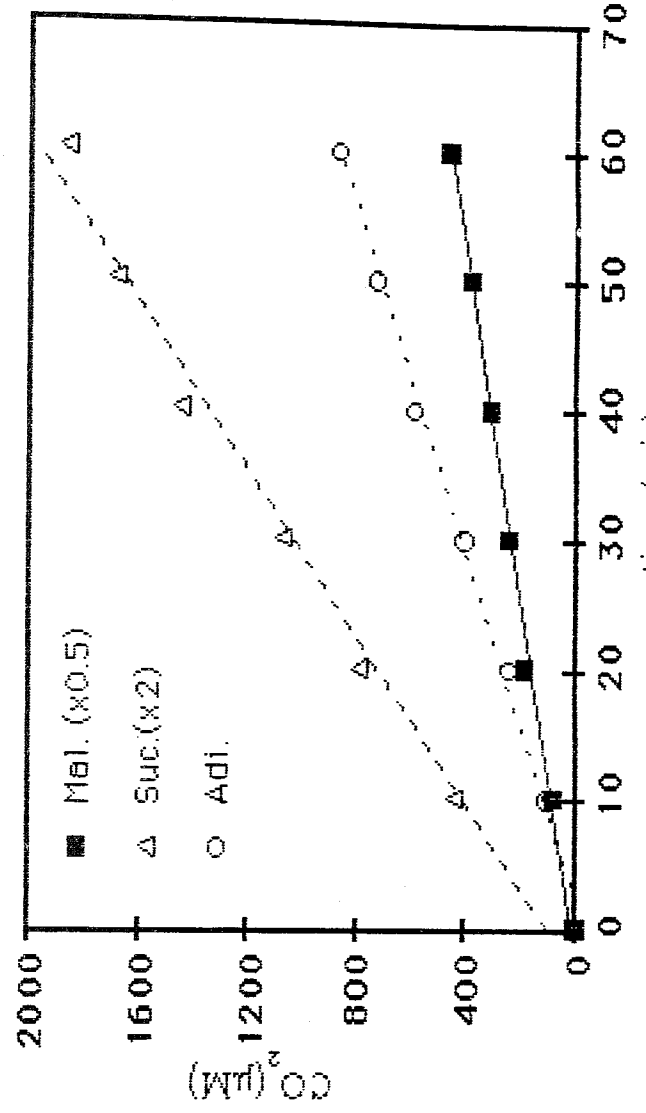

Figure 5.20. Rate of CO_2 formation after 60 min irradiation time.
Conditions: pH=natural, [acid]=$1x10^{-3}$M, T=294 K,
Intensity=$1.81x10^{-7}$ einstein/sec , [TiO_2]=1 g/L, Flow Rate =288 mL/min.

Even though maximum formation of CO_2 was not obtained at the same irradiation time, it showed linear increase during the first 60 minutes for each acid.(Figure 5.20). Therefore, to compare different results and to shorten duration of experiments, we measured CO_2 formation for 60 minutes in all cases.

5.3.4. Effect of Acid Concentration

The effect of concentration on the CO_2 formation was investigated for all acids in the (0.01-1)x10^{-3} M range by using slurries at their natural pH's and at a constant temperature of 21°C. Results of this study are illustrated in Tables 5.18, 5.19, 5.20 and are plotted Figure 5.21, 5.24, 5.27.

Table 5.18. Effect of malonic acid concentration on the CO_2 formation.

time (min)	CO_2 (µmole)			
	1x10^{-2} M	1x10^{-3} M	1x10^{-4} M	1x10^{-5} M
0	0	0	0	0
10	39.8	33.1	13.2	0.01
20	71.4	73.1	32.3	7.47
30	97.9	96.2	38.1	12.4
40	131	124	40.2	12.1
50	161	151	42.3	15.3
60	188	185	46.8	18.2

Table 5.19. Effect of succinic acid concentration on the CO_2 formation

time (min)	CO_2 (µmole)			
	$1x10^{-2}$ M	$1x10^{-3}$ M	$1x10^{-4}$ M	$1x10^{-5}$ M
0	0	0	0	0
10	68.1	43.9	32.3	11.2
20	132	78.8	48.9	13.2
30	181	107	53.9	15.3
40	237	144	57.6	14.1
50	303	168	55.5	15.3
60	335	187	57.2	14.5

Table 5.20. Effect of adipic acid concentration on the CO_2 formation

time (min)	CO_2 (µmole)			
	$1x10^{-2}$ M	$1x10^{-3}$ M	$1x10^{-4}$ M	$1x10^{-5}$ M
0	0	0	0	0
10	43.9	19.9	7.88	2.91
20	92.9	47.7	31.5	14.5
30	149	80.4	49.3	19.9
40	192	116	70.1	27.8
50	242	145	80.4	29.4
60	294	173	93.7	34.4

As it can be seen from the figures the amount of evolved CO_2 linearly increases with concentration for all dicarboxylic acids. The slopes of these straight lines which are listed in Tables 5.21, 5.22 and 5.23 are plotted versus concentration in Figures 5.22, 5.25 and 5.28.

It was observed that CO_2 formation reaches a plateau indicating that the photogeneration of CO_2 obeys a zero order kinetics and that is why in the figures y-axis is labeled as R meaning the rate of CO_2 formation.

Table 5.21. Effect of malonic acid concentration on the rate of CO_2 formation.

Equation $y=CO_2$ (µM) x=time (min)	R (µM/min)	[C] ($x10^{-3}$ M)	1/R (min/M) ($x10^4$)	1/[C] (1/M) ($x10^2$)
y=27.6+15.5x R=0.998	15.5	10	6.45	1
y=22.1+15.1x R=0.997	15.1	1.0	6.67	10
y=41.6+3.69x R=0.922	3.69	0.1	27.1	100
y=-1.39+1.61x R=0.966	1.61	0.01	62.1	1000

Table 5.22. Effect of succinic acid concentration on the rate of CO_2 formation.

Equation $y=CO_2$ (µM) x=time (min)	R (µM/min)	[C] ($x10^{-3}$ M)	1/R (min/M) ($x10^4$)	1/[C] (1/M) ($x10^2$)
y=51.9+28.2x R=0.997	28.2	10	3.54	1
y=52.6+15.6x R=0.993	15.6	1.0	6.39	10
y=96.8+4.05x R=0.827	4.05	0.1	24.4	100
y=31.6+0.941x R=0.743	0.94	0.01	106	1000

Table 5.23. Effect of adipic acid concentration on the rate of CO_2 formation.

Equation $y=CO_2$ (μM) x=time (min)	R (μM/min)	[C] ($x10^{-3}$ M)	1/R (min/M) ($x10^4$)	1/[C] (1/M) ($x10^2$)
y=-13.9+24.6x R=0.999	24.6	10	4.05	1
y=-33.7+15.1x R=0.998	15.1	1.0	6.65	10
y=-11.1+8.31x R=0.994	8.31	0.1	12.1	100
y=1.25+3.03x R=0.983	3.03	0.01	33.1	1000

The Langmuir-Hinshelwood (LH) also holds for malonic, succinic and adipic acids (Figures 5.23, 5.26, 5.29) because a plot of $1/R_{CO_2}$ versus 1/C gives a straight line where 1/k is the y intercept and 1/κk is the slope (Table 5.24).The validity of LH model confirms that the photooxidation occurs completely on the TiO_2 surface.

Table 5.24. Rate constants and adsorption equilibrium constants for acids.

Name	k(μM/min)	κ(l/μM) ($x10^3$)
Malonic Acid	8.97	21.4
Succinic Acid	13.1	7.72
Adipic Acid	15.4	24.3

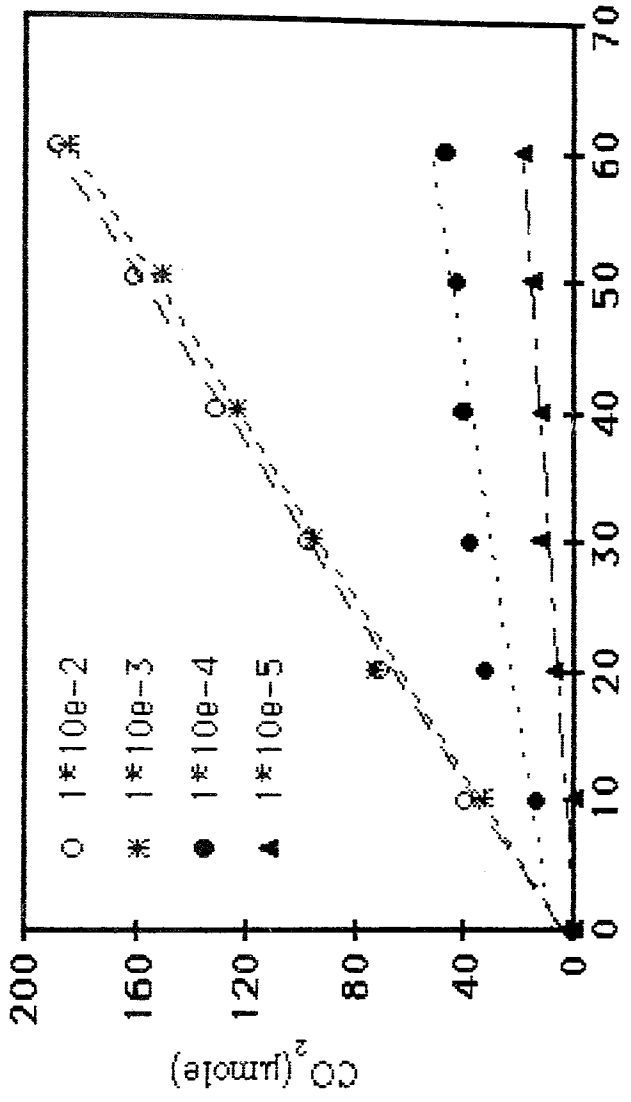

Figure 5.21. Effect of concentration on the CO_2 formation from malonic acid. Conditions: pH=3.4(natural), T=294 K, Intensity=1.81×10^{-7}einstein/sec, $[TiO_2]$=1g/L, Flow Rate=288 mL/min.

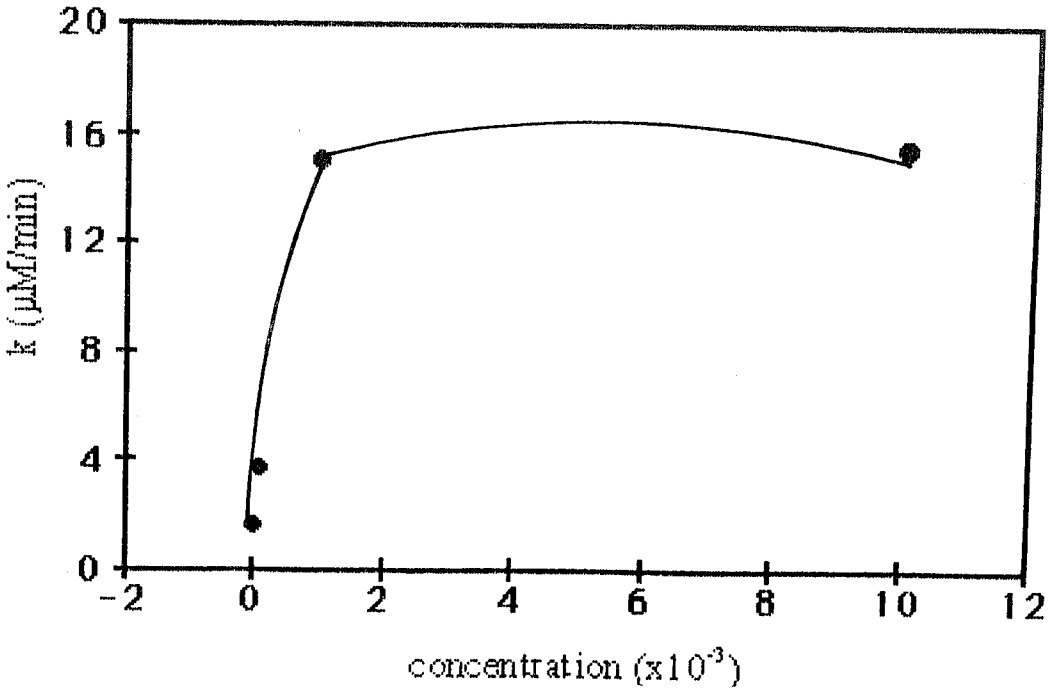

Figure 5.22. Effect of concentration on the rate of CO_2 formation from malonic acid.

Conditions: pH=3.4(natural), T=294 K, Intensity=1.81x10-7 einstein/sec, [TiO2]=1 g/L, Flow=288 mL/min.

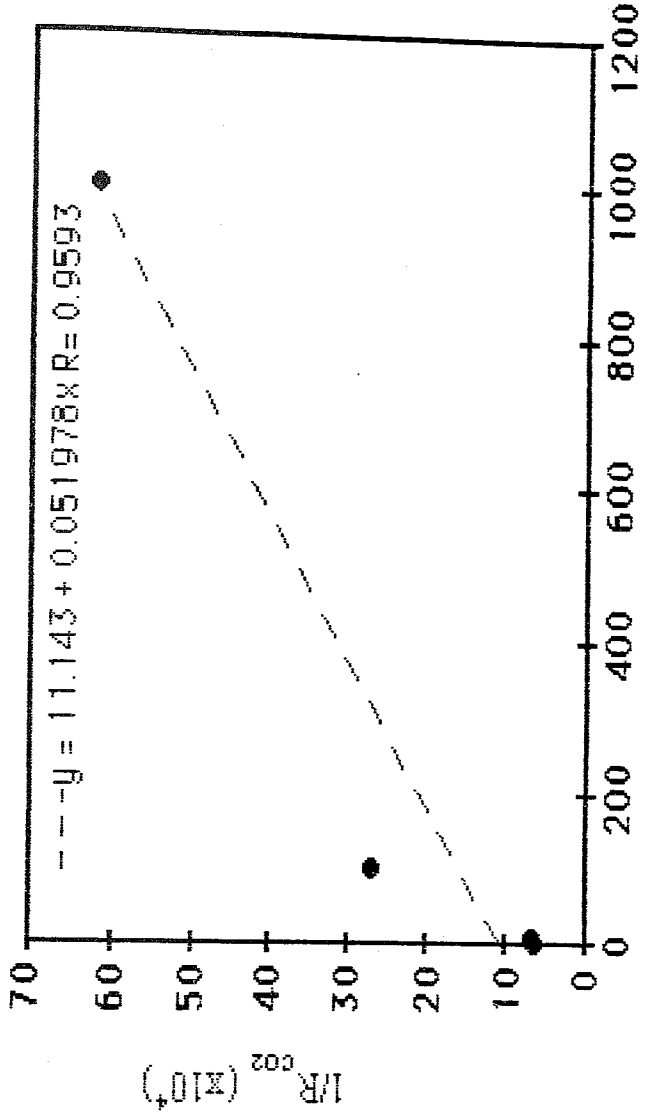

Figure 5.23. 1/Rate(CO_2) versus 1/conc for malonic acid.

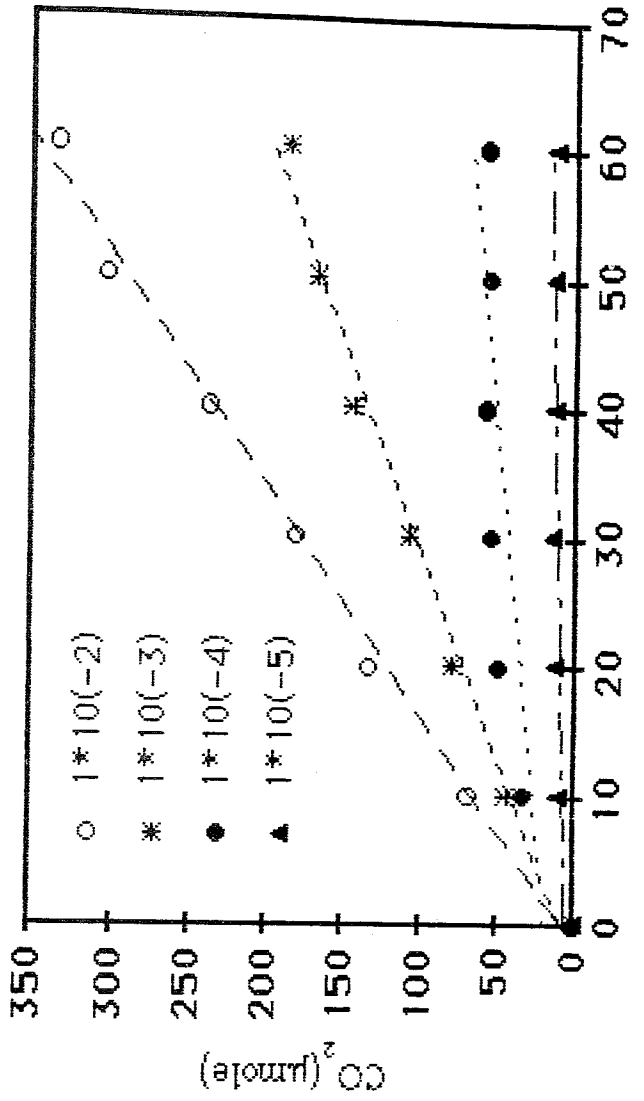

Figure 5.24. Effect of concentration on the CO_2 formation from succinic acid.
Conditions: pH=3.8(natural), T=294 K, Intensity=1.81x10-7einstein/sec,
$[TiO_2]$=1g/L,Flow=288 mL/min.

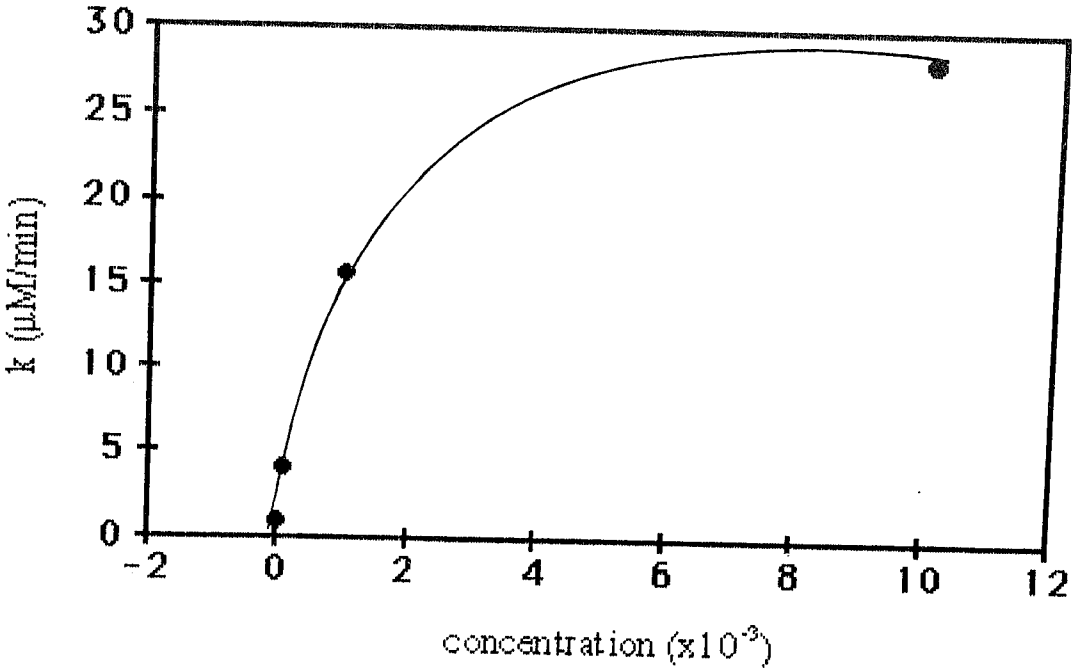

Figure 5.25. Effect of concentration on rate of CO_2 formation from succinic acid
Conditions: pH=3.8(natural), T=294 K, Intensity=1.81x10^{-7}einstein/sec,
[TiO2]=1 g/L, Flow=288 mL/min.

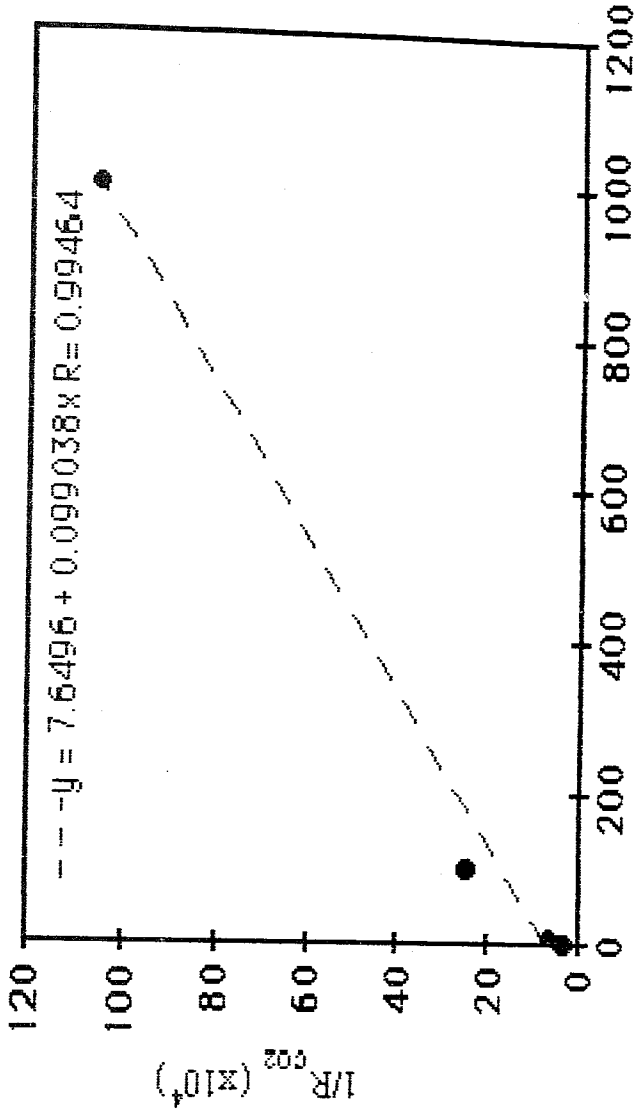

Figure 5.26. 1/Rate(CO_2) versus 1/conc for succinic acid.

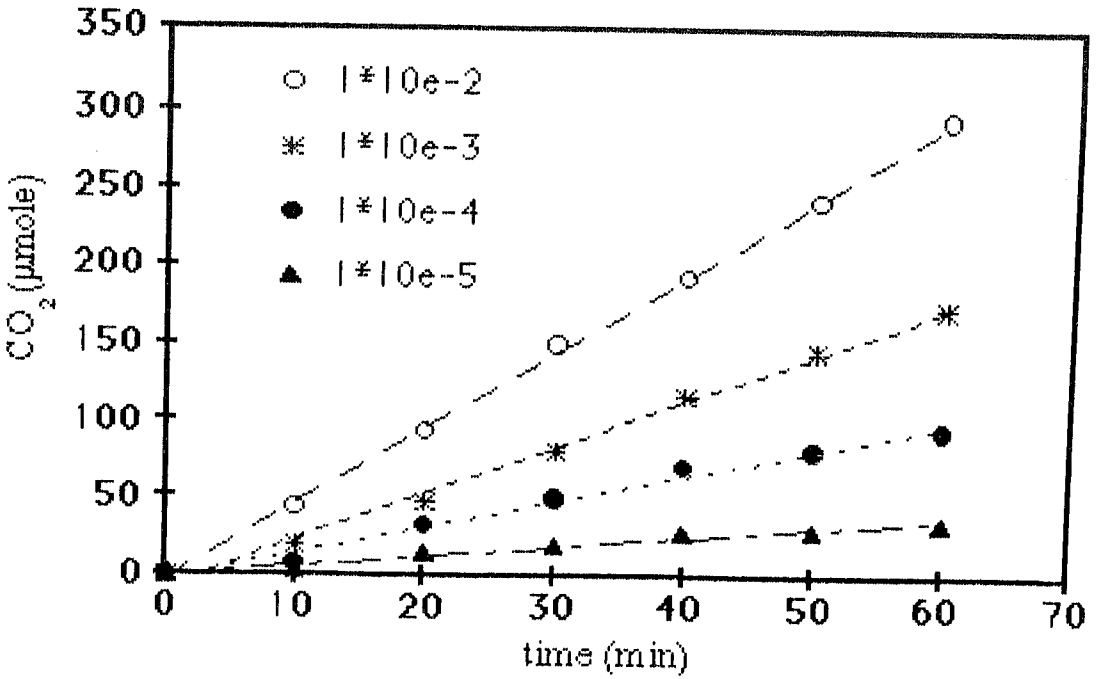

Figure 5.27. Effect of concentration on the CO_2 formation from adipic acid. Conditions: pH=3.9(natural), T=294 K, Intensity=1.81x10^{-7}einstein/sec, [TiO_2]=1 g/L, Flow Rate=288 mL/min.

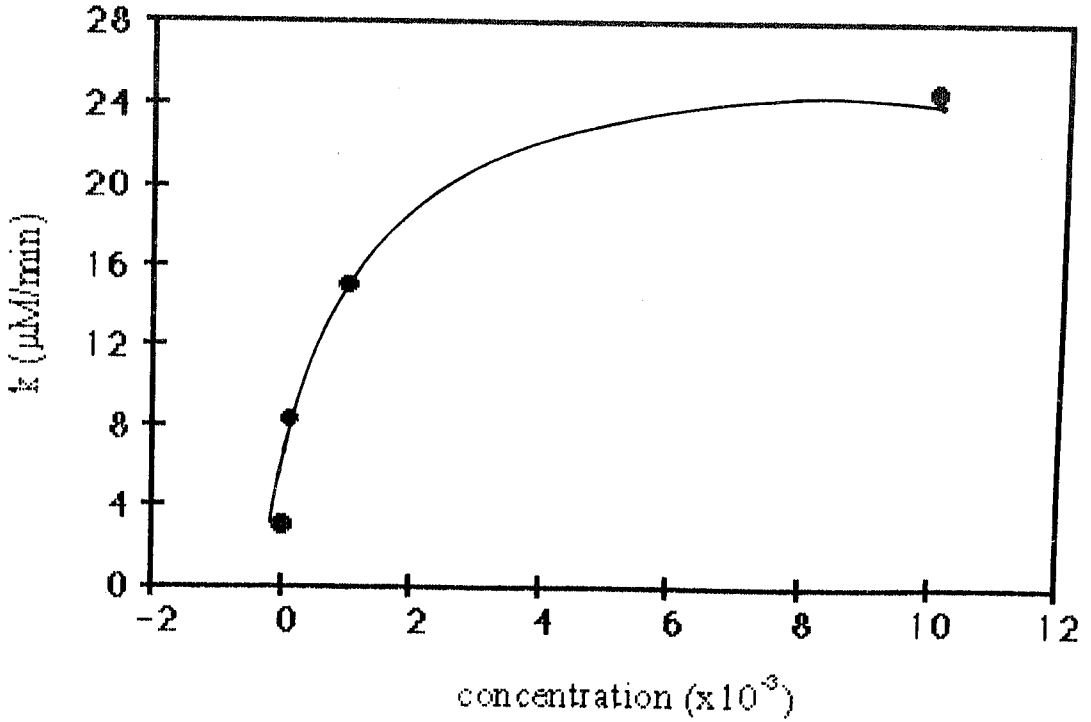

Figure 5.28. Effect of concentration on rate of CO_2 formation from adipic acid
Conditions: pH=3.9(natural), T=294 K, Intensity=1.81x10^{-7}einstein/sec,
[TiO2]=1 g/L, Flow=288 mL/min.

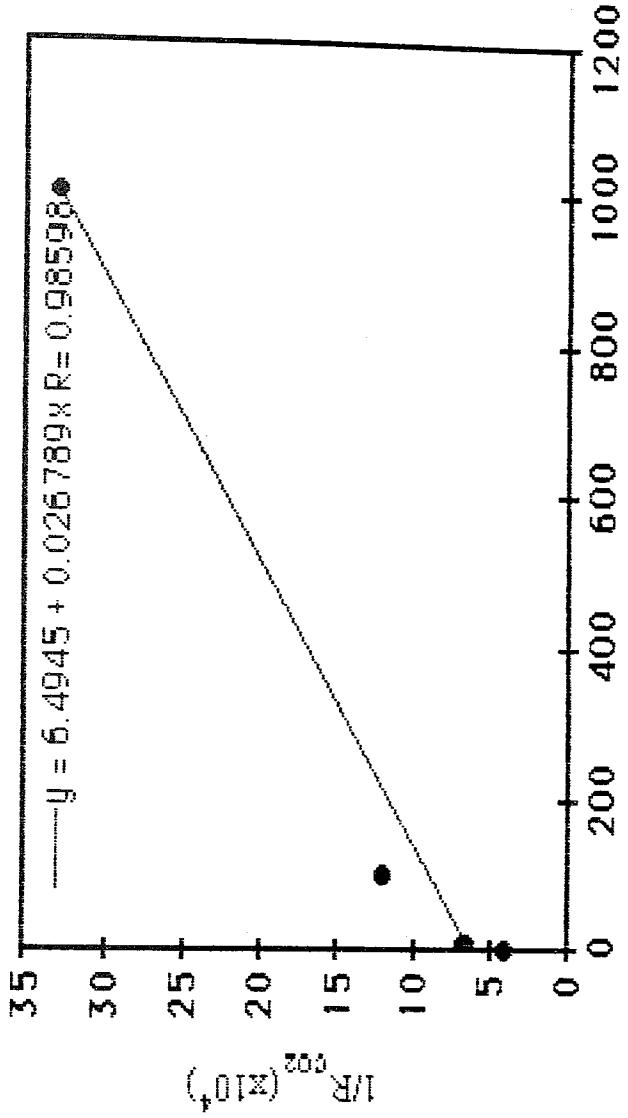

Figure 5.29. 1/Rate(CO_2) versus 1/conc for adipic acid.

5.3.5. Effect of Temperature

CO_2 formation was determined at three different temperatures (21°C, 41°C, 51°C) for each acid. Results are presented in Figure 5.30, 5.32, 5.34 and Table 5.25, 5.26, 5.27. Increases in temperature increased the CO_2 formation for all acids.

Table 5.25. Effect of temperature on the CO_2 formation from malonic acid.

Time (min)	CO_2 (µmole)		
	294 K	314 K	324 K
0	0	0	0
10	33.18	55.17	72.18
20	73.01	131.9	156.7
30	96.23	183.3	219.8
40	124.4	236.1	272.5
50	151.8	268.7	333.1
60	185.1	319.8	387.8

Table 5.26. Effect of temperature on the CO_2 formation from succinic acid.

Time (min)	CO_2 (µmole)		
	294 K	314 K	324 K
0	0	0	0
10	43.97	81.72	94.57
20	78.81	174.6	216.9
30	107.4	237.2	296.1
40	144.7	304.8	356.7
50	168.8	376.6	416.1
60	186.6	393.6	456.6

Table 5.27. Effect of temperature on the CO_2 formation from adipic acid.

Time (min)	CO_2 (µmole) 294 K	314 K	324 K
0	0	0	0
10	19.91	54.75	402.3
20	47.70	124.4	864.8
30	80.47	196.6	1165
40	116.5	243.1	1524
50	145.5	308.6	1974
60	173.8	354.2	2090

The formation of CO_2 from malonic, succinic, adipic acids was determined at three different temperatures namely 21°C, 41°C and 51°C. The correction term $\alpha(T)$ (given section 5.2.6) is calculated to take into account the decrease in the solubility of CO_2 with increasing temperature. Since most of the experiments were carried out at T=21°C, $\alpha(T)=(V_{HS}/V + V_{LP}\ K_{CO_2})$ /100 is constant and calculated as 14.02×10^{-5} mol/$[CO_2]$.

$\alpha(T)=\alpha(41°C)=(V_{HS}/V + V_{LP}\ K_{CO_2}\ T/294) / 100$

where;

V_{HS} = Volume of the head space (0.150 L)

V = Volume of one mole of gas at T=41°C and P=1 atm (27.75 L)

V_{LP} = Volume of the liquid phase (0.200 L)

K_{CO_2} = 2.3×10^{-2} mol/L atm at 41°C [46]

$\alpha(40°C)$ = 10.74×10^{-5} mol/$[CO_2]$

$\alpha(T)=\alpha(51°C)=(V_{HS}/V + V_{LP}\ K_{CO_2}\ T/294) / 100$

where;

V_{HS} = Volume of the head space (0.150 L)

V = Volume of one mole of gas at T=51°C and P=1 atm (26.57 L)

V_{LP} = Volume of the liquid phase (0.200 L)

K_{CO_2} = 1.90×10^{-2} mol /L atm at 51°C [46]

$\alpha(54°C)$ = 9.83×10^{-5} mol/$[CO_2]$.

The Arrhenious data are given in Tables 5.28, 5.29, 5.30 and are plotted as $\ln(\alpha(T)xk_{CO_2})$ versus 1/T in Figures 5.31, 5.33, 5.35 whose slopes lead to the calculation of activation energy as 9.99, 15.59, and 14.38 kj/mole for malonic, succinic, and adipic acids respectively.

Table 5.28. Arrhenious data for malonic acid.

Equation $y=CO_2(\mu M)$ x=time (min)	$\ln(\alpha(T)xk_{CO_2})$	$1/T\ K^{-1}(x10^{-3})$
y=22.05+15.06x R=0.9971	-19.98	3.401
y=54.96+26.62x R=0.9941	-19.83	3.181
y=65.33+32.16x R=0.9971	-19.57	3.091

Table 5.29 Arrhenious data for succinic acid.

Equation $y=CO_2(\mu M)$ x=time (min)	$\ln(\alpha(T)xk_{CO_2})$	$1/T\ K^{-1}(x10^{-3})$
y=52.66+15.63x R=0.9931	-19.94	3.401
y=102.1+33.94x R=0.9901	-19.43	3.181
y=158.9+38.44x R= 0.9851	-19.39	3.091

Table 5.30. Arrhenious data for adipic acid.

Equation $y=CO_2(\mu M)$ x=time (min)	$\ln(\alpha(T)xk_{CO_2})$	$1/T\ K^{-1}(x10^{-3})$
y=-33.70+15.02x R=0.9981	-19.98	3.401
y=10.66+30.16x R= 0.9981	-19.55	3.181
y=66.51+35.98x R=0.9941	-19.46	3.091

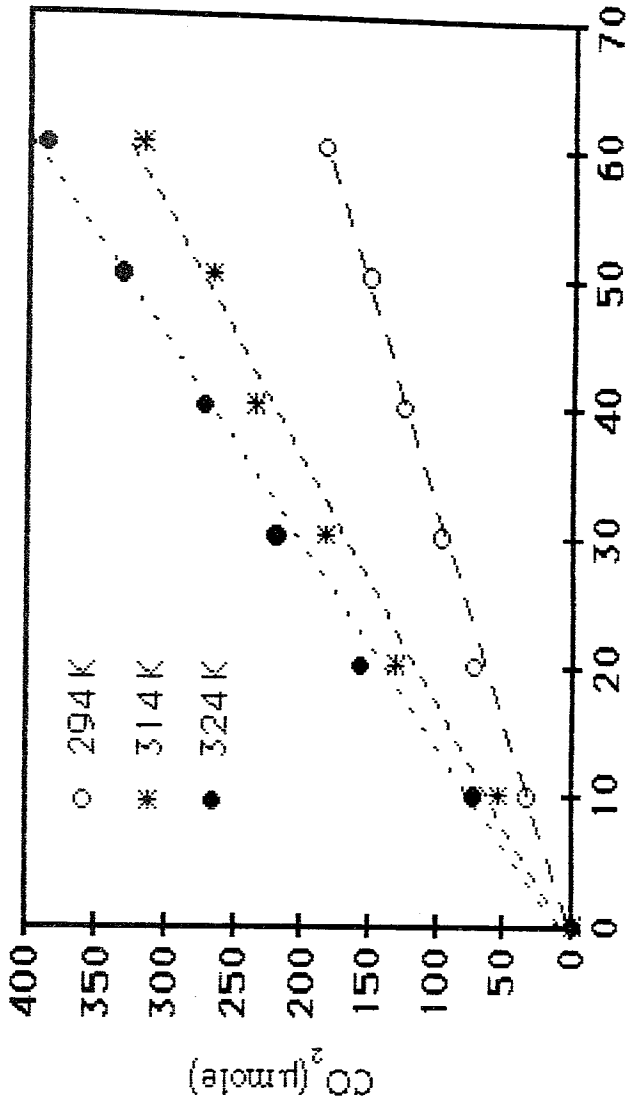

Figure 5.30. Effect of temperature on the CO_2 formation from malonic acid. Conditions: pH=3.4(natural), [acid]=1x10-3 M, Intensity=1.81x10-7einstein/sec, $[TiO_2]$=1 g/L, Flow=288 mL/min.

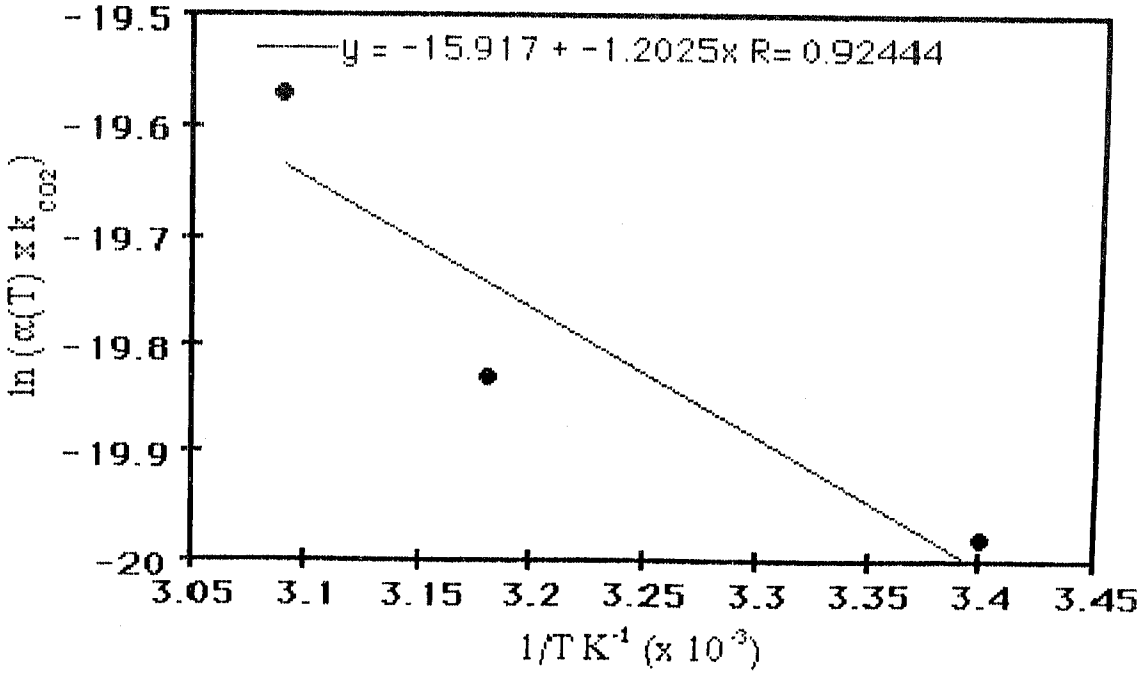

Figure 5.31. Arrhenius plot for malonic acid.
Conditions: pH=3.4, [acid]=1x10^{-3} M, Intensity=1.81x10^{-7}einstein/sec,
[TiO2]=1 g/L Flow=288 mL/min.

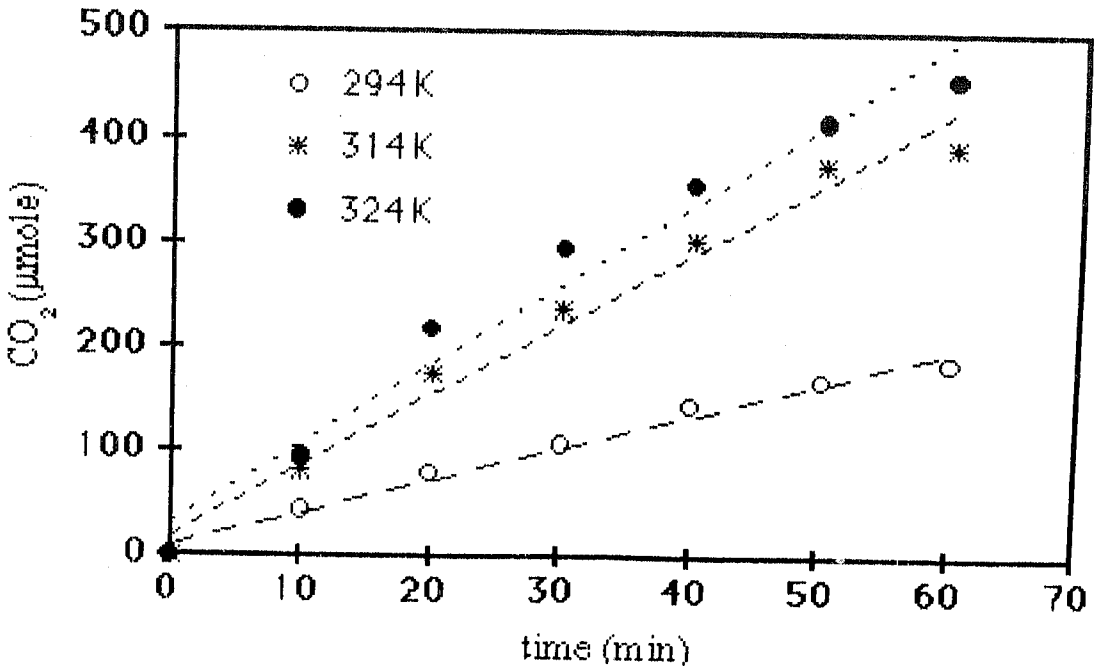

Figure 5.32. Effect of temperature on the CO_2 formation from succinic acid
Conditions: pH=3.8(natural), [acid]=$1x10^{-3}$ M, Intensity=$1.81x10^{-7}$einstein/sec,
[TiO_2]=1 g/L, Flow=288 mL/min.

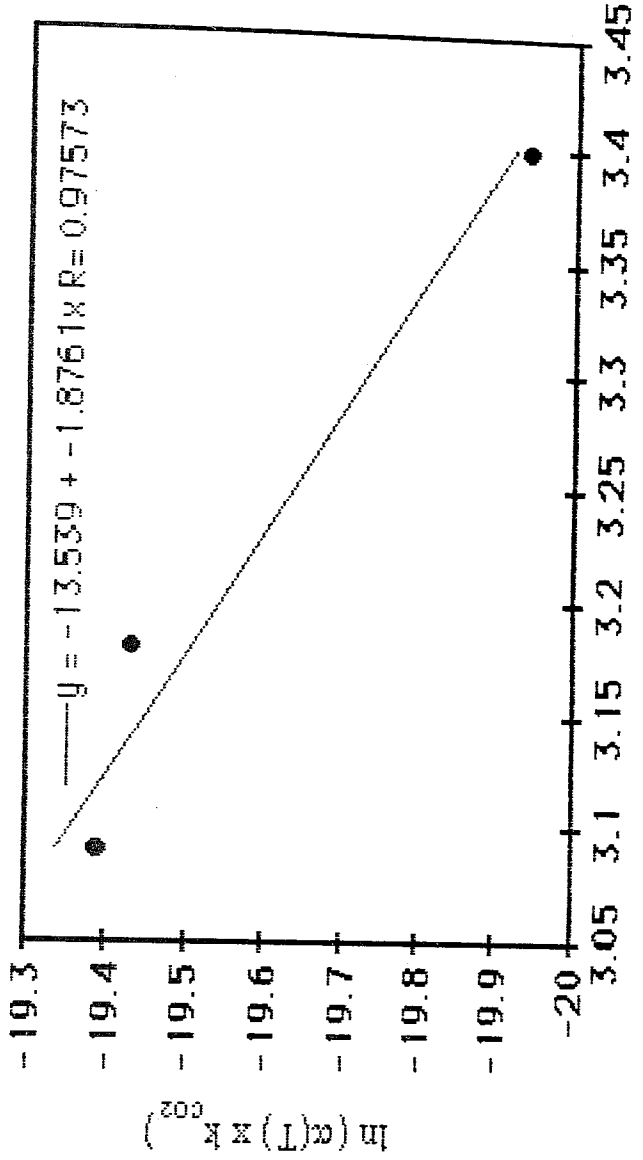

Figure 5.34. Arrhenius plot for succinic acid
Conditions: pH=3.8, [acid]=1x10-3 M, Intensity=1.81x10-7einstein/sec, [TiO2]=1 g/L, Flow=288 mL/min.

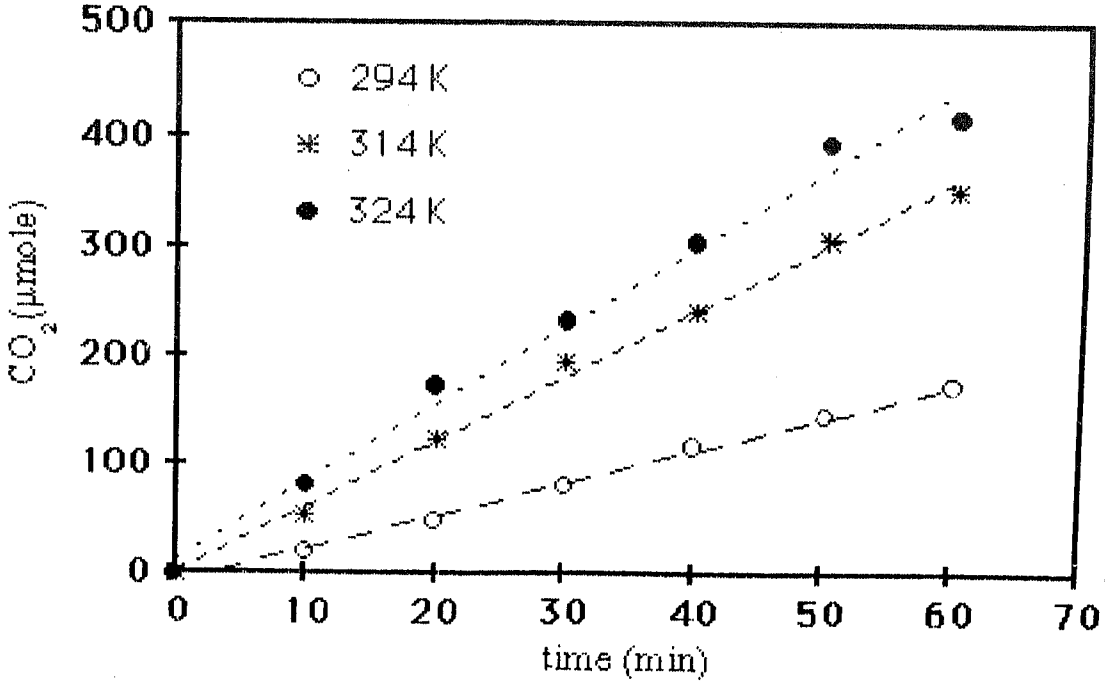

Figure 5.34. Effect of temperature on the CO_2 formation from adipic acid
Conditions: pH=3.9 (natural), [acid]=$1x10^{-3}$ M, Intensity=$1.81x10^{-7}$einstein/sec,
[TiO_2]=1 g/L, Flow=288 mL/min.

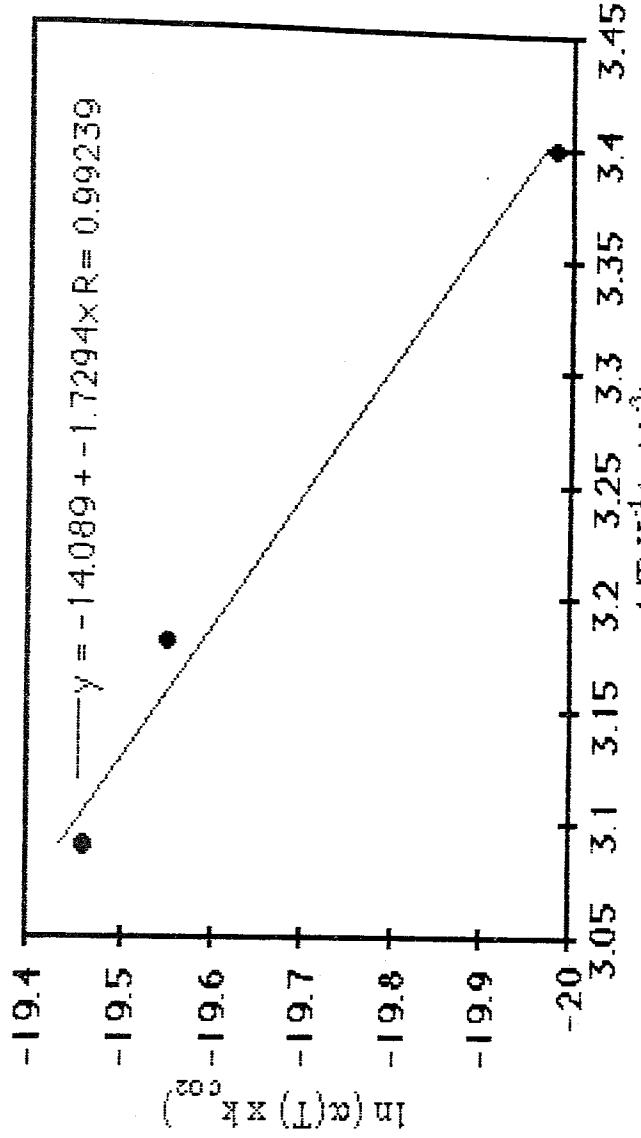

Figure 5.35. Arrhenius plot for adipic acid
Conditions: pH=3.9, [acid]=1x10-3 M, Intensity=1.81x10-7einstein/sec, [TiO2]=1g/L , Flow=200 rpm

5.3.6. Effect of Light Intensity

The irradiation intensity is another important factor for the overall mineralization efficiency, therefore, depending on the intensity of the lamps CO_2 formation for each acid was investigated. When number of lamps were increased higher CO_2 formation was observed, results were given in given in Figure 5.29, Figures 5.36, 5.39, 5.42 and Tables 5.31, 5.32, 5.33.

Table 5.31. Effect of light intensity on CO_2 formation from malonic acid.

time (min)	CO_2(µmole)					
	No=1	No=2	No=3	No=4	No=5	No=6
0	0	0	0	0	0	0
10	2.49	12.8	15.3	19.5	28.2	33.1
20	10.7	34.1	40.6	52.3	65.1	73.1
30	19.5	53.5	55.5	74.3	92.1	96.2
40	31.5	77.5	80.1	100	125	124
50	43.9	91.6	107	129	141	151
60	49.7	111	118	143	158	185

Table 5.32. Effect of light intensity on CO_2 formation from succinic acid.

time (min)	CO_2(µmole)					
	No=1	No=2	No=3	No=4	No=5	No=6
0	0	0	0	0	0	0
10	12.8	24.4	28.2	27.4	24.4	43.9
20	27.3	51.8	54.7	63.1	66.7	78.8
30	43.1	77.9	87.5	97.5	106	107
40	58.1	104	119	137	125	144
50	73.1	134	140	178	151	168
60	90.2	160	165	195	177	186

Table 5.33. Effect of light intensity on CO_2 formation from adipic acid.

time (min)	CO_2(µmole)					
	No=1	No=2	No=3	No=4	No=5	No=6
0	0	0	0	0	0	0
10	0	3.73	8.71	16.5	17.4	19.9
20	5.39	18.6	33.1	39.4	50.6	47.7
30	12.4	33.6	55.1	67.2	71.7	80.4
40	22.4	50.1	74.6	99.9	102	116
50	32.7	68.8	99.5	116	135	145
60	37.3	78.4	119	141	156	174

When reaction rates were plotted against the intensities of the lamps no linear correlation was observed (Figures 5.37, 5.40, 5.43), however, a straight line was obtained when the square root of intensities of the lamps was plotted (Figures 5.38, 5.41, 5.44). A similar linear relationship at high intensities ($>2x10^{-5}$ Einstein/m^2s)was obtained by Okamoto for photooxidation of phenol, but at lower intensities ($<1x10^{-5}$ Einstein/m^2s) a linear relationship between the rate of degradation and intensity was reported.[26]. These results can be explained in terms of an increased importance of the electron/hole recombination at higher light intensities.

Table 5.34. Effect of light intensity on the rate of CO_2 formation for malonic. acid.

Equation $y=CO_2$ (μM) x=time (min)	k (μM/min)	Intensity einstein/sec ($x10^{-7}$)	Intensity$^{1/2}$ (einstein/sec)$^{1/2}$ ($x10^{-4}$)
y=-22.6+4.51x R=0.989	4.51	0.311	1.73
y=-14.5+9.54x R=0.998	9.54	0.612	2.47
y=-11.5+10.3x R=0.997	10.3	0.871	2.95
y=-2.74+12.4x R=0.998	12.4	1.16	3.41
y=28.6+13.5x R=0.992	13.5	1.48	3.84
y=22.1+15.1x R=0.998	15.1	1.81	4.25

Table 5.35. Effect of light intensity on the rate CO_2 formation for succinic acid.

Equation $y=CO_2$ (µM) x=time (min)	k (µM/min)	Intensity einstein/sec ($x10^{-7}$)	Intensity$^{1/2}$ (einstein/sec)$^{1/2}$ ($x10^{-4}$)
y=-8.06+7.51x R=0.999	7.51	0.251	1.59
y=-8.45+13.4x R=0.999	13.4	0.542	2.34
y=4.88+14.1x R=0.998	14.1	0.851	2.91
y=-16.1+17.1x R=0.997	17.1	1.16	3.41
y=12.6+15.1x R=0.994	15.1	1.48	3.84
y=52.6+15.6x R=0.993	15.6	1.81	4.25

Table 5.36. Effect of light intensity on the rate of CO_2 formation from adipic acid.

Equation $y=CO_2$ (μM) x=time (min)	k (μM/min)	Intensity einstein/sec ($x10^{-7}$)	Intensity$^{1/2}$ (einstein/sec)$^{1/2}$ ($x10^{-4}$)
y=-25.4+3.47x R=0.978	3.47	0.301	1.59
y=-31.6+7.08x R=0.992	7.08	0.611	2.34
y=-32.1+10.3x R=0.996	10.3	0.872	2.91
y=-23.4+12.2x R=0.997	12.2	1.16	3.41
y=-24.4+13.5x R=0.998	13.5	1.48	3.84
y=-33.73+15.1x R=0.998	15.1	1.81	4.25

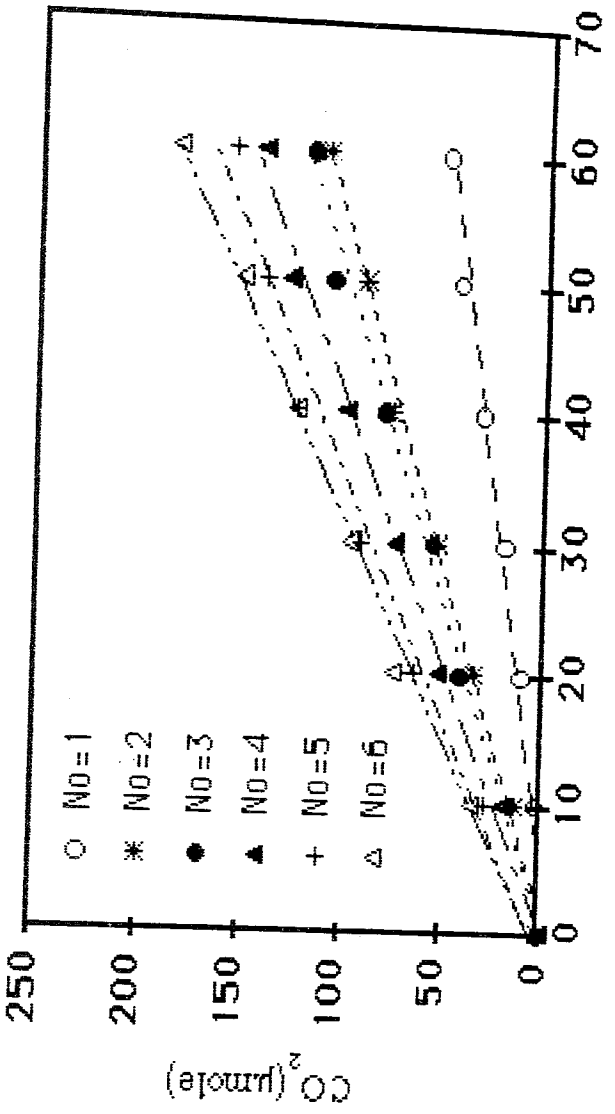

Figure 5.36. CO_2 formation from malonic acid as a function of number of lamps
Condition: pH=3.4 (natural), [acid]=1x10^{-3} M, T=294 K, [TiO_2]=1 g/L,
Flow=288 mL/min.

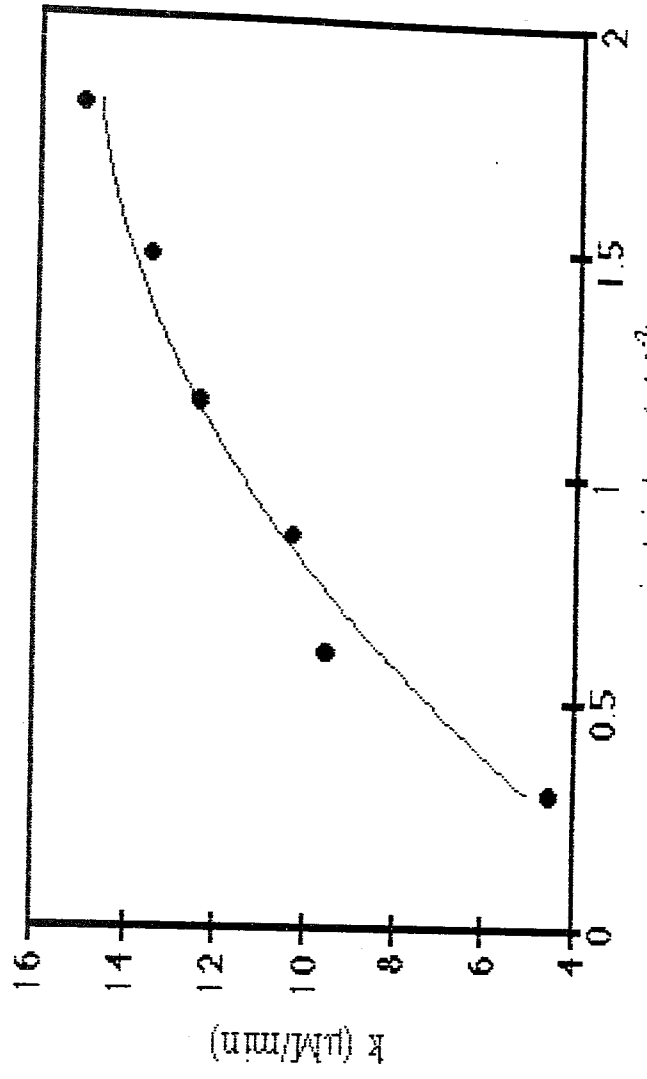

Figure 5.37. Light intensity effect on the rate of CO_2 formation from malonic acid
Conditions: pH=3.4(natural), [acid]=1x10-3 M, T=294 K, [TiO2]=1 g/L,
Flow=288 mL/min.

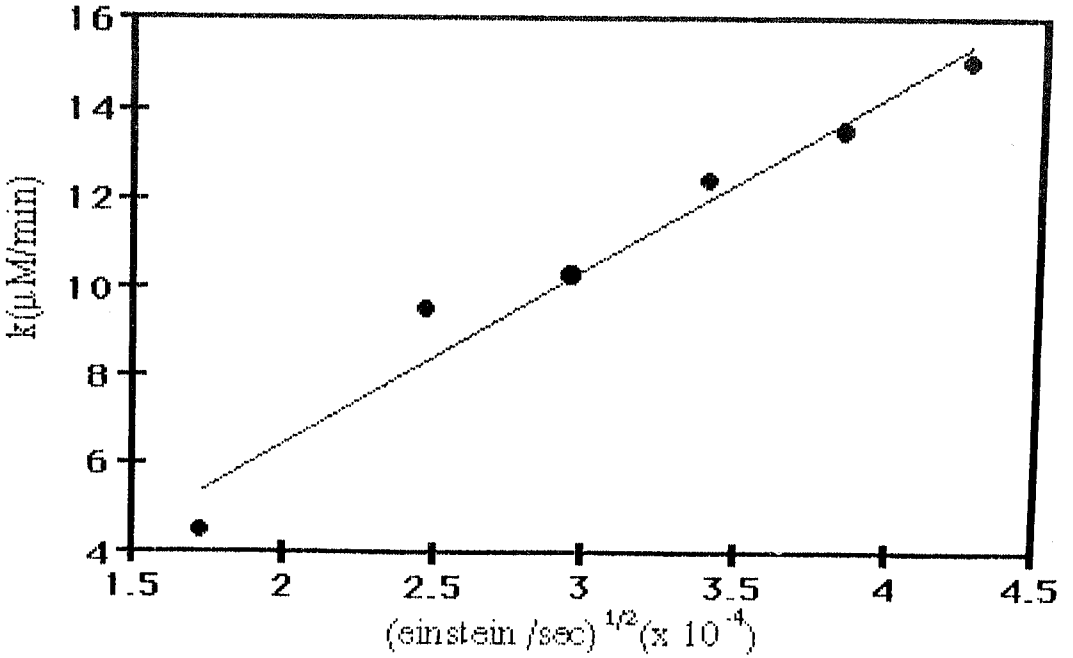

Figure 5.38. Effect of square root of light intensity on CO_2 formation from malonic acid

Conditions: pH=3.4 (natural), [acid]=1x10^{-3} M, T=294 K, [TiO_2]=1 g/L, Flow=288 mL/min.

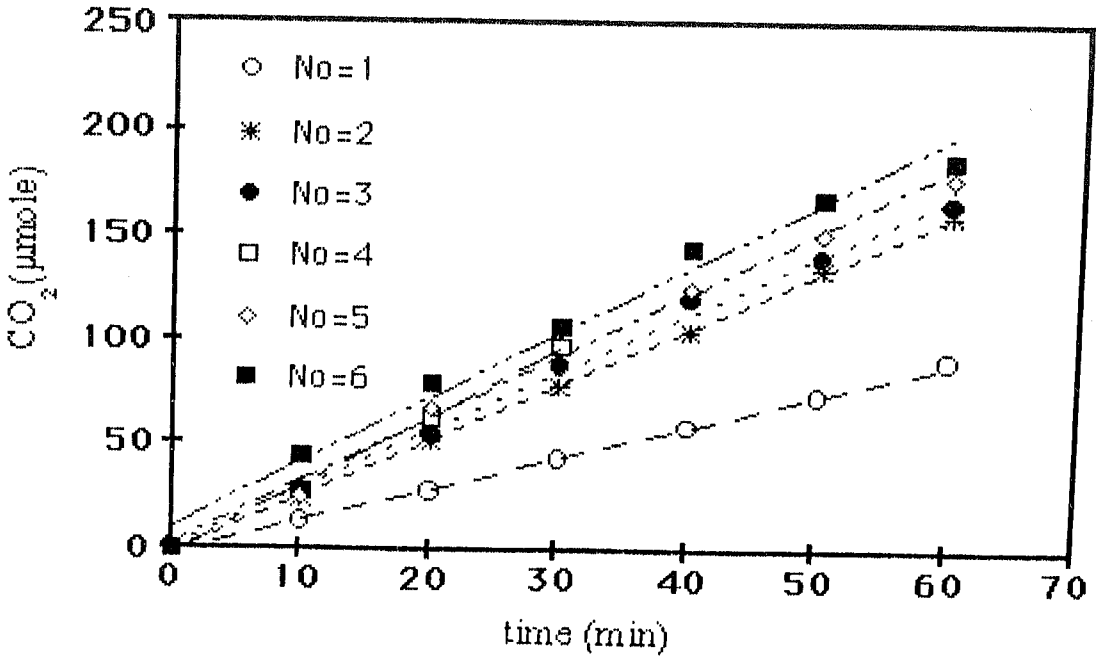

Figure 5.39. CO_2 formation from succinic acid as a function of number of lamps
Condition: pH=3.8 (natural), [acid]=1x10^{-3} M, T=294 K, [TiO_2]=1 g/L,
Flow=288 mL/min.

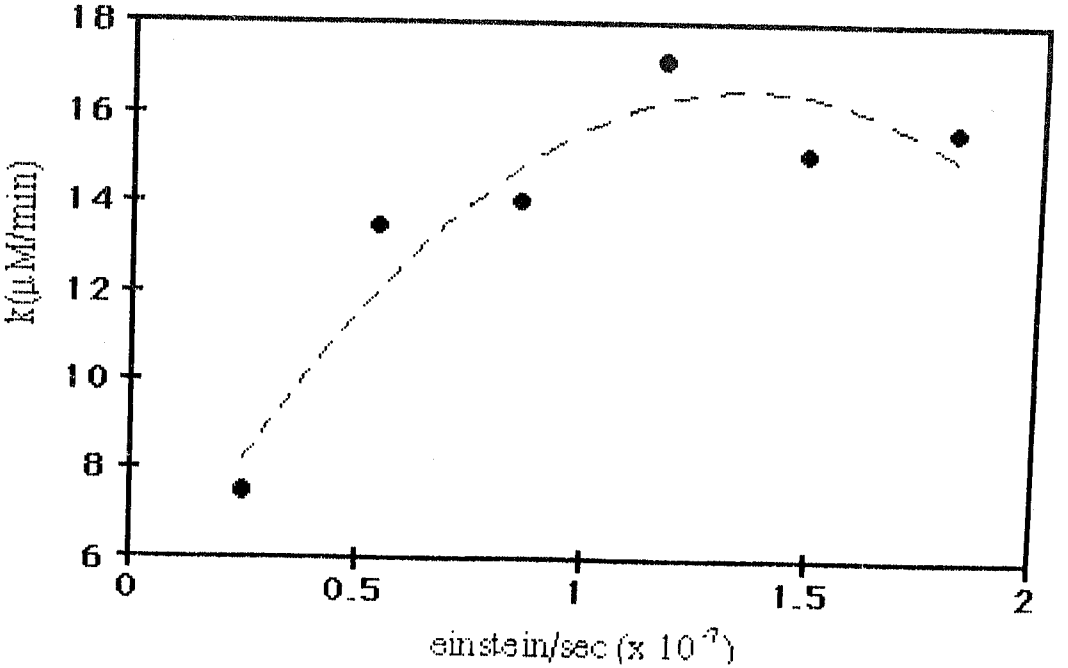

Figure 5.40. Light intensity effect on the rate of CO_2 formation from succinic acid
Conditions: pH=3.8(natural), [acid]=1x10^{-3} M, T=294 K, [TiO_2]=1 g/L,
Flow=288 mL/min.

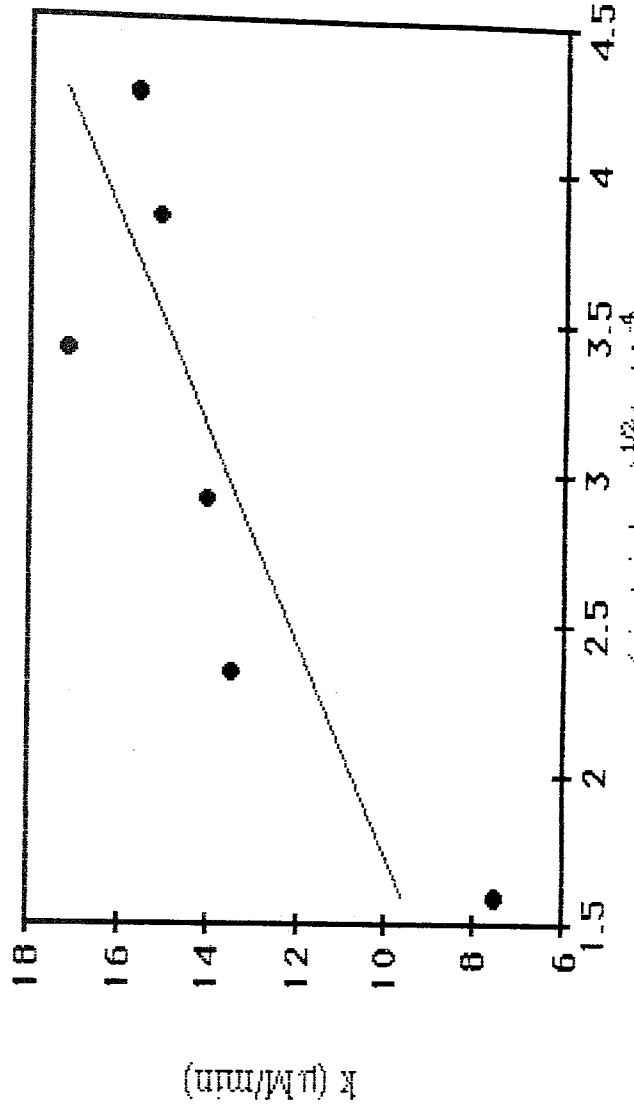

Figure 5.41. Effect of square root of light intensity on CO_2 formation from succinic acid

Conditions: pH=3.8 (natural), [acid]=1x10^{-3} M, T=294 K, [TiO_2]=1 g/L, Flow=288 mL/min.

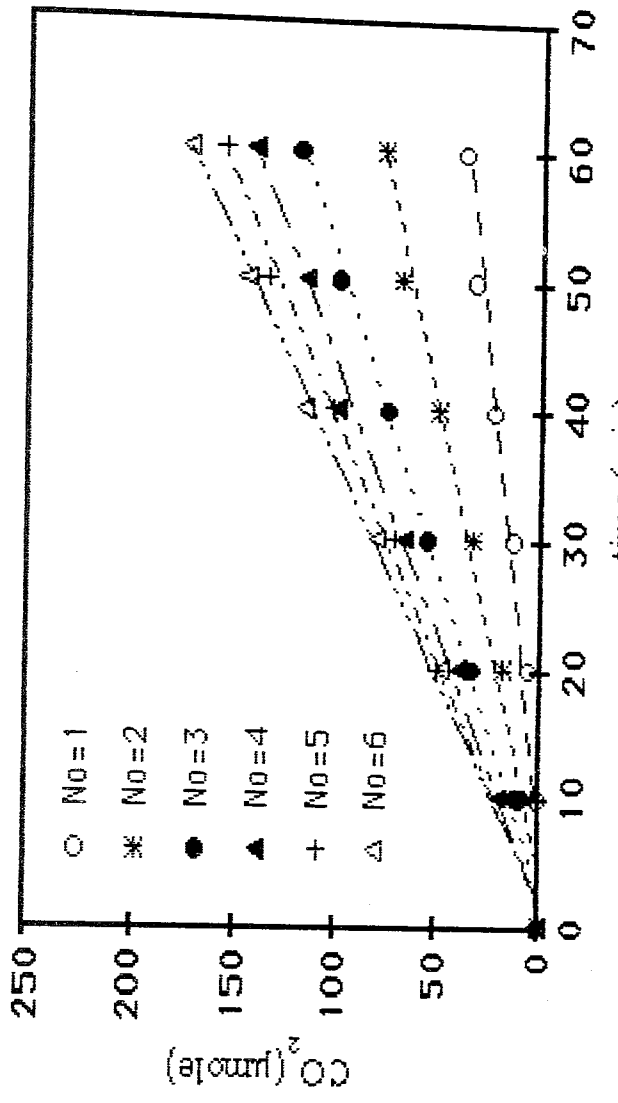

Figure 5.42. CO_2 formation from adipic acid as a function of number of lamps
Condition: pH=3.9 (natural), [acid]=1x10-3 M, T=294 K, [TiO_2]=1g/L,
Flow=288 mL/min.

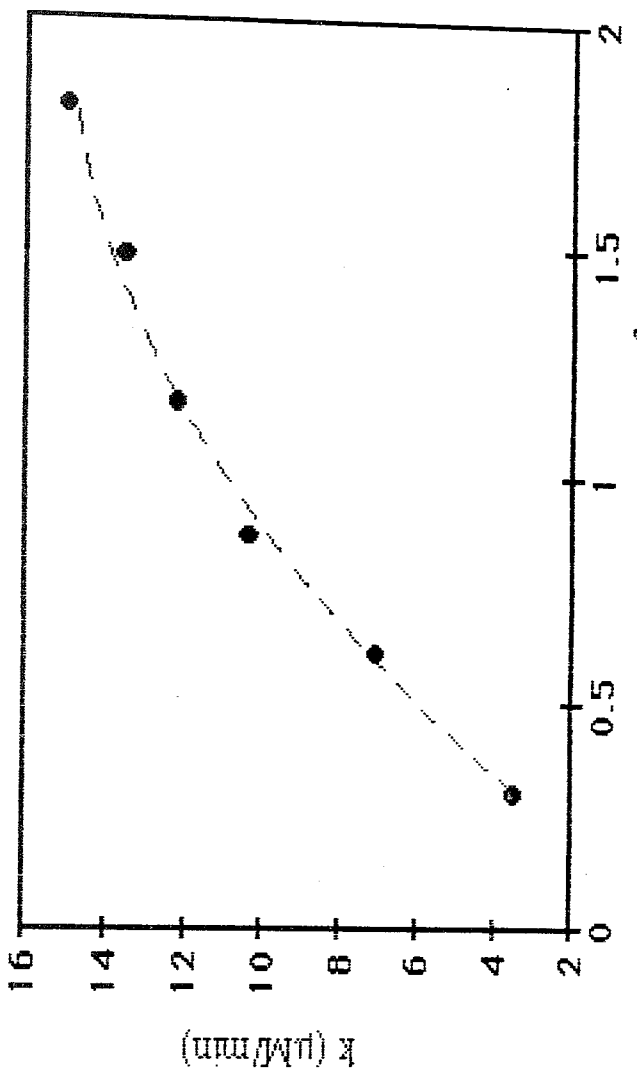

Figure 5.43. Light intensity effect on the rate of CO_2 formation from adipic acid
Conditions: pH=3.9 (natural), [acid]=1x10-3 M, T=294 K, [TiO2]=1 g/L,
Flow=283 mL/min.

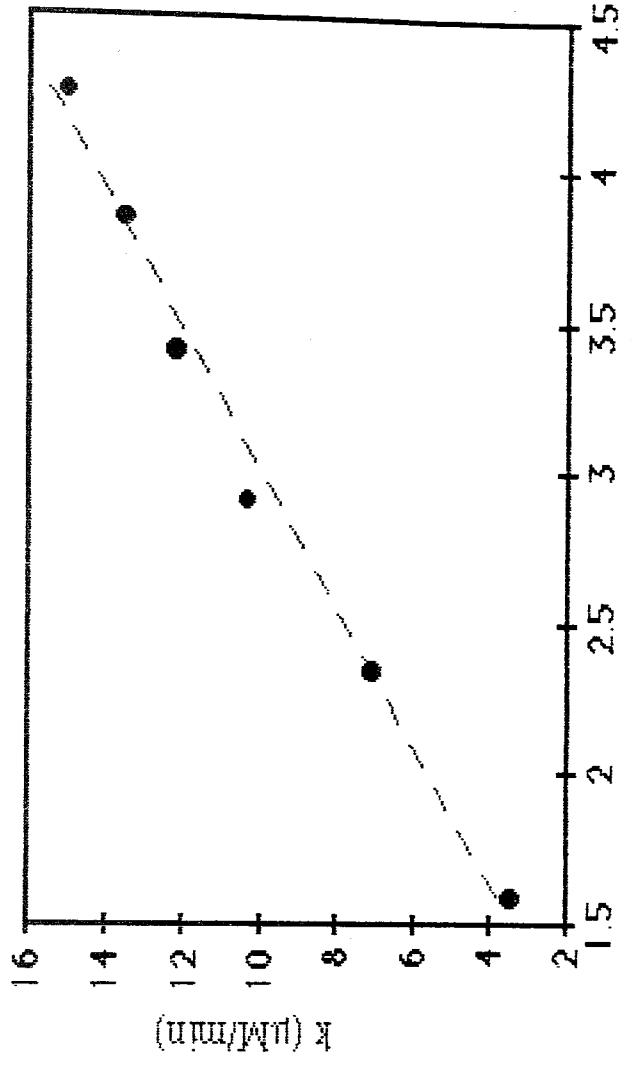

Figure 5.44. Effect of square root of light intensity on CO_2 formation from adipic acid
Conditions: pH=3.9 (natural), [acid]=1x10^{-3} M, T=294 K, [TiO_2]=1g/L, Flow=288 mL/min.

5.4. A Postulated Mechanism

The proposed reactions involved in the photooxidation of dicarboxylic acids (Table 5.37) [47,48] were given as input to a program in IBM and the following mechanisms were estimated.

Table 5.37. Proposed reactions.

$TiO_2 + h\nu \xrightarrow{k_1} e^- + h^+$
$DCA \xrightarrow{k_2} DCA^- + H^+$
$DCA^- + H^+ \xrightarrow{k_3} DCA$
$DCA^- + h^+ \xrightarrow{k_4} DCA^{\cdot}$
$DCA^{\cdot} \xrightarrow{k_5} R^{\cdot} + CO_2$
$H^+ + e^- \xrightarrow{k_6} H^{\cdot}$
$O_2 + e^- \xrightarrow{k_7} O_2^{\cdot -}$
$O_2^{\cdot -} + H^{\cdot} \xrightarrow{k_8} HO_2^-$
$HO_2^- + HO_2^- \xrightarrow{k_9} O_2 + H_2O_2$
$H_2O_2 + e^- \xrightarrow{k_{10}} OH^{\cdot} + OH^-$
$DCA + OH^{\cdot} \xrightarrow{k_{11}} R^{\cdot} + H2O$
$R^{\cdot} + H^{\cdot} \xrightarrow{k_{12}} RH$

$$d[TiO_2]/dt = -k_1 [TiO_2] (h\upsilon) = \Phi_0 I_a$$

$$d(e^-)/dt = -k_6 [H^+](e^-) - k_7 [O_2] (e^-) - k_{10} [H_2O_2] (e^-) + k_1 [TiO_2] (h\upsilon)$$

$$d(h^+)/dt = -k_4 [DCA^-] (h^+) + k_1 [TiO_2] (h\upsilon)$$

$$d[DCA]/dt = -k_2 [DCA] - k_{11} [DCA] [OH^\cdot] + k_3 [DCA^-] [H^+]$$

$$d[DCA^-]/dt = -k_3 [DCA^-] [H^+] - k_4 [DCA^-] (h^+) + k_2 [DCA]$$

$$d[H^+]/dt = -k_3 [DCA^-] [H^+] - k_6 [H^+] (e^-) + k_2 [DCA]$$

$$d[DCA^\cdot]/dt = - k_5 [DCA^\cdot] + k_4 [DCA^-] (h^+)$$

$$d[R^\cdot]/dt = -k_{12} [R^\cdot] [H^\cdot] + k_5 [DCA^\cdot] + k_{11} [DCA] [OH^\cdot]$$

$$d[CO_2]/dt = k_5 [DCA^\cdot]$$

$$d[H^\cdot]/dt = - k_8 [O_2^{\cdot-}] [H^\cdot] - k_{12} [R^\cdot] [H^\cdot] + k_6 [H^+] (e^-)$$

$$d[O_2]/dt = - k_7 [O_2] (e^-) + k_9 [HO_2^-] [HO_2^-]$$

$$d[O_2^{\cdot-}]/dt = - k_8 [O_2^{\cdot-}] [H^\cdot] + k_7 [O_2] (e^-)$$

$$d[HO_2^-]/dt = -2 k_9 [HO_2^-] [HO_2^-] + k_8 [O_2^{\cdot-}] [H^\cdot]$$

$$d[H_2O_2]/dt = - k_{10} [H_2O_2] (e^-) + k_9 [HO_2^-] [HO_2^-]$$

$$d[OH^\cdot]/dt = - k_{11} [DCA] [OH^\cdot] + k_{10} [H_2O_2] (e^-)$$

$$d[OH^-] / dt = k_{10} [H_2O_2] (e^-)$$

$$d[H_2O] / dt = k_{11} [DCA] [OH^\cdot]$$

$$d[RH] / dt = k_{12} [R^\cdot] [H^\cdot]$$

As a result the CO_2 formation rate and the quantum yield are calculated accordingly as:

$$\mathbf{R_{CO_2} = d[CO_2] / dt = \Phi_0 I_a}$$

$$\mathbf{Mean\ \Phi_0} = 0.43 \times 10^{-6}$$

VI. CONCLUSION

Irradiation of TiO_2 particles with light of wavelength about 380 nm promotes electrons from the valence band leaving positively charged holes behind. These electrons and holes both react with water and oxygen dissolved in it to create radicals that are able to oxidize toxic chemicals into a safe form.

In this study photooxidation of three different dicarboxylic acids namely malonic, succinic and adipic acids as well as phthalic anhydride were investigated, whose results can be classified as follows:

1) Effect of pH: Malonic and succinic acids were most efficient in CO_2 formation at neutral pH's. The same behavior was also observed for phthalic anhydride, however, adipic acid represented highest efficiency at its natural pH.

2) Effect of concentration: The obtained Langmuir type plot confirmed that the photooxidation reaction takes place on the surface of the TiO_2.

3) Effect of temperature: Taking into consideration that increasing temperature drastically increases the rate of CO_2 formation, the activation energy was calculated for each compound .

4) Effect of intensity: By increasing the number of the lamps the rate of CO_2 formation was increased linearly But it should be taken into account that at high intensities the probability of electron/hole recombination also increases which inhibits this linearity. In this case CO_2 formation against the square root of intensity can be plotted.

5) Effect of irradiation time: It observed that one can increase the rate of CO_2 formation by increasing the irradiation time, however, there is a limit beyond which CO_2 would be constantly evolved.

Percent CO_2 formation was calculated for each compound by the ratio between experimentally obtained CO_2 and theoretically found CO_2 (complete conversion to CO_2 was assumed). Since hundred percent CO_2 was not obtained, some intermediates can be expected, such as lower

hydrocarbons like methane, ethane, ethylene, butane, for acids, and benzoic acid for phthalic anhydride.

The percent CO_2 formations for malonic, succinic and adipic acids as well as phthalic anhydride are listed in Table 6.1.

Table 6.1. Degradation percentages after 160 minutes of irradiation.

Name	Percent CO_2 Formation
Malonic Acid	53
Succinic Acid	43
Adipic Acid	49
Phthalic Anhydride	10

BIBLIOGRAPHY

1. Matthews, R.W, and S.R.McEvoy, "Photocatalytic Degradation of Phenol in Presence of Near UV Illuminated TiO_2," Journal of Photochemistry and Photobiology A: Chemistry, Vol. 64, pp. 231-246, 1992.

2. Brezova, V., S.Vodny, M.Ceppan, and L.Lapcik, "Photocatalytic Oxidation of 2- Ethoxyethanol in a Water Suspension in TiO_2," Journal of Photochemistry and Photobiology A: Chemistry, Vol. 56, pp. 125-134, 1991.

3. Selafani, A., L.Palmisano, and M.Schiavello, "Influence of the Preparation Methods of TiO_2 on the Photocatalytic Degradation of Phenol in Aqueous Dispersion," Journal of Physical Chemistry, Vol. 94, pp. 829-832, 1990.

4. Bahnemann, D.W., J.Monig, and R.Chapman, "Efficient Photocatalysis of the Irreversible One-Electron and Two Electron Reduction of Haloethane on Platinated Colloidal TiO_2 in Aqueous Suspension," Journal of Phsical Chemistry, Vol. 91, pp. 3782-3788, 1987.

5. Harada, K., T.Hisanaga, and K.Tanaka," Photocatalytic Degradation of Organophosphorous Insecticides in Aqueous Semiconductor Suspension," Water Research, Vol. 24, pp. 1415-1417, 1990.

6. Fujishima, A., and K.Honda, "Electrochemical Photolysis of Water at a Semiconductor Electrode," Nature, Vol. 238, pp. 37-38, 1972.

7. Fox, M.A., and M.T.Dulay, "Heterogeneous Phototcatalysis," Chemical Rewievs, Vol. 93, pp. 341-357, 1993.

8. Finklea, H.O., Semiconductor Electrodes, Amsterdam: Elsevier Science Publishers B.V., 1988.

9. Finklea, H.O., "Photoelectrochemistry: Introductory Concepts," Journal of Chemical Education, Vol. 60, pp. 325-326, 1983.

10. Ward, M.D., and A.J.Bard, "Phototcurrent Enhancement via Trapping of Photogenerated Electrons of TiO_2 Particles," Journal of Physical Chemistry, Vol. 86, pp. 3599-3605, 1982.

11. Fox, M.A., and C.C.Chen, " Photocatalyzed Mechanistic Features of the Semiconductor Olefin-Two Carbonyl Oxidation Cleavage," Journal of American Chemical Society, Vol. 103, pp. 6750-6758, 1981.

12. Faust, B.C., M.R.Hoffmann,, and D.W.Bahnemann, "Photocatalytic Oxidation of SO_2 in Aqueous Suspensions of Fe_2O_3," Journal of Physical Chemistry, Vol. 93, pp. 6371-6381, 1989.

13. Official Monographs, USP XXII, 1990.

14. Morrissey, C.J., Mineral Specimens, New York: Elsevier, 1968.

15. Mellor, J.W., A Comprehensive Treatise on Inorganic and Theoretical Chemistry, London: Longmans, 1952.

16. Cockburn, J.G., and J.Bird, Thorpe's Dictionary of Applied Chemistry, New York: Longmans, 1974.

17. Bard, A.J., "Photoelectrochemistry and Heterogeneous Photocatalysis at Semiconductors," Journal of Photochemistry, Vol. 10, pp. 59-75, 1979.

18. Kiwi, J., "Ouantitative Determination of Ti^{+3} Formation in Semiconductor Dispersions Induced under Light Irradition," Journal of Physical Chemistry, Vol. 90, pp. 1493-1495, 1986.

19. Gravelle, P.C., "Surface Reactivity of Reduced TiO_2," Journal of Physical Chemistry, Vol. 71, pp. 140-148, 1972.

20. "General Discussion of the Faraday Society," Faraday Society Discussions., Vol. 52, pp. 35-37, 1971.

21. Hermann, J.M., and P.Pichat, "Heterogeneous Photocatalysis," Faraday Society Transactions I, Vol. 76, pp. 1138-1146, 1976.

22. Blake, D., J.Webb, C.Turchi, and K.Magrini, "Kinetic and Mechanistic Overview of TiO_2-Photocatalyzed Oxidation Reactions in Aqueous Solution," Solar Energy Materials, Vol. 24, pp. 584-593, 1991.

23. Rabek, J.F., Photostabilization of Polymers: Principles and Applications, London: Elsevier Applied Science, 1990.

24. Boehm, H.P., "Acidic and Basic Properties of Hydroxylated Metal Oxide Surfaces," Faraday Society, Vol. 52, pp. 264-275, 1971.

25. Day, R.E., and G.D.Parfitt, "Adsorption at the Solid-Liquid Interface III-The Thickness of the Adsorption on Rutile from Alcohol and Hydrocarbon Solutions," Journal of Physical Chemistry, Vol. 71, pp. 3073-3077, 1967.

26. Bahnemann, D., D.Backelmann, and R.Goslich, "Mechanistic Studies of Water Detoxification Illuminated TiO_2 Suspensions," Solar Energy Materials, Vol. 24, pp. 564-583, 1991.

27. Kormann, C., D.W.Bahnemann, and M.R.Hoffmann, " Photolysis of Chloroform and Other Organic Molecules in Aqueous TiO_2 Suspensions," Environmental Science and Technology, Vol. 25, pp. 494-500, 1991.

28. Matthews, R. W., "Photo-Oxidation of Organic Material in Aqueous Suspensions of TiO_2," Water Research, Vol.20, pp.569-578, 1986.

29. Finklea, H.O., and R.Vithanage, "Infrared Absorption Spectroscopy of Chemically Modified TiO_2," Journal of Physical Chemistry, Vol. 86, pp. 3621-3626, 1982.

30. Sclafani, A., L.Palmisano, and M.Schiavello, "Influence of the Praparation Methods of TiO_2 on the Photocatalytic Degradation of Phenol in Aqueous Dispersions," Journal of Physical Chemistry, Vol. 94, pp. 829-832, 1990.

31. Harvey, P.R.,and R.Rudham, "Photocatalytic Oxidation of Iodide Ions by TiO_2," Journal of Chemical Society Faraday Transactions I, Vol. 84, pp. 4181-4186, 1988.

32 Technical Bulletin: Pigments, Degussa Ltd., 1990.

33. Handbook of Chemistry and Physics, Ohio:CRC Press , 1974-1975.

34. Chamdrasekaran, K., and J.K.Thomas, "Photochemical Reactions of Amorphous and Crystalline TiO_2 Powder Suspensions in water," Journal of Chemical Society Faraday Transactions I, Vol. 80, pp. 1163-1173, 1984

35. Koller, L.R., Ultraviolet Radiation, New York: John Wiley and Sons, 1965.

36. Othmer, D.F., Encyclopedia of Chemical Technology, New York: John Wiley and Sons, 1984.

37. Akmehmet I., "Heterogeneous Photocatalytic Oxidation of Organic Compounds by TiO_2," Ph.D. Dissertation, Boğaziçi University, 1990.

38 Morrison, R.T., and R.N.Boyd, Organic Chemistry, Allyn and Bacon, 1987.

39. Calver, J.G., and J.N.Pitts, Photochemistry, New York: John Wiley and Sons, 1966.

40. Shizuka, H., and P.De Mayo, Photochemistry, New York: De Reidel Co., 1972.

41. Haciu, D., "Heteregenous Photocatalytic Elimination of Metal Ions," Ph.D. Dissertation, Bogazici University ,1992.

42. Edward, W., and E. Boschmann , "The Ferrioxalate Actinometr: A Lecture Demonstration ," Journal of Chemical Education , Vol.58, pp.655, 1981.

43. Kuhn, H.J. , S.E. Braslavsky and R. Schmidt , "Chemical Actinometry," Pure and Applied Chemistry, Vol.61, pp.187-210 ,1989.

44. Stumm ,W. and J.J.Morgan, Aquatic Chemistry, New York: Willey,1970.

45. Mills, A., and S.Morris, "Photomineralization of 4-Chlorophenol Sensitized by TiO_2: A study of the Initial Kinetics of CO_2 Photogeneration," Journal of Photochemistry and Photobiology A:Chemistry, Vol.71, pp.75-83, 1993.

46. Loewenthal ,R.E. and G.R.Marais, Carbonate Chemistry of Aquatic Systems :Theory and Application, Michigan: Ann Arbor Science Publishers, 1976.

47. Izumi,I., F.F.Fan, and A.J.Bard, "Heterogeneous Photocatalytic Decomposition of Benzoic Acid and Adipic Acid on Platinized TiO_2 Powder.The Photo-Kolbe Decarboxylative Route to the Breakdown of the Benzene Ring and to the Production of Butane," Journal of Physical Chemistry, Vol.85, pp.218-223 ,1981.

48. Lozano, A., J.Garcia ,X. Domenech, and J. Casado , "Heterogeneous Photocatalytic Oxidation of Manganese (II) over TiO2," Journal of Photochemistry and Photobiology A:Chemistry, Vol.69, pp.237-240, 1992.

49. Perry, R.H., and C.H. Chilton, Chemical Engineers' Handbook, New York: Mc-Grow Hill, 1973.